

23rd Conference and Exhibition on
OPTICAL COMMUNICATIONS 2011
Scientific Section Proceedings



11

Optics from Mb/s to Tb/s

**October 20 – 21, 2011
Prague, Czech Republic**

**Czech and Slovak Society for Photonics
Czech Technical University in Prague
Faculty of Electrical Engineering
Action M Agency**

Edited by: Vítězslav Jeřábek, Jiří Vodrážka, Stanislav Zvánovec

ISBN 978-80-86742-32-8

23rd Conference and Exhibition on Optical Communications 2011 Scientific Section Proceedings

October 20 - 21, 2011, Prague - Czech Republic

Conference Topics

- Optical Transmission Systems
- FTTx Solutions
- Optical Measurements and Diagnostics
- Optical Fibres and Cables
- Installation and Maintenance of Optical Networks
- FSO - Free Space Optics
- Passive and Active Components, their Production and Testing
- Optical Fibre Sensors
- Special Applications of Fibre Optics
- Lasers and Fibre Optics in Medicine
- Optical Nano-waveguides
- Organic Materials for Optoelectronics
- Nonlinear Optics
- Signal Processing in Optical Transmission Systems
- Optical Components
- Other Topics Related to Optical Communications

Sponsored by

- Czech and Slovak Society for Photonics
- Czech Technical University in Prague, Faculty of Electrical Engineering
- IEEE Czechoslovakia Section
- International Union of Radio Science
- The Institution of Engineering and Technology



Edited by:

Vítězslav Jeřábek, Jiří Vodrážka, Stanislav Zvánovec

Published:

Ing. Milena Zeithamlová, Agentura Action M
Vršovická 68, 101 00 Praha 10, actionm@action-m.com

Produced:

Diskus dataservis, spol. s r.o., Sokolovská 154, 180 00 Praha 8

© 2011 Agentura Action M

ISBN 978-80-86742-32-8

About the Conference

The papers included in these proceedings were presented at the scientific section of the 23rd Conference and Exhibition on Optical Communications 2011 (OK 2011) organized by the Czech and Slovak Society for Photonics, Faculty of Electrical Engineering of the Czech Technical University in Prague and Action M Agency. It was held in the beautiful historic city, the capital of the Czech Republic – Prague on October 20 and 21, 2011.

In the third decade, the conference continues the successful editions of OK conferences established by pioneer Czech optical researchers in mid eighties. The main objective is to offer an international forum for the exchange of new ideas, thoughts, and realizations on physics, technologies, and applications of optics. Even though it is impossible for the conference to cover the entire area of optical communication technology as it is intensively developing these days, it tries to focus on vivid topics of the theory and applications that have significant impact on our society's everyday life. Traditionally, the conference offers an excellent opportunity for young scientists to present their recent research results.

The submitted manuscripts were thoroughly reviewed in a two-level process. Those individuals whose papers were chosen for presentation at the conference submitted manuscripts to be published in these proceedings. Totally 17 of 26 submitted manuscripts were accepted for presentation in the scientific section.

We want to thank the volunteers who helped us to attract high-quality contributions, all those who submitted papers for review and those who provided manuscripts for publication in these proceedings. We also wish to sincerely thank the members of OK 2011 committees, our partners who supported this event, and everyone who helped to organize the conference.

Vítězslav Jeřábek, Jiří Vodrážka and Stanislav Zvánovec
Czech Technical University in Prague, Faculty of Electrical Engineering

Scientific Committee

Chairman:

Miloš Klíma, FEE CTU in Prague, Czech Republic

Members:

- Leoš Boháč, FEE CTU in Prague, Czech Republic
- Jozef Dubovan, ZU Žilina, Slovak Republic
- Pavel Honzátko, Institute of Photonics and Electronics AS CR, Prague, Czech Republic
- Vítězslav Jeřábek, FEE CTU in Prague, Czech Republic
- Anton Kuchar, APKT Prague, Czech Republic
- Rastislav Róka, FEI STU Bratislava, Slovak Republic
- František Uherek, FEI STU Bratislava, Slovak Republic
- Martin Vaculík, ZU Žilina, Slovak Republic
- Vladimír Vašínek, VSB-TU Ostrava, Czech Republic
- Jiří Vodrážka, FEE CTU in Prague, Czech Republic
- Otakar Wilfert, FEEC BUT Brno, Czech Republic
- Stanislav Zvánovec, FEE CTU in Prague, Czech Republic

Content of Scientific Section Proceedings

I. Optical Technologies and Components	
Design and Modeling of the Single Mode Optical Glass Waveguides for Passive Photonics Structures	5
<i>Ondrej Barkman, Václav Prajzler, Pavla Někviňová</i>	
Microoptical and Microwave Design and Construction of a Micromodules for WDM Receiver.....	9
<i>Vítězslav Jeřábek, Julio Armas, David Mareš, Václav Prajzler</i>	
Future All-Optical Packet Switched Networks Based on Highly Nonlinear Components.....	14
<i>Matěj Komanec, Stanislav Zvánovec</i>	
Design and Simulation of Planar Passive Optical MMI Couplers	18
<i>Anton Kuzma, František Uherek, Jozef Chovan, D. Seyringer</i>	
II. Optical Systems and Networks	
Investigation on RSOA Based WDM PON for Long-haul Operations.....	22
<i>Peter Horňák</i>	
Possibilities of Upstream Data Eavesdropping in Passive Optical Networks	27
<i>Petr Jareš, Pavel Lafata</i>	
Impairment Aware Routing Algorithm in Generalized Multi-Protocol Label Switching	30
<i>Miloš Kozák, Leoš Boháč</i>	
Dispersion Compensating Photonic Crystal Fiber with Defected Core	34
<i>Stanislav Kraus, Kenneth Botah, Michal Lucki</i>	
Advanced Testing of Multimedia Services in GPON Network	37
<i>Jan Látal, Petr Koudelka, Petr Šiška, Jan Vitásek, Jan Skapa, Vladimír Vašínek</i>	
Sharing of Fibres by Transmission Systems and Open Photonic Transmission Systems	42
<i>Josef Vojtěch, Stanislav Šíma, Lada Altmannová, Miloslav Hula, Jan Radil, Pavel Škoda</i>	
A Nearly-Zero Ultra-Flattened Dispersion Photonic Crystal Fiber With Low Confinement Loss For Broadband Transmission Systems.....	45
<i>Richard Zelený, Kenneth Botah, Michal Lucki</i>	
III. Free Space Optics	
Low Cost Free-Space Optical System and Its Application	48
<i>Pavel Lafata, Bretislav Bakala</i>	
Adaptive Techniques in FSO Networks.....	52
<i>Jiří Libich, Stanislav Zvánovec</i>	
Wave Effects in FSO link and their Influence on Transmitted Laser Beam	55
<i>Juraj Poliak, Otakar Wilfert, Jiří Komrská</i>	
Experiment with Simple Prototype for Visible Light Communication	59
<i>Jiří Vodrážka, Jaromír Hrad</i>	
IV. Optical Sensors	
The Fiber-optic Sensors for Perimeter Guarding	62
<i>Jiri Hladík, Ladislav Šašek, Leoš Boháč</i>	
Smart Optical Fiber Sensors.....	67
<i>Branislav Korenko, Josef Jasenek, Josefa Cervenová</i>	

Design and Modeling of the Single Mode Optical Glass Waveguides for Passive Photonics Structures

Ondřej Barkman¹, Václav Prajzler¹, Pavla Nekvindová²

¹ Faculty of Electrical Engineering, Czech Technical University in Prague

² Institute of Chemical Technology in Prague

Abstract—Design, modeling and fabrication of a single mode optical channel waveguide with graded refractive index is reported. Several samples of optical planar waveguides were obtained by $\text{Ag}^+ \leftrightarrow \text{Na}^+$ and $\text{K}^+ \leftrightarrow \text{Na}^+$ one step thermal ion exchange process in a molten salt. Waveguide properties were measured by optical mode spectroscopy with the METRICON system. Obtained data were used for further design and modeling of surface channel waveguides in order to improve simulation accuracy. Designs were developed by utilizing Beam Propagation Method in the BeamPROP software by RSoft Design Group. The single mode channel waveguide was designed for operation wavelength band of 1260-1625 nm.

Index Terms—Single mode waveguide, glass substrate, graded waveguide, ion exchange.

I. INTRODUCTION

PLANAR optical waveguides made by Planar Lightwave Circuit (PLC) technology represent fundamental elements for constructing photonic integrated circuits. PLCs can be utilized to fabricate several key components exploited in passive optical networks (PON), such as power splitters, couplers, Mach-Zehnder modulators, etc. PLCs can be integrated onto a single chip to significantly reduce size and cost.

Common requirements for optical planar waveguides are a low propagation loss, suitable refractive index and mode field diameter comparable to a conventional single-mode fiber, accomplished by physical and chemical stability, easy fabrication process and low price.

Several possibilities producing these PLC devices are to be mentioned. One of the most popular technologies is to fabricate silica-based planar lightwave circuits by flame hydrolysis deposition [1]. Produced waveguides are characteristic with a high difference step-index refractive profile and small core diameter. Silicon substrate with a planar silica layer is deposited from plasma under high vacuum, heated to high temperatures and patterned into device structures [2, 3].

In this paper we deal with another possibility of PLCs fabrication by the ion-exchange (IE) process into a glass

substrate. Optical glass provides an ideal substrate, because the refractive index of the substrate is close to conventional SMFs and multi-mode fibers (MMF). The coupling between optical fibers and waveguides benefits from relatively low refractive index change in ion exchanged waveguides. This results in reduced power losses in fiber-to-waveguide connections. The fabrication process is relatively simple, reproducible and cost effective.

II. ION EXCHANGE

Ion exchange is a process, in which ions in glass (usually sodium) are replaced by ions of larger size but same chemical characteristics, such as silver or potassium. Consequently, the refractive index of the glass increases and the waveguide layer is created. The following equation describes the evolution of the concentration of new ions in glass [4]

$$\frac{\partial c}{\partial t} = \frac{\partial}{\partial x} \left[\frac{D_1}{1-\alpha c} \frac{\partial c}{\partial x} \right] + \frac{\partial}{\partial y} \left[\frac{D_1}{1-\alpha c} \frac{\partial c}{\partial y} \right] \quad (1)$$

with

$$c = c_1 / c_0$$

and

$$\alpha = 1 - D_1 / D_0$$

where c_1 and D_1 are the concentration and self-diffusion coefficient of the incoming ions respectively, D_0 stands for the self-diffusion coefficient of the outgoing ions, and c_0 represents the concentration of outgoing ions present in the glass prior to the IE.

In the first step, channel waveguide with graded refractive index is created on the surface of substrate glass (Fig. 1). Refractive index change Δn and diffusion depth h are dependent on time duration of IE and molten salt temperature [5, 6].

This process enables simple fabrication combined with low propagation and coupling losses. A disadvantage of IE stems in fact, that ion exchanged waveguides provide a relatively low index difference. This implies that the bend radius must be

lower, than semiconductor based waveguides, to minimize propagation losses [8].

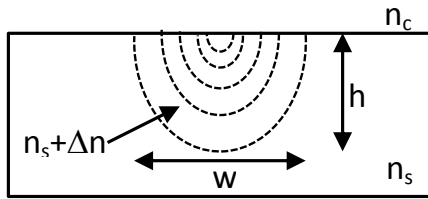


Fig. 1. Schematic representation of channel waveguide made by one step thermal ion exchange (n_c refractive index of the cover layer, n_s refractive index of the substrate).

III. EXPERIMENT

At first, four samples of optical planar waveguides were developed to obtain more accurate data for designing precise optical channel waveguide. Two types of highly pure optical glass substrates were evaluated in our experiments. A special soda-lime silica glass GIL49 and a special glass produced by Dr. Mika at the Institute of Chemical Technology in Prague. Glass properties are presented in TABLE I.

TABLE I

Composition of the substrate glass used for fabrication of optical waveguides

	SiO ₂	CaO	MgO	Al ₂ O ₃	Na ₂ O	K ₂ O	BaO
GIL49	73,28	6,10	4,10	1,20	14,87	0,45	<0,01
	NaO ₂	B ₂ O ₃	Al ₂ O ₃	TiO ₂	SiO ₂	SO ₃	
B1T1	11,65	12,59	19,20	0,00	56,56	0,30	
I1T1	14,37	14,99	17,58	1,76	51,30	0,30	

*all compounds given in wt. %

Refractive indices of chosen glass samples were measured by optical mode spectroscopy (OMS).

A. Fabrication

Three samples of optical planar waveguides were manufactured by silver IE and one by potassium thermal IE in molten salt. Process conditions are depicted in TABLE II.

TABLE II
CONDITIONS OF ION EXCHANGE PROCESS

Sample	Substrate	Ion exchange	Temperature [°C]	Time [min.]
1587	I1T1	Ag ⁺ ↔ Na ⁺	280	20
1588	B1T1	Ag ⁺ ↔ Na ⁺	280	20
1923	GIL49	Ag ⁺ ↔ Na ⁺	280	20
1924	GIL49	K ⁺ ↔ Na ⁺	400	180

Before the ion exchange process, the glass substrate must be cleaned from any impurities and dust after glass grinding and polishing. Cleaned substrate was inserted into molten salt for a defined period of time and temperature. Fabrication details are described more complex in [9].

B. Measurement

All samples were measured by OMS with METRICON 2010 system at wavelengths of 632.8, 1311 a 1552 nm while considering TE polarization. Waveguides made by silver IE

showed from three to four guided TE modes at the wavelength of 632.8 nm.

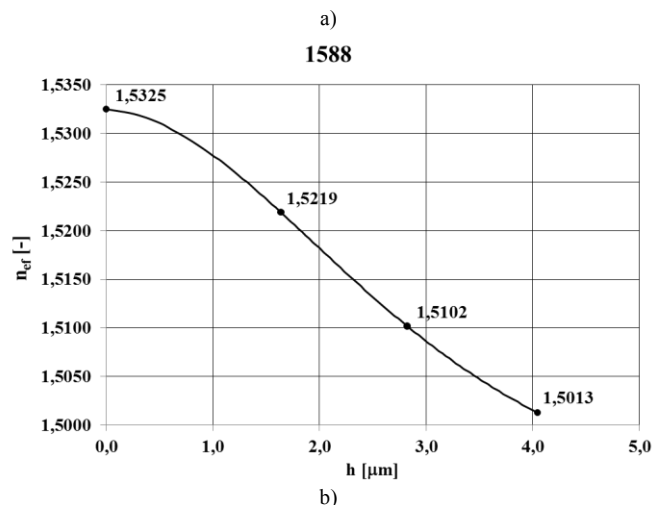
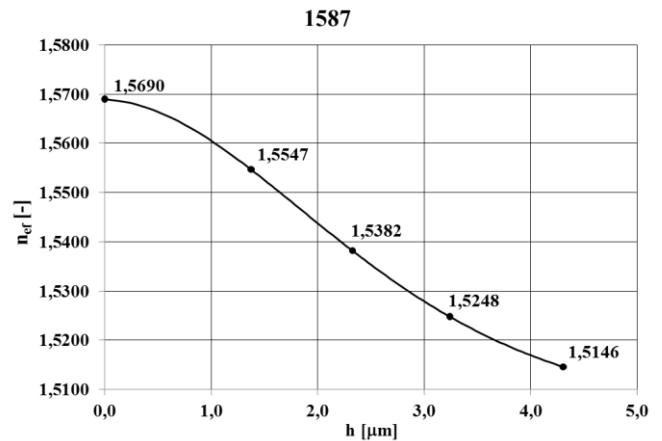
Depth of the waveguide layer was approximately 4 μm and refractive index difference in the order of hundredths. The fabricated waveguides provided single mode regime for wavelengths of 1311 and 1550 nm. Waveguide layer of the sample made by potassium ion exchange had 2 μm depth and refractive index difference in the order of thousandths. Complete properties of fabricated planar waveguides are presented in TABLE III.

TABLE III

PROPERTIES OF PLANAR WAVEGUIDES FOR $\lambda = 632.8$ NM

Sample	n_s	Δn	h [μm]	Modes
1587	1.5146	0.06	4.3	4
1588	1.5013	0.03	4.0	3
1923	1.5204	0.06	2.4	3
1924	1.5091	0.002	7.8	3

Refractive index difference was determined as a difference between refractive index on surface of planar waveguide and last guided mode. Further, the depth profile of the refractive index was measured (Fig. 2, a-d). However, we can determinate the depth profile only if the number of guided modes is greater than one. This condition satisfied only for the wavelength of 632.8 nm. Obtained data were used for design and modeling described in the following section.



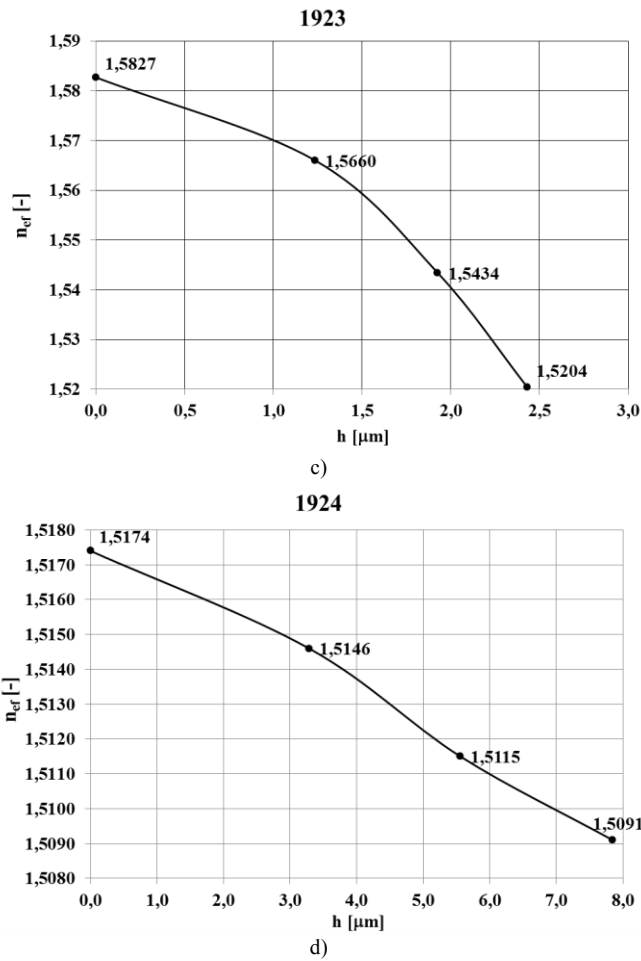


Fig. 2. Depth refractive index profile of fabricated planar waveguides. a) Sample 1587, b) Sample 1588, c) Sample 1923, d) Sample 1924

IV. DESIGN OF THE CHANNEL WAVEGUIDES

For a channel waveguide, there is no analytic solution exist, thus numerical techniques have to be employed. BeamPROP was utilized as a simulation engine [6]. This technique uses Finite Difference Time Domain (FDTD) methods to solve the well-known parabolic or paraxial approximation of the Helmholtz equation [10].

Based fabricated waveguides measurements, single mode optical channel waveguides were designed, their properties are summarized in TABLE IV.

TABLE IV PROPERTIES OF DESIGNED CHANNEL WAVEGUIDE	
n_s , ($\lambda = 1311$ nm), [-]	1.4951
n_s , ($\lambda = 1552$ nm), [-]	1.4923
Δn [-]	0.03
nc [-]	1
w [μm]	4
h [μm]	4

The design was developed for surface channel waveguide made by one step thermal IE. The diffusion profile is in BeamPROP software defined by [11]

$$n(x, y) = n_s + [\Delta n g(x) f(y)] \tag{2}$$

where function $g(x)$ is expressed as:

$$g(x) = \frac{1}{2} \left\{ \text{erf} \left[\left(\frac{w}{2} + x \right) / h_x \right] + \text{erf} \left[\left(\frac{w}{2} - x \right) / h_x \right] \right\} \tag{3}$$

where, n_s is refractive index of the substrate, Δn is maximum refractive index change produced by diffusion from an infinitely extended source, w is the width of the source in the horizontal direction, and h_x and h_y are diffusion lengths in horizontal and vertical direction respectively.

The vertical profile $f(y)$ is determined by the diffusion

shape. Gaussian diffusion shape was employed, which is defined by:

$$f(y) = \exp \left[\frac{-y^2}{h_y^2} \right] \tag{4}$$

Substituting parameters from the (2) into equations we get the refractive index profile (see Fig. 4).

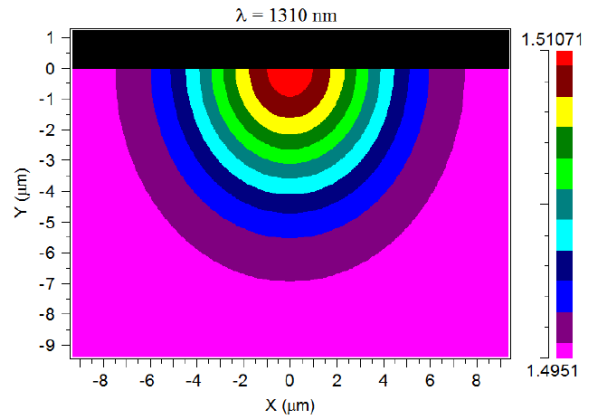


Fig. 3. Simulated refractive index profile of the designed optical channel waveguide, $\lambda = 1310$ nm.

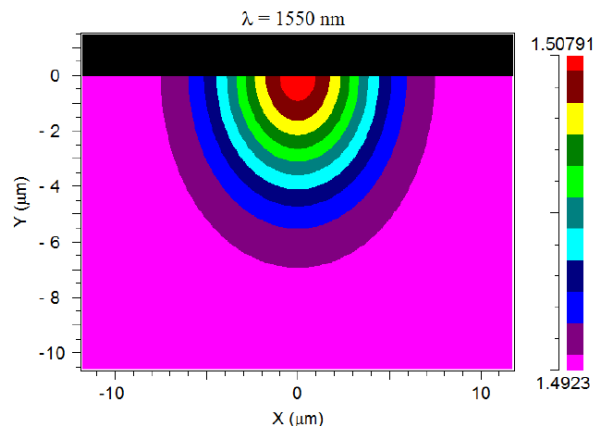


Fig. 4. Simulated refractive index profile of the designed optical channel waveguide, $\lambda = 1550$ nm.

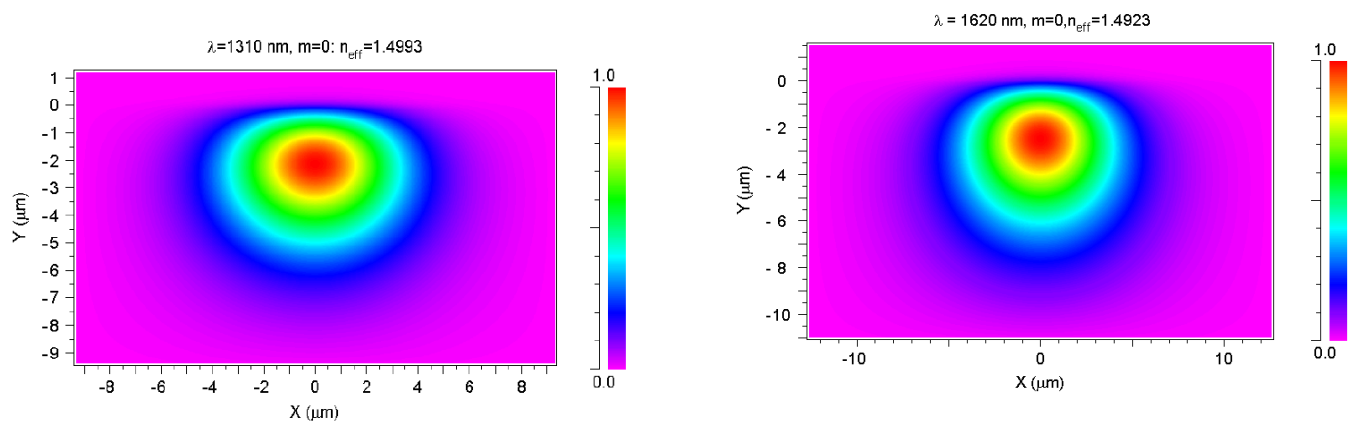


Fig. 5. Simulated electromagnetic field profile of fundamental mode designed optical channel waveguide, $\lambda = 1310$ nm.

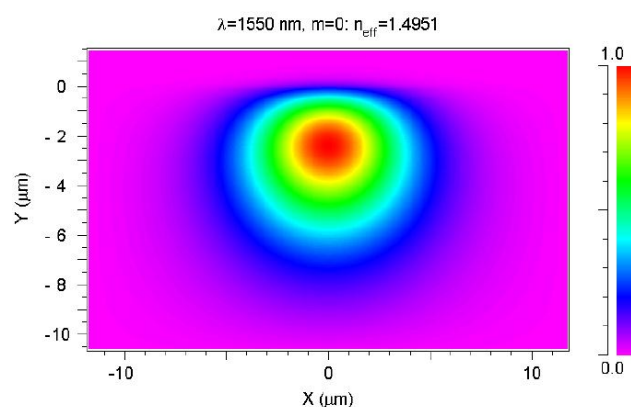


Fig. 6. Simulated electromagnetic field profile of fundamental mode designed optical channel waveguide, $\lambda = 1550$ nm.

Number of guided modes for wavelengths of 1310 nm and 1550 nm and TE polarization was verified. The transversal mode profile of the fundamental mode is shown on the Fig. 5,6. The designed waveguide is able to work in a wavelengths band of 1260-1625 nm.

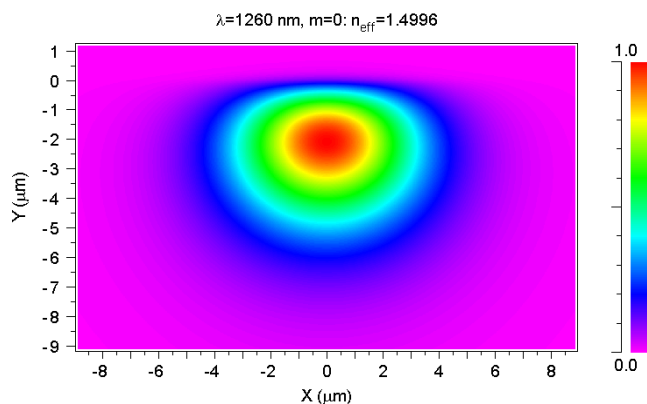
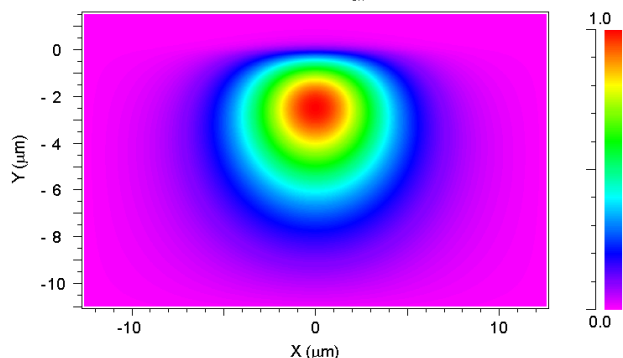


Fig. 7. Simulated electromagnetic field profile of fundamental mode designed optical channel waveguide, $\lambda = 1550$ nm.

$\lambda = 1620$ nm, $m=0, n_{\text{eff}}=1.4923$



V. CONCLUSION

An optical channel waveguide design made by thermal ion exchange in glass substrate is reported. First several samples of planar optical waveguides were fabricated and measured. Measurements showed that the depth of the waveguide layer approximately 4 μm . The refractive index difference is dependent on ion exchange properties. Base on measurements, optical single mode channel waveguide with graded refractive index for band of wavelength 1260-1625 nm was designed.

Future research will be focused on fabrication of the designed channel waveguide and design. More complex structures of photonic structures such as Y-branch power splitters will be developed and manufactured.

ACKNOWLEDGEMENT

Our research is supported by the Grant Agency of the Czech Republic under grant number 102/09/P104, the research program MSM6840770014 of the Czech Technical University in Prague and project "POLYPLAN" (MPO 61/110002).

Special thanks belong to company SQS Vlčkovná optika a.s. and Prof. Ing. J. Čtyrský, DrSc for collaboration and consultation.

REFERENCES

- [1] H. Takahashi, "Planar lightwave circuit devices for optical communication", 2003, Proc. of SPIE Vol.5246
- [2] B. West, M.C. Gupta, J. Ballato, "Handbook of Photonics: Ion-exchanged Glass Waveguides" 2007, CRC Press
- [3] Čtyrský, Hüttel, Schröfel, "Integrovaná optika", 1986, SNTL
- [4] K. Novotný, "Optická komunikační technika", 2007, ČVUT, Praha.
- [5] J. Albert, G. L. Yip, "Wide Single-mode Channels and Directional Couplers by Two-step Ion-exchange in Glass" 1988, Journal of Lightwave technology, Vol. 6, No. 4
- [6] S. Yliniemi, "Studies on Passive and Active Ion-exchanged Glass Waveguides and Devices, 2007, Doctoral thesis, ch. 3, Helsinki university of Technology
- [7] Madasamy, West, Morrel, Geraghty, Honkanen, Peyghambarian, "Buried Ion-exchanged Glass Waveguides: Burial-depth Dependence on Waveguide Width", 2003, Optics Letters, Vol. 28, No. 13
- [8] M.B.Pereira, S. Pelli, G.C. Righini, F. Horowitz, "K⁺/Ag⁺ Ion-exchange Glass Waveguides: Concentration and Graded-index Profile Analysis from EDS, m-line and DNS measurements, 2002, Annals of Optics-XXV ENFMC
- [9] O. Barkman, "Návrh optických kanálkových difuzních rozbočnic na skleněných podložkách", 2011, Master thesis, ČVUT
- [10] RSoft design group, "RSoft CAD Environment 8.1, User Guide", 2008
- [11] RSoft design group, "BeamPROP 8.1 User guide, 2008

Microoptical and Microwave Design and Construction of a Micromodules for WDM Receiver

Vítězslav Jeřábek, Julio Armas, David Mareš, Václav Prajzler

Faculty of Electrical Engineering, Czech Technical University in Prague

Abstract—We report about microoptical and microwave design and construction of WDM receiver module useable for the passive optical network PON of a fiber to the home FTTH topology. The WDM receiver uses a microoptics hybrid integration technology with volume holographic Bragg grating triplex filter (VHGT) and a collimating lenses for wavelength demultiplexing. A VHGT filters are ideal optical beam distribution element having high diffraction efficiency wavelength and very low insertion losses and optical crosstalk for radiation wavelength 1490 nm and 1550 nm. The optical imaging system was design in the paraxial approximation by ray-transfer matrix. The optical WDM receiver was constructed using system of a three micromodules in the new circle topology. OE receiver micromodules were designed by use small signal equivalent electrical circuit model and noise model, from which the mathematically solved the transmittance function, which was used for calculation and simulation of the optimal frequency characteristics and signal to noise ratio. The optoelectronics microwave receiver micromodules using integrated circuit (IC) Pseudomorphic High Electron Mobility Transistor (HEMT) amplifier for transimpedance OE receiver micromodule and Heterojunction Bipolar Transistors (HBT) Monolithic Microwave Integrated Circuit MMIC amplifier for low impedance OE receiver micromodule for receiving download information (internet and digital TV signals). The advantage of the hybrid integration technology is in using existing soft technology plant, piecing together different devices, which have been substantially optimized on a given substrate.

Index Terms— Collimating lens, Microoptical hybrid integration, Volume holographic grating triplexer, WDM Receiver.

I. INTRODUCTION

THE micromodules for WDM receiver are considered to be the key component for realizing fiber-to-the-home networks. Especially, an optical WDM Receiver module that can receive a 1490 nm download data as well as a 1550 nm download video signals for cable TV applications.

A microoptical lightwave hybrid integration technology enables us to construct a microoptical integrated lightwave circuits (MLC) and planar integrated lightwave circuits (PLC) by combining components with passive function (optical fiber, lens, VHGT, planar optical waveguides) and active optoelectronics devices (laser diodes, optical amplifiers and photodiodes) hybridized on one substrate for collimating,

focusing, imaging, branching, receiving and transmitting of an optical beams [1], [2].

WDM transceiver Fig. 1 was constructed by using system of a four micromodules set on the substrate in the new circle topology [3]. The optical demultiplexing micromodule is created by multimode optical fiber, collimating lens and volume holographic grating triplexer) diffraction filter (VHGT) [4] the two type microwave optoelectronic receiver micromodules (OE receiver micromodules) with bandwidth 2.5 GHz or 1.25 GHz and optoelectronic transmitter micromodule (OE transmitter micromodule). In the OE receiver micromodules, each diffracted beam from VHGT was focused on the active area of the PIN PD connected to microwave amplifier. The microoptical WDM receiver system will be assembled in DIL case.

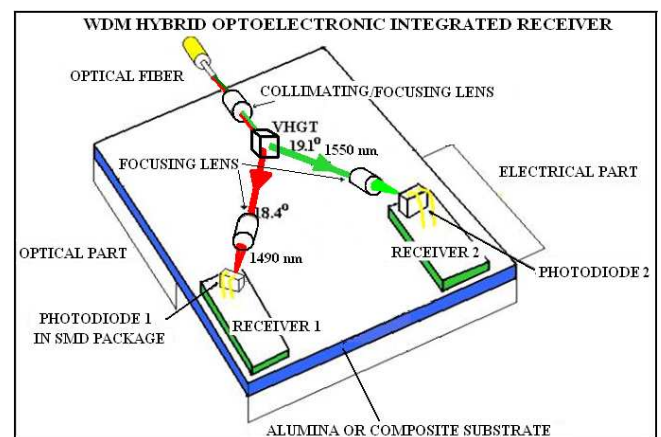


Fig. 1. WDM Receiver optical system with VHGT

II. SYSTEM DESIGN AND MEASUREMENT OF OPTICAL MICROMODULE

The OE receiver micromodule is represented by the block diagram shown in Fig 2. A special cylindrical lens is used in the WDM receiver to collimate the beam before the VHGT. The VHGT surface is covered antireflection layers. The collimated beam is diffracted by the VHGT and focused on the active area of PIN photodiodes by lenses. The PIN PD converts the received optical power of the radiation into a photocurrent [5].

We analyze the optical system and calculate parameters of

the optical micromodules - focal lengths and insertion losses of the lenses, angles of diffraction, diffraction efficiency, diffraction crosstalk on the VHGT for the wavelengths 1490 nm and 1550 nm.

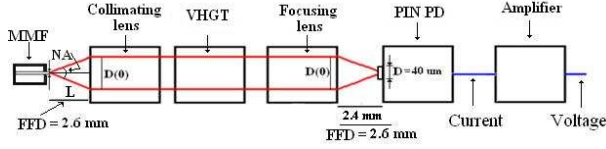


Fig. 2. Block diagram of WDM receiver signal path.

A. Analysis of optical collimating/focusing imagine

WDM receiver high efficiency optical system uses collimating/focusing lenses (lenses) for optical processing of the beam and spot transformation. The radiation propagates from the multi mode fiber (MMF) across the first collimating lens, VHGT and focusing lenses on the active area of the PIN PD's connected by microstrip electrical waveguides to the input of the electronic amplifiers. The main parameters of the system were the focal distance of the lenses and the diameter of the beam spot, which had a significant influence on VHGT optical characteristics (diffraction efficiency, optical crosstalk etc.).

The optical analysis by ray-transfer matrix describes optical systems in the paraxial approximation. The ray-transfer matrix (S_I) is used in order to find simple and explicit expressions for determination of the beam optimal structural parameters of the focusing system. The modal field profiles in the MMF and collimating lenses are assumed, to be circular symmetric and Gaussian and consider the propagation of a ray in a homogeneous medium [6]. The schema of the collimating system composed of the MMF and the collimating lens is shown in Fig. 3.

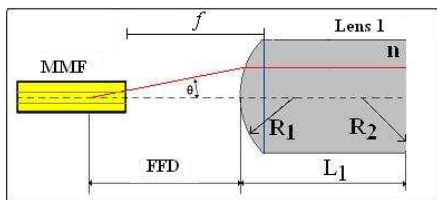


Fig. 3. Collimating system: MMF - cylindrical lens 1. (FFD - first focal distance, L_1 - length of the collimating lens, R_1, R_2 - radius of curvature of the lens, n_2 - refractive index, f - focal length, θ angle of numerical aperture).Block diagram of WDM receiver signal path.

The ray-transfer matrix (S_I) of the collimating lens was calculated as the multiplication of the translation matrix T_1 and the refraction matrices M_1 and M_2 shown in formulas (1), (2) and (3).

$$S_1 = M_1 T_1 M_2 \quad (1)$$

$$S_1 = \begin{bmatrix} 1 & 0 \\ \frac{n_2 - 1}{R_1} & 1 \end{bmatrix} \begin{bmatrix} L_1 \\ 0 \end{bmatrix} \begin{bmatrix} 1 & 0 \\ \frac{n_2 - 1}{R_2} & 1 \end{bmatrix} \quad (2)$$

$$S_1 = \begin{bmatrix} 1 + P_1 t & t \\ P_1 + P_2 + P_1 P_2 t & 1 + P_2 t \end{bmatrix} = \begin{bmatrix} A & B \\ C & D \end{bmatrix} \quad (3)$$

where P_1, P_2 and t are defined by (4), (5) and (6)

$$P_1 = \frac{n_2 - 1}{R_1} \quad (4)$$

$$P_2 = \frac{n_2 - 1}{R_2} \quad (5)$$

$$t = \frac{L_1}{n_2} \quad (6)$$

The focal plane of the collimating lens is defined by (7)

$$\begin{bmatrix} 0 \\ \beta_{out} \end{bmatrix} = \begin{bmatrix} 1 & b \\ 0 & 1 \end{bmatrix} \begin{bmatrix} A & B \\ C & D \end{bmatrix} \begin{bmatrix} y_{in} \\ 0 \end{bmatrix} \quad (7)$$

this implied that

$$0 = (A + b \cdot C) y_{in} \quad (8)$$

therefore

$$b = -\frac{A}{C} \quad (9)$$

where b is the front focal distance FFD of the lens and defined by (10)

$$FFD = b = -\frac{1 + P_1 t}{P_1 + P_2 + P_1 P_2 t} \quad (10)$$

The parameters of the optical system are: $L_1 = 3.0$ mm, $R_1 = 2.3$ mm, $R_2 = \infty$ (the concave radius of curvature of lens back surface). The calculated values of first focal distance (FFD) and attenuation in the collimating lens due to Fresnel reflection at the interfaces A_F for different wavelength are shown in the Table I.

TABLE I
THE CALCULATED VALUES OF THE COLLIMATING LENSES AND OPTICAL ATTENUATION FOR THE WAVELENGTH 1310 NM, 1490 NM AND 1550 NM.

λ [nm]	n	FFD [mm]	A_F [dB]
1550	1.4865	2.709	0.151
1490	1.4870	2.705	0.104
1310	1.4885	2.692	0.128

For the focusing process it was important to analyze the active area of the PIN PD covering by the radiation cone, formed behind focusing lens. The diameter of the beam spot exposition of the PIN PD active area depends on the distance between the focusing lens, PIN PD active area and the diameter of the beam spot. For the diameter active area $D = 40\mu\text{m}$ of PIN PD was calculated and measured distance from the focusing lens $FFD = 2.43$ mm.

B. Analysis and measurement of VHGT

For the optical demultiplex of the wavelength 1490 nm and 1550 nm optical beam in WDM receiver was in the optical micromodule used the VHGT filter from Ondax Ltd with double grating system. This transmission type grating filters has high diffraction efficiency, very low insertion losses and optical crosstalk.

The Bragg diffraction condition is given by (11)

$$\lambda_B = 2 \cdot \Lambda \sin\left(\frac{\theta_{diff}}{2}\right). \quad (11)$$

where Λ is Bragg constant, λ_B is the Bragg wavelength, θ_{diff} is the diffraction angle. From equation (11) were determine Bragg constants of VHGT by use measurement of the diffract angle. The Bragg constant $\Lambda = 4.66 \mu\text{m}$ and $\Lambda = 4.671 \mu\text{m}$ was calculated, where $\theta_{diff} = 18.4^\circ$ for $\lambda_1 = 1490 \text{ nm}$ and $\theta_{diff} = 19.1^\circ$ for $\lambda_2 = 1550 \text{ nm}$.

The diffraction efficiency η_B for VHGT was defined as the ratio between the diffracted intensity and the incident intensity, without considering absorption and Fresnel reflections at the interfaces. When the Bragg condition is satisfied for wavelength λ_B , the diffraction efficiency η_B is given for transmission gratings first diffraction order [4] as (12).

$$\eta_B = \sin^2\left(\frac{\pi \cdot n_1 \cdot D}{\lambda_B \cos \theta_n}\right) \quad (12)$$

where θ_n is the Bragg-matched incident angle in the medium, n_1 is grating strength refraction index modulation, D is thickness of the grating, and λ_B is the Bragg wavelength. For the compromise position of both gratings VHGT systems the diffraction efficiencies were calculated as 71.0% and 74.9% for 1550 nm and 1490 nm respectively. The space distribution of VHGT optical beams are shown in Fig. 4.

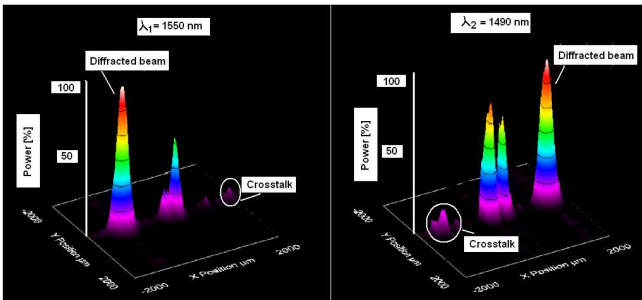


Fig. 4. The diffracted beams with crosstalks in 3D for the wavelength $\lambda_1 = 1550 \text{ nm}$ and $\lambda_2 = 1490 \text{ nm}$.

The measured values are shown in Table II.

TABLE II

THE MEASURED DIFFRACTION EFFICIENCIES η_B AND DIFFRACTION LOSSES A_F OF THE VHGT.

λ [nm]	P_{IN} [μW]	P_D [μW]	η_B [%]	A_F [dB]
1550	367	268.7	73,21%	1.35
1490	879	659	75,0%	1.24

where P_{IN} is incident optical power, P_D is diffracted optical power and A_F [dB] is attenuation in the VHGT due to non diffracted beam and crosstalk. The attenuation in the VHGT due to Fresnel reflection at the interfaces is very low because the VHGT has antireflection coated surfaces.

By the measurement the space distribution of an optical power was investigated that in center of diagram Fig. 5, exist two peaks of radiation no diffracted, which don't equal of Bragg condition. These radiations have to be filtered, when VHGT will be used in three wavelength WDM receiver or transceiver. At opposite side of the space distribution power diagram is clear perceptible peaks diffracted to opposite direction as optical crosstalk. In the next measurement of optical crosstalk was used the formula (13).

$$A_\lambda = 10 \log\left(\frac{P_{1\lambda}}{P_{2\lambda}}\right) \quad (13)$$

where $P_{1\lambda}$ is the is optical diffracted power, $P_{2\lambda}$ is optical power diffracted at the same direction than $P_{1\lambda}$.

The minimal optical crosstalk of the optical beams for two wavelengths was very important requirement for the good BER. The optical crosstalk was given by optical power, which was diffracted to wavelength opposite direction. For BER = 10^{-9} it was needed optical crosstalk attenuation $A_\lambda > 11 \text{ dB}$. The optical crosstalk for the wavelength $\lambda_1 = 1490 \text{ nm}$ and $\lambda_2 = 1550 \text{ nm}$ with the total power normalized to $P_{IN} = 360 \mu\text{W}$, was measured the crosstalk $P_{2\lambda}$ for λ_1 and λ_2 . It correspond $A_\lambda = 18.29 \text{ dB}$ and 18.4 dB as is shown in Table III.

TABLE III

THE OPTICAL CROSSTALK OF THE VHGT BEAMS MEASUREMENT.

λ [nm]	Total Power P_{IN} [μW]	Diffracted Power $P_{1\lambda}$ [μW]	Crosstalk $P_{2\lambda}$ [μW]	A_λ [dB]
1550	360	268.7	15 ₁₄₉₀	12.44
1490	360	659	4 ₁₅₅₀	18.29

For measurement of the optical power space distribution in 2D or 3D was used beam profiler head BP 104 IR from Thorlabs with special software. The crosstalk measured shows us that using the VHGT is possible diffract two beams at the same time without undesired effect from each other.

III. SYSTEM DESIGN AND MEASUREMENT OF RECEIVER MICROMODULE

For OE receiver micromodules were used two types of the OE receivers. For construction of the 1.25 GHz optoelectronic microwave micromodules with transimpedance OE receiver was used SMD technology, which is sufficient for this dynamics response devices. OE receivers were designed by use small signal equivalent electrical circuit model and noise model. The internal structure of the transimpedance OE receiver, with the ATF-36163 amplifier, InGaAs PIN photodiode and the bias circuitry is presented in the Fig. 5. The all components the PIN PD, capacitors, resistors and inductance in SMD were assembled on composite low loss substrate (Rodgers), with Au/ Cu microstrip line and

waveguide motive. The focusing lens was fixed on Au/ Cu currier in front of PIN PD.

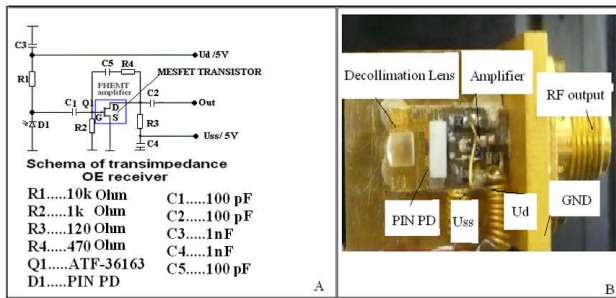


Fig. 5. Design and construction of the optoelectronic micromodule. A) The electrical schema of the transimpedance OE receiver B) The real microwave optoelectronic micromodule assembly

The low impedance OE receiver for 2.5 GHz bandwidth optoelectronic micromodules were realized by the thin layer hybrid integration technology.

For realized OE receiver micromodules the electro/optical transmission, dynamic response and noise figure characteristics parameters were designed and measured. The low impedance OE receiver was composed of the InGaAs PIN photodetector C30616 ECER with bandwidth 3.5 GHz and HBT monolithic amplifier HM 396 made by GaAs/ InGaP heterojunction bipolar transistors technology (HBT) with bandwidth 8GHz and gain 20 dB. In microwave signal path was used a microstrip waveguide, connecting the PIN PD to the signal input of HBT amplifier. The thin film Au microstrip waveguides was formed by a standard lithographic sputtering process assembly on an alumina substrate (thin layer technology), in which the passive and active components in chip form are mounted directly on Au strip waveguide lines and fix by epotek.

The parameters of WDM receiver were calculate and measured. The low frequency transmittances were 140 V/W and 170 V/W for low and transimpedance OE receivers respectively. The dynamic measurement results of modulation frequency characteristic OE receivers, $f_T = 2.5$ GHz for low impedance OE receiver and $f_T = 1.25$ GHz for transimpedance OE receiver as is shown in Fig. 6.

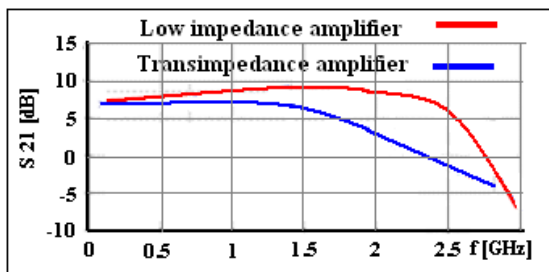


Fig. 6. The measured S21 frequency characteristics of the OE receiver for low impedance and transimpedance amplifier

The signal to noise ratio (SNR) of WDM receiver was calculated and measured for both type of OE receivers. In the case of the transimpedance OE receiver was measured SNR = 27.3 dB and in the case of the low impedance OE receiver SNR= 23.6 dB. This corresponds with optical attenuation

reserves 5.7 dB for transimpedance and 2 dB for low impedance OE receiver. We presume the fiber loss 0.2 dB/ km and SNR=21.6 dB for BER=10⁻⁹. These values correspond to the transmission distance of the 28.5 km or 10 km optical SM fiber. When we subtract optical losses 1.4 dB, of the demultiplexing optical system of WDM receiver, the transmit distance drop to 21.5 km or 3 km of optical SM fiber.

The WDM receiver Rx has been constructed using system of a three micromodules in the new circle topology set on the alumina or composite substrate. The fundamental layout of the hybrid integrated microoptical WDM receiver is given on Fig. 7.

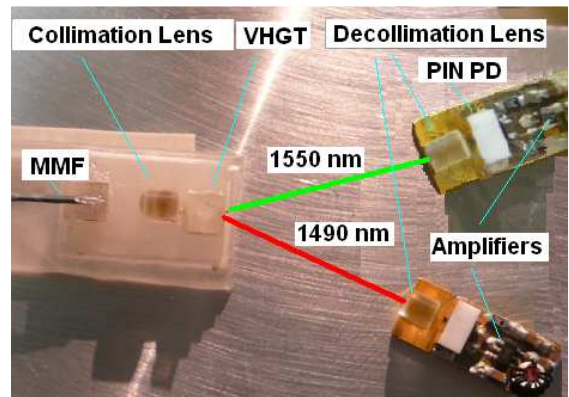


Fig. 7. WDM receiver module based on microoptical hybrid integration technology

IV. PLC HYBRID INTEGRATION FOR WDM TRANSCEIVER

WDM transceiver in PLC hybrid integration technology is shown in Fig. 8. Our works was focused on design a PLC ridge waveguide with interference or microring resonators MUX/ DEMUX filter, which was made from polymer materials. For design was used BMP program from R Soft.

As polymer we choose NANOTM SU-8 2000 polymer from Micro Chem Corp. due to good optical and mechanical properties (this polymer has optical losses less than 1 dB/cm at the wavelengths 1 300 and 1 550 nm).

The polymer layers were deposited by using spin coating method on silica on silicon. Before lithography the samples were prebake for 10 min. at 90°C. The channel waveguides would be fabricated by using UV lithography. As a last step the post backing (200 °C at 120 min or 90°C at 15 min.) would be carried out to stabilize optical properties. The photodetectors and laser is placed in the groove for elimination height offset.

The optimum distance among optical waveguides facet on base polymer SU8-2000 and optical fiber or photodetector in the receiving part was specified by BMP program simulation. The optoelectronic part was made same as at microoptics type WDM transceiver.

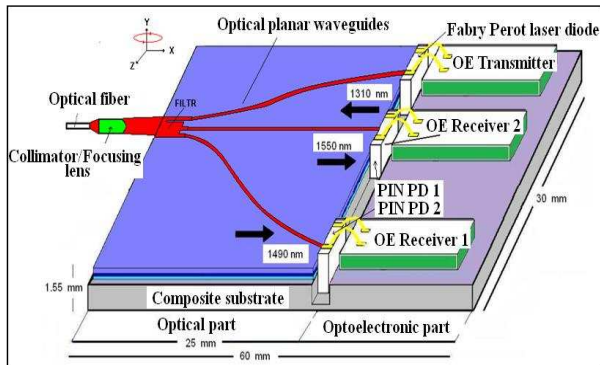


Fig. 8. WDM planar hybrid integrated transceiver.

V. CONCLUSION

The paper presents design a novel topology and technology solution of IC microoptical hybrid integrated WDM receiver, composed of the optical and optoelectronic micromodules. The optical micromodule use volume holographic grating triplexer (VHGT) as unique optical multiwavelength demultiplexing element in WDM microsystem, The downstream microoptical imagine system was verified by construction and measurement of the microoptical hybrid integrated WDM receiver. Very low insertion optical losses and optical crosstalk of VHGT element imply the high sensitivity and the transmit distance of optical SM fiber. Further work was concentrated on design and construction of WDM transceiver realized by planar lightwave circuit hybrid integration technology. The optical part will be solved by polymer or glass interference filter or microoptical resonators.

ACKNOWLEDGMENT

This research has been supported by MPO-TIP grant Nos. and the research program MSM6840770014 of the Czech Technical University in Prague.

REFERENCES

- [1] K. Kato, at all, "PLC Hybrid Integration Technology and Its Application to Photonic Components," *IEEE J. Quantum Electron*, pp. 4–13, 2000.
- [2] T.-Hatta, at all, "Hybrid Integration of Waveguide Photodiode and Preamplifier IC Using Au Stud Bump," *J. of Lightwave Technology*, pp. 3187–3194, 2006
- [3] J. Armas, V. Jeřábek, K. Bušek, D. Mareš, V. Prajzler, "Microoptical Triplexer System with High Efficiency for WDM Hybrid Optoelectronic Receivers," *Proc. EDS IMAPS CS Conf*, Brno, pp. 126–128, 2010
- [4] Ondax Inc., Volume Holographic Gratings (VHG), *Whitepaper*, 2005.
- [5] Judson Technologies Technical Documentation, PIN PD J22-CO2-RO 40U
- [6] G. Kloos, "Matrix methods for optical layout," *SPIE*, vol. 6, 2007
- [7] Han, Y., at all, "Fabrication of a TFF- Attached WDM-Type Triplex Transceiver Module Using Silica PLC Hybrid Integration Technology," *Journal of Lightwave Technology*, vol. 24, No. 12, 2006.

Future All-Optical Packet Switched Networks Based on Highly Nonlinear Components

Matej Komanec, Stanislav Zvanovec

Faculty of Electrical Engineering, Czech Technical University in Prague

Abstract—Novel optical packet switch for future all-optical packet switched networks and IP routing is presented. Chalcogenide-based nonlinear glass fabrics are evaluated for the proposed switching configuration. Particular research results of the optical packet switch development will be introduced. Future major research challenges are discussed as well, focusing on sophisticated labeling techniques.

Index Terms—optical packet switching, optical networks; nonlinear optics, chalcogenide fibers, fiber tapering, labeling techniques.

I. INTRODUCTION

ALL-OPTICAL networks discarding slow and power-demanding electronic processing introduce the indisputable solution for the future data communication, such as 3D multi-media data streams, extreme high quality video, etc. Although simple switching methods of data streams based on wavelength routing [1], space-switching [2] or broadcast and select method [3] have already been presented, the situation changes rapidly, when sophisticated label recognition and/or IP based optical routing is going to be included. Recently pure optical processing of a 4-bit optical packet label was presented in [3].

Another problem will arise with new spectrally efficient modulation formats appearing in optical networks, e.g. differential phase shift keying (DPSK), differential quadrature phase shift keying (DQPSK) [4], multiple-quadrature amplitude modulation (M-QAM) [5, 6], orthogonal frequency division-multiplexing (OFDM) [7], where modulation processing is significantly more complicated and it is therefore suitable to preserve the signal only in an optical form.

Nonlinear switching techniques exploiting the Kerr effect (four-wave mixing, FWM and cross-phase modulation, XPM) are evaluated for the proposed OPS, offering many possibilities for the design of novel planar and fiber optical devices for all-optical switched networks [8]. They also provide extremely fast switching speeds (in orders of nanoseconds or even picoseconds).

In contrast to conventional fused silica fibers, highly nonlinear materials could serve as a core building block of an OPS network. From the wide range of nonlinear media glasses based on chalcogenide (ChG) can provide one of the best options due to their optical parameters [9].

Development of an optical packet switch (OPS) at the Czech Technical University in Prague in a joint co-operation with the Institute of Photonics and Electronics, Academy of Sciences of the Czech Republic, and SQS fiber optics (medium-sized enterprise) is presented.

At first, basic operational principle of an OPS is discussed. Afterwards, buffering techniques are summarized. State-of-art research of suitable switching fabrics is discussed together with an analysis of nonlinear materials for optical packet switching. Based on analysis results, ChG glass fibers based on sulfide (As_2S_3) and mainly selenide (As_2Se_3) are considered in the next steps of OPS development.

Main aim was to optimize high-speed data switching with combination of particular nonlinear element while utilizing more sophisticated packet labeling format.

The paper is concluded with a brief summary of so far obtained results and proposed future work.

II. BASIC PRINCIPLE OF AN OPTICAL PACKET SWITCH

Generalized operational principle of an OPS is demonstrated in Fig. 1. An optical packet composed of a label (header) and data payload arrives at the input of the OPS. The payload carries user data, e.g. video, voice, etc. The label serves only as a destination information, where header includes whole IP address.

The label is segregated and converted into electrical format and processed by the CPU (in most cases a field programmable gateway array, FPGA). Label segregation is carried out by an optical filter or a spectrally-narrow fiber Bragg grating (FBG). Payload is delayed in an optical delay line as long as the label is being processed. Then according to the generated routing signal the payload is imprinted onto the routing signal, i.e. is wavelength converted and sent to the desired output. A new label is attached at the output of the OPS for further network processing.

Several approaches to packet switching have been

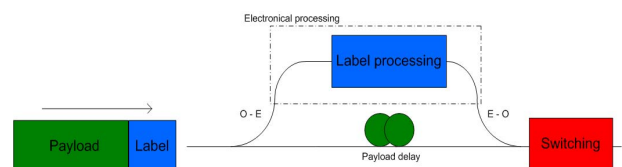


Fig. 1. OPS generalized operational scheme (O-E – opto-electrical conversion)

proposed. Main difference in scientific teams currently dealing with the OPS development can be found in the labeling method [3, 10-11] and the switching technique respectively [12-15].

III. BUFFERING TECHNIQUE

As long as optical memories will be unavailable in a simple form, buffering is required to prevent collision of incoming optical packets at the input of the OPS. It is usually achieved by employing multiple delay lines, with a different fiber length, i.e. different time delay.

A pure optical design is definitely an advantage. Therefore several concepts have been proposed. Figure 2 presents a recirculation fiber loop, the so called resonator, which was developed as a substitute for conventional delay lines in one of our former research works [16]. It works on the principle of conserving maximum energy in the loop (energy is coupled into the loop by a directional 99/1 coupler). Resonator application may be found not only in OPS, but also in optical sampling [17] and other signal processing.

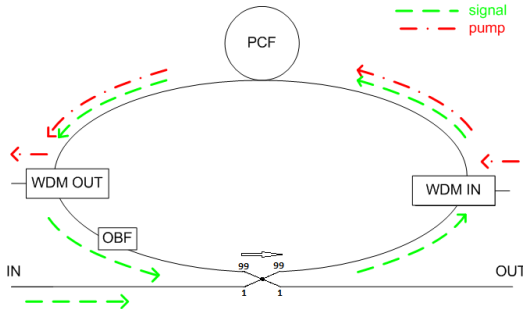


Fig. 2. Delay-line in a resonator setup with inserted amplification [16]; WDM – wavelength-division multiplexer, OBF – optical bandpass filter, PCF – photonic crystal fiber

IV. SWITCHING FABRIC

Switching fabrics, mostly aiming for monolithic integration, based on indium phosphide (InP) [10,15] or lead zirconium titanate doped with a little lanthanum (PLZT) [13] have been deeply studied recently.

On the other hand from the fiber point of view chalcogenide fibers can offer much higher nonlinear refractive index n_2 than conventional silica fibers, thus offering a possibility of drastic length reduction, while preserving relevant performance parameters.

By additional tapering of the ChG fiber even shorter component length may be achieved. Chalcogenide As_2Se_3 fiber with numerical aperture $NA \approx 0.20$, having $170\mu\text{m}$ cladding diameter and $6\mu\text{m}$ core diameter respectively was utilized for the tapering process [18]. A taper with a waist diameter of $7.1\mu\text{m}$ has been already technologically obtained, meaning a reduction factor of almost 24, thus decreasing core diameter to a value of $\approx 0.25\mu\text{m}$.

Considering the nonlinear coefficient defined as:

$$\gamma = \frac{2\pi n_2}{\lambda A_{eff}}, \quad (1)$$

where λ is wavelength, A_{eff} stands for the effective mode area. In case of an untapered ChG As_2Se_3 fiber, at 1550nm , $\gamma \approx 1408 \text{ W}^{-1}/\text{km}^{-1}$ was obtained. For the tapered fiber at the same wavelength it corresponds to $\gamma > 15600 \text{ W}^{-1}/\text{km}^{-1}$, where an exact value is hard to define, due to complicated mode area measurement methods and mode conversion in the taper.

The attenuation limit was set according to the ITU recommendation G.671 for optical switches [19]. For extremely tapered core diameters, it is expected, that greater losses are obtained due to insufficient field confinement in the taper core. It meets the practical point of view, where it is extremely complicated to technologically produce tapers with waist diameter in orders of nanometers.

V. LABELING METHOD

Most of current proposed state-of-art optical label encoders utilize the in-band labeling [3], where multiple labels at different wavelengths are inserted between the ITU-grid data channels. Its main advantage is in including the packet label into the spectrum of the data and then separating it with a very narrow filter, not distorting the data spectrum. The label separation is done usually by a narrow fiber Bragg grating, which allows filtering in orders of 0.1nm or even less.

Other labeling techniques to be mentioned are the out-band labeling [9], which exploits the wavelength spectrum. Employing the out-band label ensures the simplest approach for achieving good label detection without distortion of the data spectrum. The serial labeling [10] exploits the OTDM principle. The label consists of a specified bit sequence to identify its front (typically a predefined stream of binary zeros and ones). Synchronization is needed to detect the label properly. The payload is either delayed until the label is processed or if the guard time is longer than label processing time, no delay for the payload is necessary. Next to mention are the optical carrier suppression and separation (OCSS) labeling technique [8] and the modulation diversity labeling method [11].

In the OPS proposed by our research team, the in-band labeling technique was employed. Data payload was placed on the 100GHz ITU-defined wavelength grid, where labels were placed between the ITU-grid wavelengths, minimizing distortion of the data spectrum, while maximizing spectral efficiency.

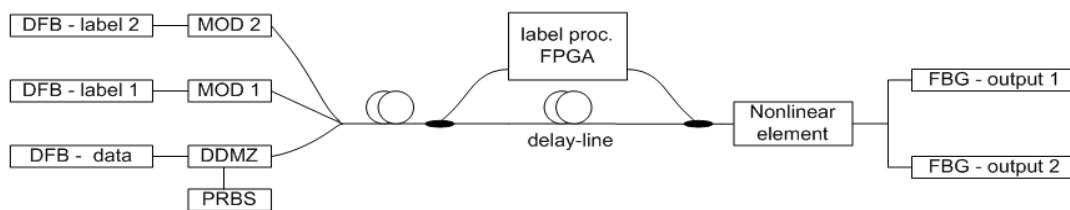


Fig. 3. Experimental setup of the proposed optical packet switch; DFB – distributed feedback laser diode, MOD – modulator, DDMZ – dual-drive Mach-Zehnder modulator, PRBS – pseudo-random binary sequence generator, FPGA – field-programmable gateway array, FBG – fiber Bragg grating

VI. EXPERIMENTAL SETUP

The experimental setup is demonstrated in Fig. 3. It included a high-speed data source laser diode externally modulated with a pseudo-random binary sequence (PRBS) in a dual-drive Mach-Zehnder (DDMZ) modulator.

Several label generators were employed. Both label generators and data source were distributed-feedback (DFB) laser diodes, which enabled large wavelength tuning span via temperature or current control. This allowed measurements of various spectral parameters and different optical packet compositions. A label processing unit included a FPGA utilizing a decision algorithm, generating a routing signal according to label content. As a delay-line a segment of conventional optical fiber can be employed or a fiber loop resonator as proposed in our previous work [16]. Nonlinear switching element (NSE) together with fiber Bragg gratings (FBG) provided switching of the packet at desired output.

Via the XPM effect, the data signal was imprinted on the routing signal and sent to the desired output port, where it was filtered by the FBG.

VII. CONCLUSION

Results from development of the optical packet switch were presented. The evaluated data show very promising results, mainly incorporation of untapered and tapered chalcogenide fibers into the switch. Simulations showed very promising implementations of such a ChG As_2Se_3 fiber taper for ultrafast optical switching. Thanks to the natural ultrafast response of the ChG medium, switching speeds in orders of nanoseconds were obtained. Influence of the labeling technique was also evaluated and preliminary results suggest that in-band labeling method together with complicated label format, utilizing nonlinear element also for label recognition may propose the future solution for optical IP routing.

ACKNOWLEDGMENT

The research activities were supported by Technology Agency of the Czech Republic grant TA01011105. Additional analyses and simulation background was supported by the Grant Agency of the Czech Technical University in Prague, grant No. SGS11/065/OHK3/1T/13.

REFERENCES

- [1] T. Segawa, S. Matsuo, T. Kakitsuka, Y. Shibata, T. Sato, and R. Takahashi, "A monolithic wavelength-routing switch using double-ring-resonator-coupled tunable lasers with highly reflective mirrors," *Indium Phosphide & Related Materials (IPRM)*, pp. 1-4, 2010.
- [2] C. Guillemot, M. Renaud, P. Gambini, Ch. Janz, I. Andonovic, R. Bauknecht, et al., "Transparent optical packet switching: the European ACTS KEOPS project approach," *J. of Lightwave Tech.*, vol. 16, pp. 2117-2134, 1998.
- [3] N. Calabretta, H.-D. Jung, E. Tangdiongga, and H. Dorren, "All-Optical Packet Switching and Label Rewriting for Data Packets Beyond 160 Gb/s," *IEEE Photonics J.*, vol. 2, pp. 113-129, April 2010.
- [4] C. Schmidt-Langhorst, L. Reinhold, D.-D. Gros, L. Molle, M. Seimetz, R. Reund and C. Schubert, "Generation and coherent time-division demultiplexing of up to 5.1 Tb/s single-channel 8-PSK and 16-QAM signals," *Optical Fiber Communication - includes post deadline papers (OFC)*, pp. 1-3, March 2009.
- [5] A. H. Gnauck, G. Charlet, P. Tran, P. J. Winzer, C. R. Doerr, J.C. Centanni, E.C. Burrows, et al., "25.6-Tb/s WDM Transmission of Polarization-Multiplexed RZ-DQPSK Signals," *J. of Lightwave Tech.*, vol. 26, pp. 79-84, January 2008.
- [6] Z. Xiang, Y. Jianjun, H. Ming-Fang, S. Yin, W. Ting, P. Magill, et al., "32Tb/s (320x114Gb/s) PDM-RZ-8QAM transmission over 580km of SMF-28 ultra-low-loss fiber," *Optical Fiber Communication - includes post deadline papers (OFC)*, pp. 1-3, March 2009.
- [7] H. Takahashi, A. Al Amin, S. L. Jansen, I. Morita and H. Tanaka, "DWDM transmission with 7.0-bit/s/Hz spectral efficiency using 8x65.1-Gbit/s coherent PDM-OFDM signals," *J. of Lightwave Tech.*, vol. 28, pp. 406-414, 2010.
- [8] G. P. Agrawal, *Nonlinear fiber optics*, 4th ed. Amsterdam; Boston: Elsevier / Academic Press, 2007.
- [9] A. Zakery, and S. R. Elliott, *Optical Nonlinearities in Chalcogenide Glasses and their Applications*, Springer, 2010.
- [10] J. P. Mack, K. N. Nguyen, M. M. Dummer, E. F. Burmeister, H. N. Poulsen, B. Stamenic et al. "40 Gb/s buffered 2x2 optical packet switching using photonic integrated circuits," *Lasers and Electro-Optics, Quantum electronics and Laser Science Conference (CLEO/QELS)*, pp. 1-2, 2009.
- [11] A. Chowdhury, J. Yu, and G.-K. Chang "Same Wavelength Packet Switching in Optical Label Switched Networks," *J. of Lightwave Tech.*, vol. 24, pp. 4838-4849, December 2006.
- [12] K. Huybrechts, T. Tanemura, Y. Nakano, R. Baets, and G. Morthier, "Fast 40 Gb/s optical packet switching using an all-optical flip-flop based on a single distributed feedback laser," *Optical Fiber Communication Conference, OFC*, pp. 1-3., 2009
- [13] M. Takagi, H. Imaizumi, T. Tanemura, S. Iio, M. Seuhiro, Y. Nakano, et al., "200Gb/s Multi-Wavelength Optical Packet Switching with 2ns ultra-fast optical switch," *OptoElectronics and Communications Conference (OECC)*, pp. 1-2, 2009.
- [14] N. Wada, S. Shinada, and H. Furukawa, "Modulation format free optical packet switching technology," *Transparent Optical Networks (ICTON)*, pp. 1-4, 2010.
- [15] I. M. Soganci, N. Calabretta, T. Tanemura, W. Wang, O.Raz, K. Higuchi, et al., "160-Gb/s Optical Packet Switching Subsystem With a Monolithic Optical Phased-Array Switch," *IEEE Phot. Tech. Letters*, vol. 22, pp. 817-819, 2010.

- [16] M. Komanec, and S. Zvanovec, "Analysis of Fiber Pulse Replicators for Single-Shot All-Optical Measurements," ICECom 2010 Zagreb: KoREMA 2010.
- [17] M. Komanec, P. Honzatko and S. Zvanovec, "Single-shot all-optical sampling oscilloscope using a polarization-maintaining resonator for pulse replication, Microwave and Opt. Tech. Letters, vol. 52, pp. 2452-2456, November 2010
- [18] T. Martan, J. Kanka, I. Kasik, and V. Matejec: "Theoretical analysis and preparation of tapered suspended core microstructure fibers", Int. J. Optomechatronics 3 (3), pp. 233-249, 2009.
- [19] "Transmission Characteristic of Passive Optical Components," ed. Recommendation ITU-T Rec. G.671, 2009

Design and simulation of planar passive optical MMI splitters

A. Kuzma^{1,2}, J. Chovan¹, F. Uherek^{1,2} and D. Seyringer³

¹ International Laser Centre, Bratislava, Slovakia

² Institute of Electronics and Photonics, Faculty of Electrical Engineering and Information Technology, Slovak University of Technology in Bratislava, Slovakia

³ FH Vorarlberg, Dornbirn, Austria

Abstract - The paper deals with the design and simulation of planar passive optical splitters. Splitters were designed for 16 output waveguides. We designed two types of MMIs: MMI with a low index contrast (0.75%) and also with a high index contrast (58.9%). The simulations were performed by Rsoft CAD. The simulated results as insertion losses, the size of the splitters and the dependence of the output power on the used input wavelength were compared with one another and discussed.

Index Terms – optical splitter, design, MMI, waveguide

I. INTRODUCTION

Splitting and combining of multiple optical beams plays important role in the integrated optics. One way how to split optical signals is to use multimode interference (MMI) splitters that have been implemented for a variety of optical signal processing functions such as splitting, switching and routing. The MMI splitters feature a large splitting number and stable splitting ratio, ensuring good uniformity over all the output signals. Another advantage is their good fabrication tolerance because the splitting is performed in the multimode section.

In this paper we present the design of 1x16 MMI with both, the low and high index contrast. For the design and simulation we have used Rsoft CAD that is the core program in the Rsoft Photonics Suite, and acts as a control program for passive device simulation module BeamPROP.

The first part of paper explains shortly the design theory of planar passive optical MMI splitter.

The second part describes the fabrication of both MMI splitters (low and high index contrast material systems). This part of paper describes difficulties of mode of productions of MMI splitters, too.

The third part focuses on the design of MMI splitters. After the design topology of both MMI splitters (low index contrast and high index contrast) an analysis options are defined.

Last part presents a comparison of achieved simulated parameters of both designs. Some advantages and disadvantages of MMI splitters with low and high index contract for telecom applications are discussed.

II. MULTIMODE INTERFERENCE SPLITTER

Geometry of the conventional 1×16 MMI splitter is illustrated schematically in Fig. 1. The Optical signal propagates in the fundamental mode through the input

waveguide to the multimode region across the junction. Abrupt change in the geometry and symmetry of the device ensures that the fundamental mode excites the even modes in the multimode segment. Propagation constants are uniformly spaced and constructive interference occurs between the modes. This results in the bright spots (maxima) in the cross-section of the splitter. By cutting the splitter at particular length, L_{MMI} , N split output signals can be obtained. The length of the splitter was designed to achieve 16 output optical signals. The output single mode waveguides (channels) are located at the end of multimode region to collect these optical signals each having the 6.25% of input optical power.

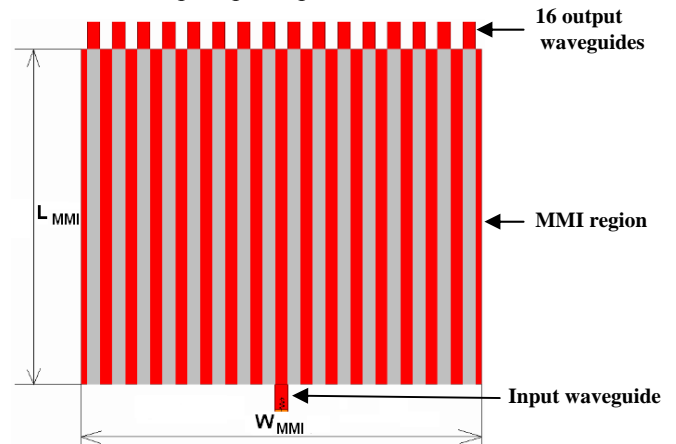


Fig. 1. Schematic view of 1x16 MMI splitter design.

The length, L_{MMI} is wavelength dependent, because the beat length depends on the difference in propagation constants between successive pairs of modes, which depend on the wavelength of the source [1]. Equation (1) is used to determine a correct length of MMI region. L_{π} is defined as the beat length of the first two modes. L is L_{π}/N , where N is number of channels, λ_0 is central wavelength, n_f is effective refractive index and W_{MMI} is width of MMI region.

$$L_{\pi} = \frac{4n_f \cdot W_{MMI}^2}{3 \cdot \lambda_0} \quad (1)$$

Note that this simple model assumes that the modal fields are zero at the side-wall. This error can be partly compensated by using an effective index and effective width. But, strictly speaking, effective index and effective width will vary with mode number [2].

III. FABRICATION

A. Low index contrast waveguides

Si-doped silica-on-silicon waveguides with low refractive index contrast are fabricated with combination plasma enhanced chemical vapor deposition (PECVD) and reactive ion etching (RIE) technique. The fabrication process consists of five steps which are graphically described in Fig. 2. The first step is wet oxidation of the silicon wafer forming a thick silica buffer layer (with refractive index n_{cl}). PECVD creates the doped SiO_2 active layer (*core*) with refractive index (n_c) higher than the refractive index of the cladding. Optical lithography and dry etching define then the waveguide structure. In the lithography process the wafer photoresist is applied and it is exposed. Waveguide structure is transferred from mask into the photoresist. Photoresist is developed and the core is etched by RIE. The rest of the photoresist is then striped. The growth of upper cladding (co-doped silica) with the refractive index matching the lower cladding, n_{cl} is the last technological step [3].

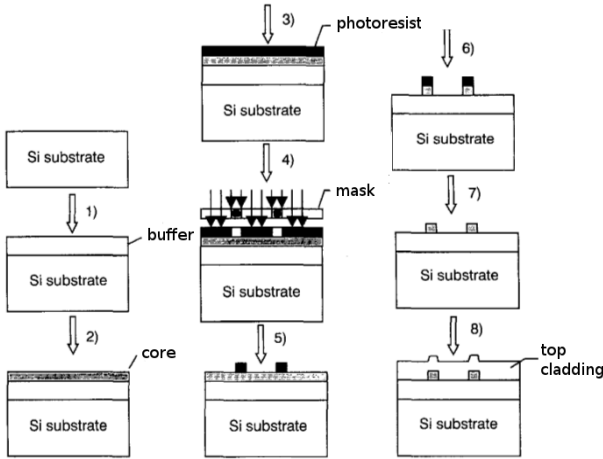


Fig. 2. Fabrication steps for a rib silica-on-silicon waveguide.

1. buffer layer growth, 2. core layer deposition, 3.-5. photolithography,
6. core layer etching, 7. stripping of photoresist,
8. top-cladding layer deposition [3]

B. High index contrast waveguides

The fabrication of the silicon-on-insulator (SOI) waveguide is relatively simple in comparison to the fabrication of silica-on-silicon waveguides. There are some important steps like creating a mask, etching the silicon and cladding oxide deposition. Structure is protected by mask until the Si is etched. Mask consists of SiO_2 . Deposition of SiO_2 is made by low temperature oxide (LTO) process in a low pressure chemical vapor deposition (LPCVD) furnace. Template of waveguide is transferred to oxide mask by photolithography. Dry oxide etching is used in parallel-plate plasma etcher. Silicon is etched using inductively coupled plasma (ICP) type reactive ion etcher provided by surface technology systems (STS). Etching process is used as a modification of the STS advanced silicon etches (ASE) process. The etching and passivation gases are SF_6 and C_4H_8 , respectively. Continuous passivation is way to obtain extremely smooth etched sidewall. The flow rate of passivation gas is linearly increased as the etching reached deeper. The Si etch rate is around 440 nm/min in ICP etching. The etching process is figured in Fig. 3 [4].

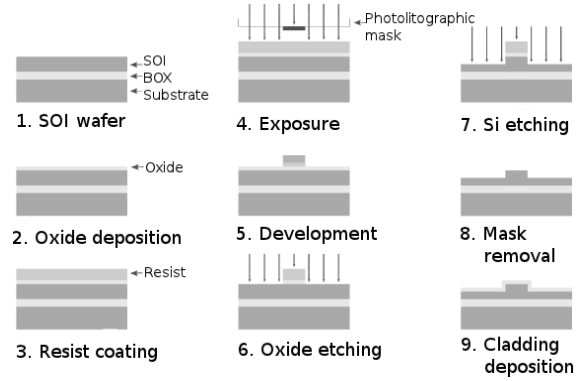


Fig. 3. Fabrication steps for a rib SOI waveguide [4].

IV. DESIGN OF MMI SPLITTERS

We have designed two 1×16 MMI splitters: low index MMI with the index contrast $\Delta n = 0.75\%$ and high index MMI with the index contrast $\Delta n = 58.9\%$.

As a first step the waveguide structure was designed. Both splitters were designed with step-profile index contrast materials system. As a next step the MMI structure was created. The structure of MMI splitter consists of input waveguide, MMI region and $N=16$ output waveguides. The used design parameters for both, the waveguide and for the MMI structure are listed in Tab 1. After the MMI structure was created, pathways and monitors were configured for the analysis.

TABLE I
DESIGN PARAMETERS OF MMI SPLITTER STRUCTURE

Variable	Value – low index contrast	Value – high index contrast
Simulation Tool	BeamPROP	BeamPROP
Model Dimension	3D	3D
Free Space Wavelength	1.55 μm	1.55 μm
Background Index	1.444	1.4472
Index Difference	0.011	2.074
Waveguide Width	6 μm	0.9 μm
Waveguide Height	6 μm	0.38 μm
L_{MMI}	2300 μm	120.5 μm
W_{MMI}	192 μm	28.8 μm
L_{in}	200 μm	10 μm
L_{out}	200 μm	10 μm

Description: L_{MMI} – MMI segment length, W_{MMI} – MMI segment width, L_{in} – input waveguide length, L_{out} – output waveguide length

Optimal length of MMI region L_{MMI} was determined through the simulation. It is the length where sixteen bright spots in the MMI splitter cross-section were obtained in one line. The output of the simulation is the field distribution having 16 split output signals.

Design and simulation software

The MMI splitter was designed in Rsoft CAD environment, which allows the user to define the material properties and structural geometry of a device. All simulations are performed in Beam PROP simulation engine. It is part of the Rsoft Photonic Suite, and is based on advanced finite-difference beam propagation (BMP) techniques. It is fully integrated into the Rsoft CAD environment.

V. RESULTS AND DISCUSSION

A. MMI splitter structure

The design and simulation of low index MMI splitter is shown on Fig. 4. The width of the MMI region $W_{MMI} = 192 \mu\text{m}$ and the length $L_{MMI} = 2300 \mu\text{m}$. The structure of the input/output waveguides is $6 \mu\text{m} \times 6 \mu\text{m}$ (see Table 1).

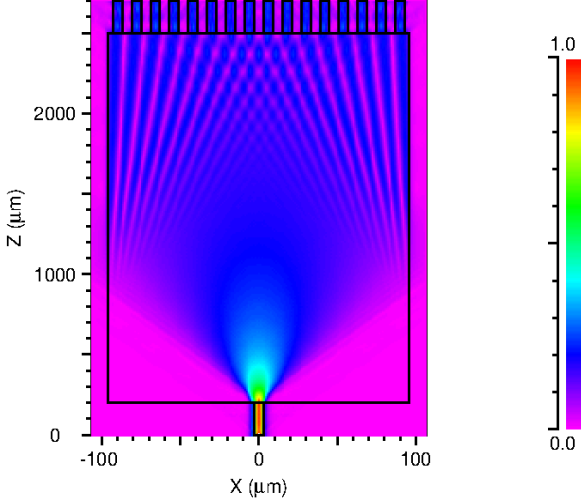


Fig. 4. Design and simulation of low index MMI splitter with 16 output waveguides.

The design and simulation of high index MMI splitter is shown on Fig. 5. The splitter consists of MMI region, which is only $28.8 \mu\text{m}$ wide (W_{MMI}) and $120.5 \mu\text{m}$ long (L_{MMI}). The structure of the input/output waveguides is $0.9 \mu\text{m} \times 0.38 \mu\text{m}$ (see Table 1).

From the Table 1 can be seen that the structure of the MMI splitter designed with a low refractive index contrast is almost seven times wider and almost fifteen times higher than the structure of the MMI splitter designed with a high refractive index contrast. Also the waveguide structure used in the high index MMI splitter design is much smaller than the waveguide structure used in the low index MMI splitter design (it was designed to keep the single mode). Small dimensions are important for better integration in optical integrated circuits.

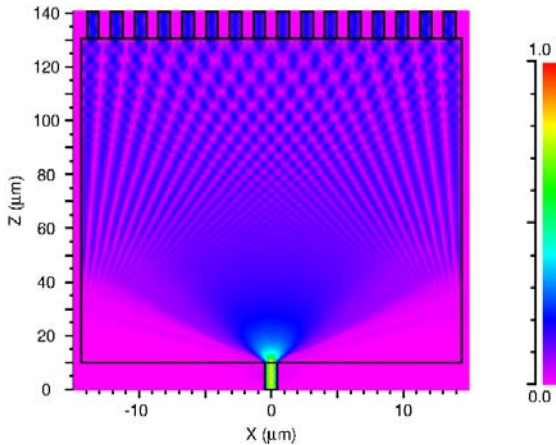


Fig. 5. Design and simulation of high index MMI splitter with 16 output waveguides.

B. Insertion loss

The simulated insertion losses are different for each design. Coupling losses in high index MMI splitter are higher than coupling losses in the low index MMI splitter because it is much more difficult to couple optical power into such small cross-section waveguide. Therefore the insertion losses in the output waveguides of the high index MMI splitter are higher than the insertion losses in the output waveguides of the low index MMI splitter. The Fig. 6 shows the level of optical power in the output waveguides of low index contrast MMI splitter. Fig. 7 shows the case of the high index design. From both figures can be seen that the insertion losses are about 1 dB higher than 12 dB (that is a typical reduction in optical power for 1x16 optical splitter).

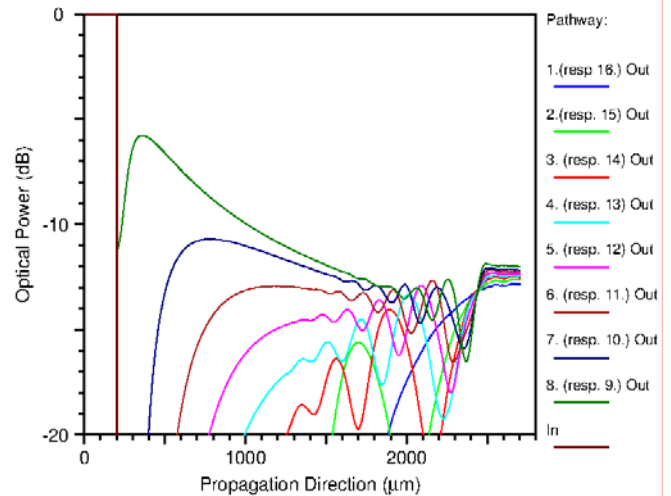


Fig. 6. Level of optical power in channels of low index MMI splitter.

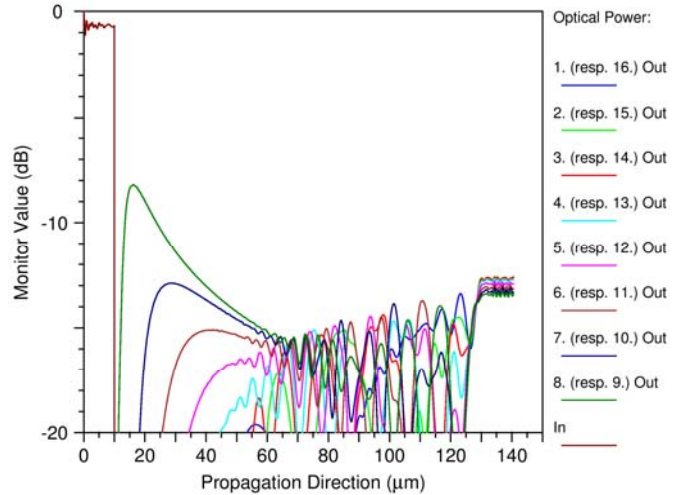


Fig. 7. Level of optical power in channels in MMI splitter designed on a high refractive index contrast.

C. Output power dependence on the input wavelength

The main disadvantage of MMI splitters results from the fact that the length of the multimode section is wavelength dependent, i.e. the MMI splitters are designed solely for one wavelength and can only operate in a narrow wavelength region. This dependence is shown in Fig. 8 for both designs. As can be seen the high index MMI splitter is more

depended on the input wavelength and also features higher insertion losses (caused by higher coupling losses ≈ 1 dB).

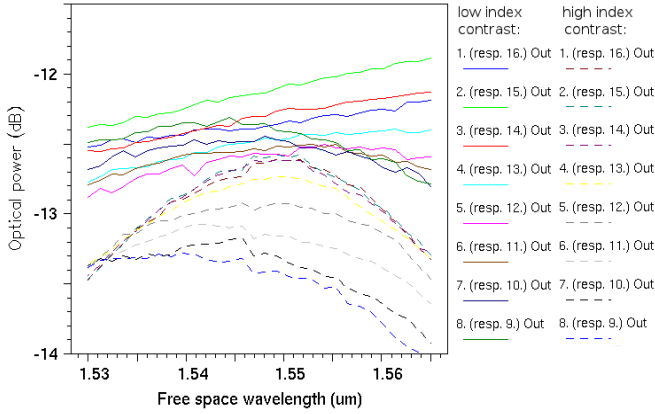


Fig. 8. Output power dependence on input wavelength
Continuous line – low refractive index contrast
Dashed line – high refractive index contrast

D. MMI splitters with 127μm output waveguide spacing

For telecom applications where MMI splitter has to be packaged and pigtailed with single mode optical fibers the output waveguide spacing is required 127 μm. High refractive index contrast is allowed to use bends with smaller radius without extra insertion losses. Output waveguide can be shorter and losses are lower. Equation (2) is used for determination an optical losses expressed in dB/cm.

$$a[dB/cm] = 10 \times \log \frac{P_{L1cm}}{P_{L0cm}} \quad (2)$$

In Fig. 9 and Fig. 10 the optical power is expressed in dB and optical losses are about 0.01 dB/cm and 0.18 dB/cm for design with low refractive index contrast and with high refractive index contrast respectively.

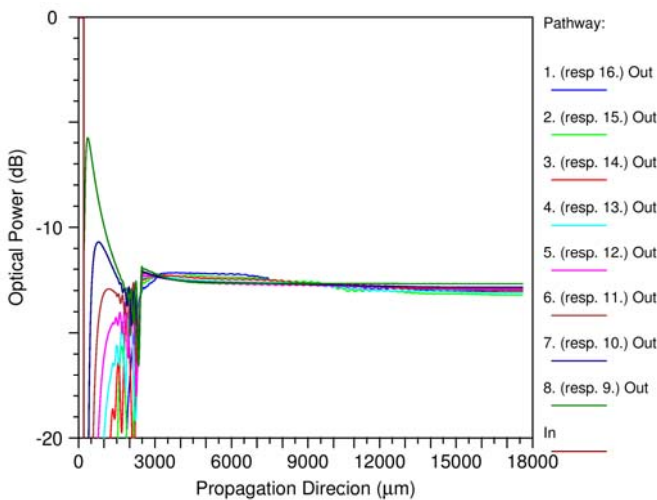


Fig. 9. Level of optical power in channels in MMI splitter designed with low refractive index contrast with 127 μm output waveguide spacing.

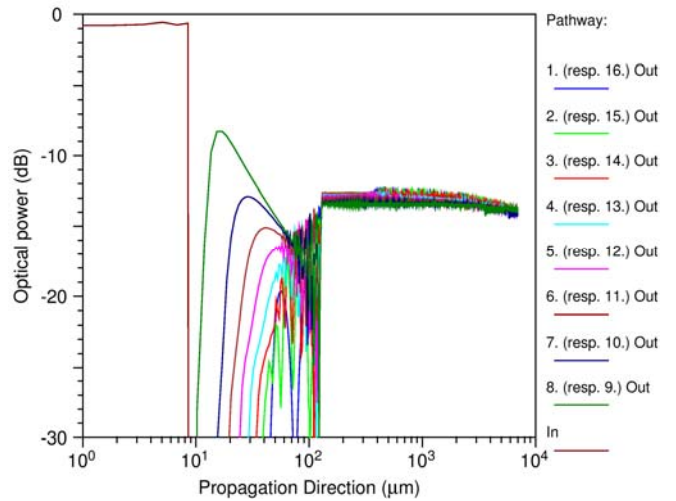


Fig. 10. Level of optical power in channels in MMI splitter designed with high refractive index contrast with 127μm output waveguide spacing.

VI. CONCLUSION

In this paper we presented the designs of two, low index and high index, 1x16 channel MMI splitters. The simulation results show that the high index contrast MMI splitter is more suitable for photonics integration circuit although it has higher insertion losses. These losses are not critical in photonics integrated circuit where distances are in order 100 μm.

The low refractive index contrast MMI is more useful for division optical power between optical fibers. This design is less depended on input wavelength. This is preferred in telecommunication applications.

ACKNOWLEDGMENT

This work was supported by projects No. 1/0787/09 of VEGA grant agency of Slovak Ministry of education and APVV-0424-10, APVV-0262-10, SK-AT-0010-10 from Slovak research and development agency of Slovak Ministry of education and SK 13/2011 from Austrian Agency for International Cooperation in Education and Research (OeAD-GmbH).

REFERENCES

- [1] J. A. Besley, J. D. Love, and W. Langer, "A multimode planar power splitter (Periodical style)," in *Journal of lightwave technology*, vol. 16, no. 4, pp. 678–684, April 1998.
- [2] L. Cahill, "The modelling of MMI Devices," in *2006 ICTON Conf.*, pp. 138-141.
- [3] H. Ou, "Different index contrast silica-on-silicon waveguides by PECVD (Periodical style)," *IEEE Electronics Letters*, vol. 39 no. 2, pp. 212–213, Jan. 2003.
- [4] J. Williams, "Fabrication of microphotonic waveguide components on silicon (Thesis or Dissertation style)," Ph.D. dissertation, Dept. of Elect. and Com. Eng., Helsinki Univ., Espoo, April 2007.

Investigation on RSOA-based long reach WDM PONs

P. Horňák

*Institute of Electronics and Photonics, Faculty of Electrical Engineering and Information Technology,
Slovak University of Technology in Bratislava*

Abstract— The main focus of this paper is to provide up-to-date information on the state-of-the-art of wavelength division multiplexed passive optical networks and results of our recent research activities aimed at extending the FTTx platforms over large areas. In addition, the paper provides a draft version of an analytical model of the WDM PON access network and some experimental results. Currently, the reflective semiconductor optical amplifier-based WDM PONs seem to be the most promising method how to extend the reach of WDM PON access networks. Implementation of this method can be done by employing the RSOAs in Optical Network Units (ONUs) where they re-modulate and re-amplify the downlink signals and send them back in the uplink direction. In this way it is possible to extend the operating range and increase the transmission distance over 100 km without using any additional in-line optical amplifiers .

Index Terms— WDM PON, Long Reach, Reflective SOA, Access Networks, FTTx

I. INTRODUCTION

Since the last decade, a lot of research activities in optical communications were devoted to FTTx access networks (where X can mean the home, curb, cabinet, building etc.). The FTTx platform is a very attractive solution for provisioning different broadband services to subscribers. The Internet traffic has multiplied over the last few years mainly due to IP-based video services such as IPTV, video streaming, etc. As a result, access networks are required enabling data transmission at higher bit rates and with low latency over longer reach. In order to fulfill all these requirements as well as the end user needs, it is necessary to find some cost-effective solutions. Utilization of wavelength division multiplexing in passive optical networks is a promising solution to meet the requirements.

WDM PONs are considered as the final solution for new generation of access networks since they provide almost unbounded bandwidth and bit rate transparency for each end user. WDM PONs also offer greater security and protocol end-to-end connectivity on a per-wavelength basis. However, current solutions are still too expensive for massive deployment and operation mainly due to the high cost of the relevant components in the ONUs and OLTs. For that reason the economical model for a densely penetrated WDM PON

has not been justified yet.

II. STATE OF THE ART

Optical access networks (FTTx) present the basis of the broadband infrastructure and comprise its last section (last mile) connecting the end users. These networks are the bottleneck of the communication networks. Their development is the most demanding process in building the broadband telecommunication infrastructure.[2] From the WDM PON access network point of view, this requires certain replacement of current architecture in all legacy systems, for example, the replacement of optical power splitters by arrayed waveguide gratings (AWGs). ONUs in WDM PON require new transmitters working on different wavelengths, thus a good option is to use colorless ONUs either with tunable lasers or RSOAs (Reflective Semiconductor Optical Amplifier). However, the price of currently available RSOAs is one order of magnitude higher than the price of an entire (EPON based) ONU. The tunable lasers may be more expensive. A WDM PON with cascaded TDM PON (hybrid PON) can dynamically allocate unused bandwidth from one ONU to other ONUs.[6]

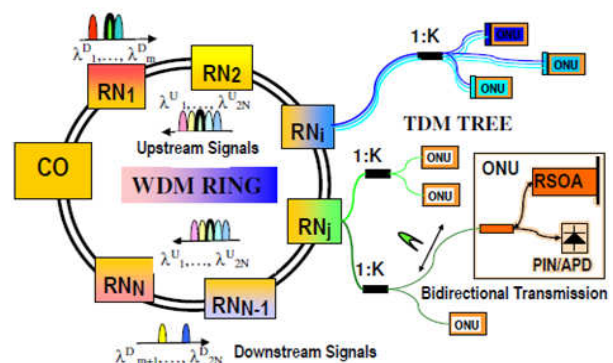


Fig. 1. Example of a long reach WDM/TDM hybrid PON utilizing a WDM ring, TDM trees and reflective SOAs in Optical Network Units [4]

Addition of a splitter in one or more fiber drops allows time sharing of the dedicated wavelengths among some ONUs in the PON branches, which can significantly increase the

maximum number of ONUs and accommodate more subscribers over a relatively wide geographical area. This solution also allows extension of passive optical access networks. One of the promising solutions for such a long reach WDM PON seems to be implementation of reflective semiconductor optical amplifiers (RSOAs) in ONUs that simultaneously re-modulate and re-amplify the downlink continual laser light wave carrying the downlink signals for uplink transmissions. The RSOA-based WDM PONs have the potential to increase transmission distances over 100 km without using any additional in-line optical amplifiers (EDFAs)[1]. The next chapter deals in more detail with the basic principles of RSOA-based WDM Passive Optical Networks.

III. PRINCIPLE OF RSOA-BASED WDM PONs

Exploitation of loop-back architecture

The RSOA-based WDM PON are mostly configured as the so called loop-back architecture for colorless operation in ONUs. The seed light, which is transmitted from the central office (CO) side, is then detected, modulated and amplified by the RSOA on the ONU side in one step (with a switching time in the ns range), therefore, the need for additional amplification is to a large extent reduced. Furthermore, the wide amplification bandwidth of RSOAs provides wavelength independency of the ONUs, where the light is finally reflected at the end facet of the RSOAs and afterwards sent back to the OLTs in the CO modulated with the uplink data. From this point of view, we can distinguish two main approaches to realization of WDM PONs both leading to the use one single wavelength

- WDM PONs with seeded reflective transmitters
- WDM PONs with wavelength re-use.

In the first approach, the injection seeding with separated uplink and downlink bands, where the optical carriers are remotely generated and then distributed to the ONUs Here, the RSOAs can be used to modulate the uplink signal. In the second approach, each downlink wavelength is amplified and re-used to handle the uplink traffic. This should be performed on the same fiber to avoid the downlink and uplink interference

A. WDM PON with seeded reflective transmitters

The light sources used for seeding the reflective transmitters (transmitter arrays) are based on Multi-Frequency Lasers (MFLs). Compared to spectrally sliced broadband sources like ASE sources or LEDs, MFLs have the advantage of higher power levels which translates to longer reach performance. The seed light is spectrally separated and each wavelength is injected into the corresponding OLT transmitter (RSOA or Reflective Electro-Absorption Modulator - REAM). The PON

shown in Figure 2 is based on two MFLs, one for seeding a reflective transmitter array in the OLT, and the second MFL for seeding the ONUs. In a simplified implementation these MFLs can work in two different wavelength bands, e.g., in C-band and L-band. [5]

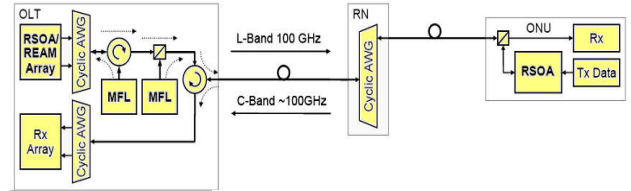


Fig. 2. WDM PON with seeded reflective (RSOA/REAM) OLT transceiver array and seeded reflective ONU based on RSOA

The downlink data are transmitted to ONU receivers through two circulators, a feeder fiber, and a remote wavelength filter. The downlink optical signal injected into the RSOA in a ONU is utilized as the seed light with the aid of a special electrical circuit for the RSOA, where the intensity modulated downlink light is transformed into the uplink light, which is in turn modulated with uplink data, and then transmitted to the OLT receiver over the same optical path as the downlink. Hence, as the uplink wavelength is identical with the downlink wavelength, there is no need of the cyclic wavelength function for the WDM filters neither in the OLT nor in the remote node (RN). The transceiver employs the RSOA as a colorless transmitter and a specially designed electric receiver circuit to be able to receive the downlink optical signal in the ONU with a large noisy logic 1-level, both of which provide high quality, high performance and cost effective transceiver functions. In order to significantly increase the maximum reach of the WDM PON with seeded ONU, the use of dedicated seed fibers has been proposed. These dedicated fibers can run all the way down to ONUs (end-to-end) or they can be used between the OLT and the RN only. Provisioning of end-to-end seed fibers has the advantage of complete elimination of the Rayleigh crosstalk.

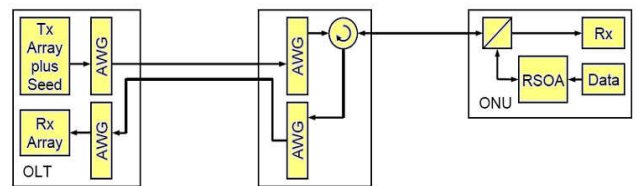


Fig. 3. Decrease of Rayleigh crosstalk through use of dedicated upstream feeder fiber

Another example of a high performance seeded PON is based on an active remote node together with hybrid WDM/TDM PON architecture for wavelength sharing. This variant is called Super PON (sometimes also called L-R PON) and is also usable for longer reach as well as for increasing the splitting ratio of splitters. As a consequence of using an active remote node, this architecture is not considered as pure passive optical network. Nevertheless, by employing in-line

amplifiers it would be possible to span distances over 100 km (e.g. 90 km of feeder fiber and 10 km of distribution fiber). Furthermore, in combination with wavelength division multiplexing, this allows to connect hundreds of subscribers to one access network. For achieving higher sensitivity of receivers in ONU/ONTs it will become necessary to supersede the currently often used PIN detectors by avalanche photo diodes. Such a combination with very long reach and very high user count could be cost effectively achieved only with the help of employing active components in the optical distribution network. For this purpose, the use of R-P EDFA (Remotely-Pumped Erbium-Doped Fibers Amplifier) and RSOAs are considered. Also implementation of colorless transmitters at ONUs is all important in this case. The above mentioned use of RSOAs is also one of the possible solutions for data transmission at rates of 1.25 Gbit/s or 2.5 Gbit/s .

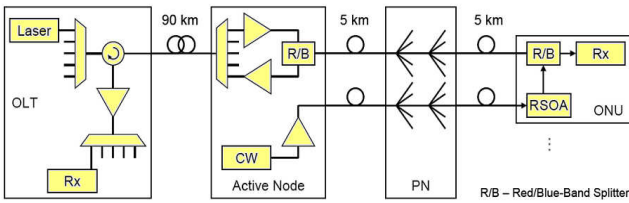


Fig. 4. An example of Super PON (L-R PON) with active remote node

B. WDM PON with wavelength re-use

A WDM PON system, where each ONU is served by a single wavelength, allows to increase the network capacity and to simplify the network management since all the connections are point-to-point. In addition, implementation of colorless ONUs allows centralizing the wavelength management, enabling further architectural simplification and cost savings. In this way, the downlink wavelengths are reused in the uplinks, that is, wavelength bi-directional channels are created thus doubling the system capacity. Such wavelength re-use requires the downlink modulation to be cancelled before applying the uplink data on the wavelength. This leads to additional penalty to the uplink signal caused by the residual downlink modulation and optical reflections arising along the optical fiber link. [5]

Availability of broadband multi-wavelength sources, athermal AWGs and reflective SOAs enabling wide band amplification and operations at rates up to 2.5Gb/s opens the way to practical deployment of WDM PONs based on colorless reflective ONUs. However, in order to provide full re-modulation of the downlink traffic, the RSOAs must operate in a saturation regime. In an ONU, part of the downlink signal is tapped and sent to the RSOA. If the power of the tapped signal is sufficiently high, the RSOA is saturated, thus cleaning the downlink modulation. The uplink data can then be applied to the RSOA's electrical input with only a small penalty due to the residual modulation. In practice, the input power needed to saturate the RSOAs limits the achievable power budget in practical systems.[3]

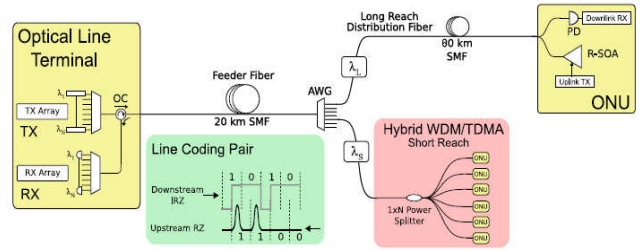


Fig. 5. WDM PON architecture with IRZ/RZ coding [1]

The use of Inverse Return-to-Zero (IRZ) optical line coding for the downlink and of the Non-Return-to-Zero (NRZ) coding for the uplink allows performance improvement in comparison to the saturated RSOA without using any additional optical components resulting in remarkable cost reduction. The downlink signal is coded 50% IRZ and the RZ uplink signal is shifted by half a bit in time with respect to the downlink IRZ. The use of 50% IRZ in the downlink and of RZ coding in the uplink signal results not only in symmetrical bandwidth. In addition, the RSOAs can operate far from the saturation regime, thus relaxing the constraints on the ONUs' received power. By using this technique, re-modulation with full downlink signal modulation erasure by seeding the RSOAs with power levels as low as -35 dBm average power over an extended reach of 100 km, with no in-line amplification, can be achieved. The PON power budget is then improved without increasing the operational expenses associated with in-line amplification. This technique may also be used to increase the power splitting ratio in the hybrid WDM/TDM PONs (allowing to serve more than one user on a single wavelength). Optionally, these two solutions may be implemented simultaneously in the same WDM PON on different wavelengths.[5]

IV. ANALYTICAL MODEL OF WDM PONS

Figure 6 depicts an analytical model of the WDM PON access network. Its topology consists of three main parts: OLTs, ODN and ONUs. For transmission, frequencies of 193,1 THz (for downlink) and 193,2 THz (for uplink) are used modulated at 2.5 Gbit/s transmission bit rate. The network is designed only for one end user in order to simplify its structure as much as possible.

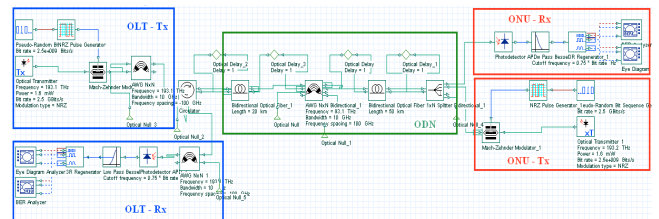


Fig. 6. Analytical model of WDM PON access network: blue part (OLT), green part (ODN), red part (ONU)

Optical Line Terminal - OLT

The OLT is realized by splitting the receiving and the transmitting parts. The transmitting part consists of a WDM transmitter block sending a Pseudo Random Bit Sequence (PRBS) to the Non-Return to Zero (NRZ) pulse generator. The optical transmitter has the following parameters: Optical power = 1.6 mW, optical frequency = 193.1 THz, the channel grid spacing is 200 GHz.

The receiving part consists of an avalanche photo diode (APD) acting as a photo detector, low pass Bessel filter and a 3R regenerator. A BER analyzer is used for measuring the level of the received signal and the eye diagram.

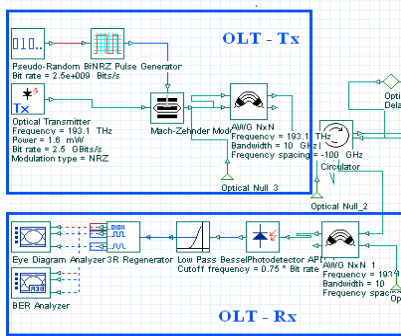


Fig. 7. A block diagram of Optical Line Terminal with its transmitting and receiving parts

Optical Distribution Network - ODN

The optical distribution network is based on a 2x2 bidirectional AWG de/multiplexor, which in this case represents the remote node. A bidirectional SMF feeder fiber with fiber length of 20 km and attenuation equal to 0.2 dB/km is used for connecting the AWG de/multiplexor to the OLT. In order to draw comparison between 50 km and 100km transmission distance, the distribution fiber link consists first of 30 km long bidirectional SMF section followed by a 80 km long fiber section. The transmission frequency used on both fibers is set to 193.1 THz. At the end of the ODN a bidirectional passive optical splitter section is placed which distributes the downlink signal to the ONU and counter-propagates the uplink signal to the OLT.

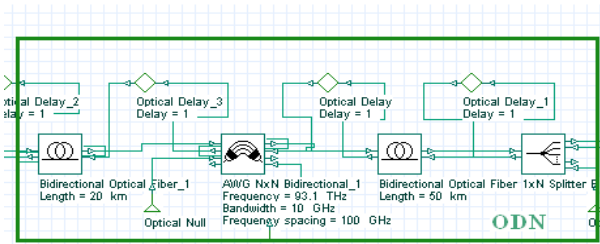


Fig. 8. Block diagram of Optical Distribution Network with AWG as remote node

Optical Network Unit - ONU

The ONU is realized in the same way as the OLT, so the receiving and transmitting part are separated from each other. The only difference here is that the frequency is set to 193.2 THz (the channel grid spacing remains 200 GHz). A BER analyzer producing also eye diagrams is used as a measuring device.

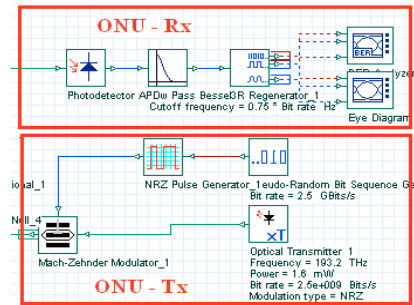


Fig. 9. A block diagram of Optical Network Unit with its transmitting and receiving part

Figure 10 presents a comparison of the final eye diagrams at the ONU side. The first diagram characterizes the WDM PON with total reach of 50 km consisting of 20 km feeder fiber and of 30 km distribution fiber. The second diagram applies to the WDM PON with total reach of 100 km consisting of a 20 km long feeder fiber and of 80 km long distribution fiber. The results show a significant change in the level of the received signal, since the BER value increased by three orders of magnitude from 2.501×10^{-10} (50 km reach) to 4.058×10^{-7} (for 100 km reach).

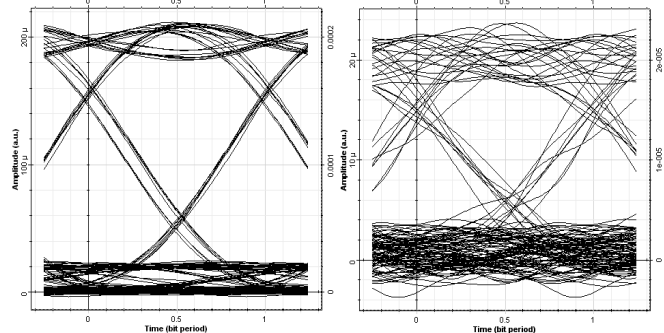


Fig. 10. Comparison of eye diagrams for 50 km long WDM PON (left diagram) and 100 km long WDM PON (right diagram)

V. CONCLUSION

In this paper we focused on providing evidence that the WDM PON networks are the most cost-effective solution for developing FTTx broadband access networks in the near future. Although this technology has not been standardized yet, neither has its economical model been justified, such access networks will most likely be able to provide dedicated bandwidth more than 100 Mbit/s per subscriber over a pretty

wide geographical area. To provide even higher bandwidth and greater coverage, the RSOA based WDM PON access networks are intended for implementation mainly due to their ability to re-modulate and re-amplify the downlink signal simultaneously in the ONUs. The RSOA-based WDM PONs are mostly configured in the loop-back architecture with two main approaches: with seeded reflective transmitters and with wavelength re-use. These solutions are suited for operations in new generation networks with ultra long reach but also in hybrid WDM/TDMA PON with high power splitting ratio. Finally the draft of WDM PON access network is depicted, where the whole topology, main blocks and parameters are described. As a result, the final eye diagrams for 50 km and 100 km WDM PON network are shown in order to compare results obtained for these two transmission distances. However, the analytical model used in this paper applies to WDM PONs without RSOAs. To achieve significantly better transmission parameters, RSOAs have to be employed on the ONU side.

REFERENCES

- [1] P. Horňák, "Súčasný prieskum WDM PON založených na RSOA pre prístupové siete s dlhým dosahom," OK2010 Praha, October 2010.
- [2] P. Horňák, "Analytický model WDM pasívnej optickej prístupovej siete," FEI STU Bratislava, March 2011.
- [3] M. Presi, R. Proietti, K. Prince, G. Contestabile, E. Ciaramella, "A 80 km Reach Fully Passive WDM-PON based on Reflective ONUs, Optical Society of America (2008)
- [4] L. Sandstrom, "Advances in Next Generation FTTH: WDM Enables Optical Technologies," ADTRAN, 2010.
- [5] OASE, "Survey of Next-Generation Optical Access System," OASE WP4 D4.1, October 2010.
- [6] M. De Andrade, G. Kramer, L. Wosinska, J. Chen, S. Salent, B. Mukherjee, "Evaluating Strategies for Evolution of Passive Optical Networks," University of California, Davis, USA; Broadcom Corporation, USA; Royal Institute of Technology, Sweden; Universita Politecnica de Catalunya, Spain; November 2010.

Possibilities of Upstream Data Eavesdropping in Passive Optical Networks

Petr Jareš, Pavel Lafata

Czech Technical University in Prague, Faculty of Electrical Engineering, Department of Telecommunication Engineering, Czech Republic

Abstract—Passive optical networks represent a promising solution for modern access networks that could meet the increasing requirements of transmission rate for demanding multimedia services. The essential component of optical distribution networks is a passive optical splitter, which is used to split optical signals. The downstream traffic in passive optical networks is based on broadcasting the entire signal to all optical network units, therefore, it is necessary to provide a robust and complex data encryption to prevent their eavesdropping and misusing by an unauthorized person. On the other hand, the upstream traffic represents a simple burst mode with the system of reserved transmission intervals (windows) to exclude collisions between data transmitted by each optical network unit. It is assumed that upstream traffic due to the passive optical splitters can propagate only between a specific optical network unit and the central optical line termination. Therefore, the passive optical network in the upstream direction is a point-to-point network and it is not necessary to encrypt transmitted data at all. However, due to the reflections on various interfaces (connectors, splices, splitters) and in several specific situations, the upstream traffic can be passively eavesdropped and it could be possible to obtain transmitted upstream data of neighbor users. In this article, the possibilities of upstream traffic eavesdropping under certain specific conditions are investigated. In addition, several measurements were carried out on a real passive optical network.

Index Terms—Eavesdropping, Optical Return Loss, Passive Optical Network, Splitter, Upstream Monitoring.

I. INTRODUCTION

NOWADAYS, the passive optical networks (PONs) are widely deployed as a modern solution for access telecommunication networks, as they provide fast and reliable network connection mainly for households, business centers, offices and for industrial applications. The current generation of PON networks uses TDMA (Time Division Multiple Access) together with WDD (Wavelength Division Duplex) duplex method for sharing the optical fibers among all active users in both transmission directions. The character of transmission in the downstream direction is based on broadcasting of multiframe containing all time slots, therefore, it needs to be encrypted and protected against eavesdropping. On the other hand, the upstream traffic is carried out as a point-point communication being transmitted exclusively between each optical network unit (ONU) and the optical link termination (OLT). Therefore, it is not necessary

to provide any encryption of the upstream traffic, so even the system and management messages are not encrypted and protected [1].

The optical distribution network (ODN), which ensures the connection of all optical units and contains optical fibers, splices, connectors, passive filters and splitters, is completely passive with no power consumption nor management and controlling mechanisms. The process of optical beam splitting is purely passive thanks to the passive optical splitters. These splitters consist of simple Y-junctions, which are cascaded to realize a desired splitting ratio. The Y-junctions can be realized either by fusing short fibers together, or by using a planar technology. There are several important parameters and characteristics, which each passive splitter must meet. One of them is the optical return loss (ORL) and a directivity, which defines the attenuation of a misdirected optical beam in dB.

As described in the text above, in perfect ODN network with ideal splitters it is assumed that the upstream traffic of a particular ONU cannot be obtained by any other ONU due to the high directionality of all optical components used in ODN, especially of passive splitters. Theoretically, no ONU should be able to detect the upstream traffic of neighboring ONUs, which would make the upstream completely secure from eavesdropping and therefore it would not require any encryption. Moreover, the complete immunity of upstream traffic makes it an ideal and secure medium for exchanging the encryption keys, which are subsequently used to encrypt downstream traffic from the OLT individually for each ONU.

However, the perfect directionality of passive components, especially passive splitters, is usually questionable in practice. There have been several cases already reported by network operators and PON providers, that the reflections and directionality are not so perfect in practice mainly by dirty connectors and splitters or excessive bending of optical cables and patchcords. From experience described in [2] it follows that dirty connectors affecting the transmissions and quality of services can be often found in real optical access infrastructure.

But the most serious impact of such dirty connectors could result in reflections of the upstream optical beams. Since the ORL of used connectors and directivity of passive splitters might not be perfect, it would be possible to have situations, where the reflections in the upstream direction are big enough

for a malicious ONU to obtain the traffic of a victim ONU, but not big enough to prevent the upstream transmission from passing through, making the situation undetectable for the network operator [3]. Moreover, the malicious ONU could eventually obtain the encryption keys and be able to decrypt the downstream transmission of a victim ONU, as well.

Therefore, several measurements and practical tests were performed to discover, if such situation is possible to emerge and if so, under what conditions. Tests were made in our EPON laboratory (Ethernet PON network) with the use of various passive splitters, fibers and optical spectrometers and power meters to explore and describe this situation.

II. PRACTICAL MEASUREMENTS AND RESULTS

First, optical components in our laboratory workplace were used to create a simple PON infrastructure. While there are several minimum and maximum limits of attenuation, ORL and other parameters, which the ODN must meet for correct operation of PON, for testing optical fiber with the length of 1.6 km, several short optical patchcords with SC/APC connectors, PLC optical splitter (planar), fused optical splitter and optical spectrometer were chosen. The resulting test optical distribution network is presented in Fig. 1.

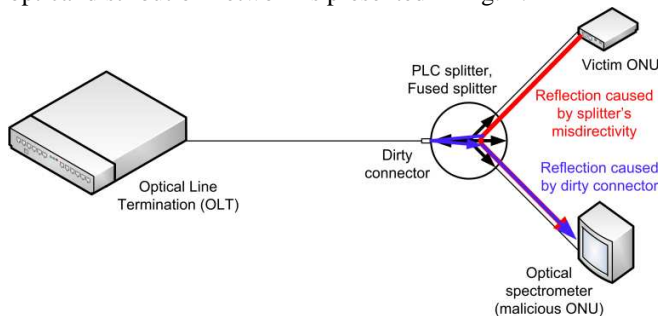


Fig. 1. Experimental workplace of EPON for analyzing possible reflections in the upstream ONU traffic.

The first measurement was performed with standard PLC passive optical splitter with the splitting ratio 1:2. The output connector of the splitter was soiled to increase the reflections. We tried to simulate the situation from practical applications of optical cables and patchcords, which can be possibly soiled usually by a dust and human fingerprints due to their frequent usage. The connector we used in our experiment is a SC/APC type on the splitter's side and SC/PC on OLT's and ONU's side. This scenario is given by the connector types used by the manufacturers of used optical components. The APC connector has usually higher ORL in practice and the results of our measurements could be slightly different if we use only SC/APC connectors. This is one of the possible future tasks in our research. According to the datasheet, the directivity of the splitter should be better than 55 dB and the return loss better than 55 dB. Fig. 2 presents the results that were obtained from an optical spectrometer.

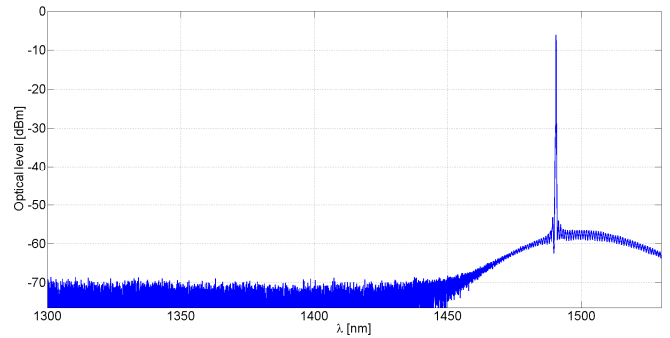


Fig. 2. The results of reflection measurement on a PLC passive splitter.

It is obvious that the PLC splitter has a good directivity and even the reflections caused by the dirty connector are not detectable (the level of optical noise is lower than -70 dBm). The same measurements were performed also with a fused type of passive splitter. These splitters contain short optical fibers fused together. Their parameters of directivity and ORL are typically worse in comparison with PLC splitters.

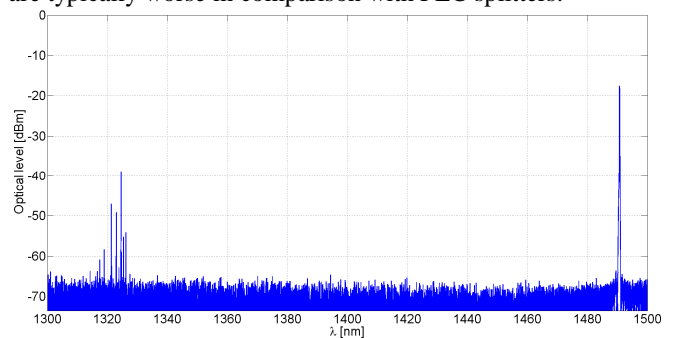


Fig. 3. Reflections detected in upstream transmission in case of using a fused optical splitter.

As opposed to the first measurement, there are several detectable reflections of the upstream traffic from a fused optical splitter. They are caused by the worse splitter's directivity together with the reflections caused by a dirty optical connector. Their optical level is not enough for a malicious ONU to be able to obtain victim's data in this case, however, by using appropriate optical amplifier (e.g. SOA amplifier) their optical level could be enhanced thus making the reflections readable.

The results described above clearly illustrate that in case of using fused passive splitters, the upstream traffic of neighboring ONUs can be detected. This can subsequently result in a potentially dangerous situation, because the upstream traffic also contains encryption keys used for downstream transmission.

III. CONCLUSION

This paper presented investigation of possible upstream data eavesdropping by exploiting reflections caused by dirty optical connectors (interfaces) and passive splitters with lower directivity. The results demonstrate that using the fused type of passive splitters in PONs can cause a potential risk of possible upstream traffic eavesdropping, whereas the modern PLC splitters with high directivity offer a good immunity to

potential reflections and passive eavesdropping. The upstream traffic also usually contains encryption keys for a downstream transmission thus this threat should be taken seriously.

ACKNOWLEDGMENT

The work presented in this paper was supported by the grant No. VG20102015053 - The modern structure of photonic sensors and new innovative principles for intrusion detection systems, integrity and protection of critical infrastructure (GUARDSENSE).

REFERENCES

- [1] W. Shawbaki, A. Kamal, "Security for FTTx Optical Access Networks," in *Proceedings 2006 of 31st IEEE Conference on Local Computer Networks*, pp. 221-228.
- [2] D. Gutierrez, J. Cho, L. G. Kazovsky, "TDM-PON Security Issues: Upstream Encryption is Needed," in *Conference of Optical Fiber Communication and the National Fiber Optic Engineers, 2007. OFC/NFOEC 2007*, pp. 1-3.
- [3] S.-W. Wong, W.-T. Shaw, S. Das, L. G. Kazovsky, "Enabling Security Countermeasure and Service Restoration in Passive Optical Networks," in *Global Telecommunications Conference. GLOBECOM '06. IEEE, 2006*, pp. 1-5.

Model of impairment aware routing algorithm for Generalized Multi-Protocol Label Switching

Milos Kozak, Leos Bohac

Faculty of Electrical Engineering, Department of telecommunication technology, Czech Technical University in Prague, Prague, Czech Republic

Abstract— This paper deals with impairment aware routing and wavelength assignment problem in all optical networks. It provides information about current state of the art of GMPLS impairment aware interface for patch computation. The paper gives suggestion to use OMNeT++ simulation tool for evaluation of routing and wavelength assignment problem especially in its enhanced version encompassing physical properties of fibers. The paper discusses nonexistence of models for simulations of impairment aware routing and wavelength assignment problem and thus suggests a model that could fulfill the gap. The model implementation is clearly described and mathematical evaluation of fiber model is provided. The evaluation is based on attenuation of fiber that causes optical signal to noise ratio (OSNR) and consequently bit error rate (BER) degradation. Evaluation is made using Artis OptSim simulator and OMNeT++. Measurement of BER is carried out using both simulators and results are compared. The correlation of results verifies that model is correct. The following discussion provides information about additional model extension and calculations of impairment aware routing and wavelength assignment problem for Generalized Multi-Protocol Label Switching framework.

Index Terms—Impairment aware, wavelength switching, Generalized MPLS, Simulations, OMNeT++

I. INTRODUCTION

OPTICAL communication systems are growing in importance today. It is caused by rapid growth of a variety of new services deployed onto smart mobile phones, triple play and bandwidth growth of DSL for residential, high Internet penetration and a variety of new traffic demanding services. A few years ago the penetration was so high that it was not possible to handle it by the contemporary systems and therefore some improvements were introduced. In the beginning only wavelength division multiplex (WDM) as a way for fiber multiple use was implemented but now we are facing the problem of high power consumption of transmission systems due to excessively used optical-electrical-optical (OEO) conversion [1]. These systems are point-to-point using lasers at output ports and detectors at input ports. Each laser consumes a lot of energy and the way how to make this more efficient is to use only one laser for the whole lightpath from a starting edge node to the terminating edge node of transmission systems. All optical lightpath can reduce power consumption significantly but on the other hand

it introduces a lot of new problems such as a need of wavelength switching mechanisms. In networks where interconnecting fibers are too long that fiber properties affect signal propagating routing algorithms must be extended to take these physical properties into account. Wavelength switching in WDM was at the beginning managed manually using optical add drop multiplexers (OADMs) and later by reconfigurable OADMs (ROADMs) allowing automatic lightpath setup. ROADMs allow to avoid OEO in the whole optical network. Such network is generally called an all-optical network (AON). AONs need management because the main optically switched part can transmit the light only. However, there is a variety of mechanisms used in traditional OEO based networks for management. One of the most massively used carrier grade networking framework is multi-protocol label switching (MPLS). Because of AON MPLS was extended to generalized version it does not rely on Ethernet frames and Internet Protocol (IP) packets only. The generalized version of MPLS is called GMPLS and allows switching of IP packets; Ethernet frames; time domain multiplex (TDM) frames used for voice transmission in synchronous digital hierarchy (SDH) and newly is supplemented by the Wavelength Switching Optical Network (WSO) framework allowing incorporation of ROADMs into design of GMPLS network. GMPLS enables switching and routing on first three layers of OSI reference model. Switching abilities of GMPLS are depicted on Fig. 1.

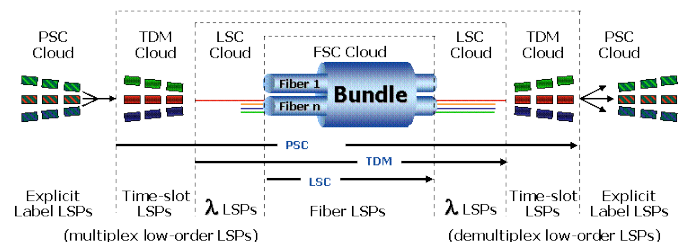


Fig. 1. GMPLS switching hierarchy.

Currently GMPLS framework does not use physical properties of fibers along the lightpath for path computation best knowledge. There are some IETF documents [2] addressing the problem of routing and wavelength assignment (RWA), IETF draft documents on the topic of impairment aware interface [3] describe three types of calculation

mechanisms taking into account impairments of optical fibers along a lightpath. GMPLS impairment aware interface [3] allows each GMPLS node to gather and keep current data about physical properties of each fiber between any of two GMPLS nodes in the AON. Based on up-to-date data each GMPLS node can calculate lightpath using impairment aware (IA) RWA [4],[5] algorithm. The reasonable way of IA-RWA evaluation is through simulations. This paper presents calculations using event driven simulator OMNeT++ which was designed and proven for simulations of complex communication systems. Simulator allows easy model deployment and tests in current systems. This way valuable feedback can be obtained.

The paper is organized as follows: Chapter 2 gives overview of current state of problem in viewpoint of simulation frameworks. Chapter 3 outlines information about simplifications made to the traditional optical simulators in the fiber model used in our simulation. Chapter 4 contains evaluation of presented fiber module. Results from the model are compared with results from Artis OptSim. Chapter 5 discusses model implementation and future extension.

II. RELATED WORK

Several algorithms for dynamic lightpath establishment have been already proposed and some simulation frameworks were used in literature but they are not publicly available. There is only one well known public available model of GMPLS node [6]. Its WSON extension is proposed in work [7]. This model uses shortest path algorithm for routing decisions and the wavelength blocking ratio is used for a calculation of network metric (1), (2). In this model, the first-fit method for the lambda election is used at each egress port. The work [7] extends metric (1) to (2), because it has a better performance but (1) is used in a case of low traffic load where it scales well.

$$w = 1 - \frac{\lambda_d}{\lambda_c} \quad (1)$$

$$w = -\log \left[1 - \left(1 - \frac{\lambda_d}{\lambda_c} \right)^{\lambda_d} \right], \quad (2)$$

where w stands for metric, λ_d stands for amount of currently available wavelengths in the fiber and λ_c stands for total amount of available wavelengths at the egress port. A number of wavelengths is given by a spectral grid. Currently GMPLS node model implementation [7] considers only wavelength constraint, but an impairment aware extension is not introduced at all. For comfortable IA-RWA evaluation in OMNeT++ a model of optical fiber is needed and the following text describes important steps verifying model relevance for further use of IA-RWA evaluation.

III. OMNET++ MODEL OBJECTIVES

Due to the existence of the mathematical description of light propagation in an optical fiber the above mentioned model can be created. In the propagation model of light in fiber a linear

and nonlinear terms that are important in WDM systems [8] will be considered, but model presented in this paper does not take into consideration a nonlinear part. A linear phenomenon like the group velocity is calculated from fiber parameters such as the core index of refraction (3).

$$t(e) = n \cdot c/e \quad (3)$$

where n stands for core index of refraction, c for velocity of light and e stands for a fiber length. Attenuation effect of a fiber is obtained from (4). Equation (4) models amplitude weakening introduced by a fiber with different length. It means that ingress signal's amplitude is decreased by a factor of α multiplied by length of the fiber.

$$\frac{\partial A}{\partial z} = -\frac{\alpha}{2} A \quad (4)$$

A is intensity of electric field and α is the fiber attenuation coefficient. Equation (4) is used for OSNR evaluation that is consequently converted into BER by (5) for on-off keying and (6) binary phase shift keying (BPSK) and quadrature phase shift keying (QPSK).

$$BER_{OOK} = \frac{1}{2} \operatorname{erfc} \left(\sqrt{\frac{\text{OSNR}}{2}} \right) \quad (5)$$

$$BER_{BPSK,QPSK} = \frac{1}{2} \operatorname{erfc}(\sqrt{\text{OSNR}}) \quad (6)$$

For general M-state quadrature amplitude modulation (QAM) model implements estimation of symbol error ratio (SER) (7). SER is not evaluated in this article.

$$SER_{QAM_m} = \left(1 - \frac{1}{\sqrt{M}} \right) \operatorname{erfc} \left(\sqrt{\frac{3}{2(M-1)} \text{OSNR}} \right) \quad (7)$$

IV. MODEL EVALUATION

The model evaluation is a three step process. It involves direct BER estimation based on (5)-(7) directly in the proposed model, verification of BER based on significantly long bit stream and Artis OptSim fiber model which is used as reference because of its accurate mathematical model based on NLSE. Simulation network used in Artis Optsim is depicted in Fig. 3. OMNeT++ test network is depicted in Fig. 2. Network consists of traffic generator *gen* and a traffic consumer *sink*. Model *sink* evaluates incoming packets transmitted from *gen* and prepares statistics based on it. The model evaluation is based on a change of fiber length from 0 km to 180 km that introduces attenuation of transmitted signal and as a result reduction of OSNR. The simulation was also carried out in Artis OptSim. Fiber parameters are outlined in Table I. These parameters are based on standard ITU-T G.652.A [9] which

defines properties of optical fibers that are generally used in telecommunication networks.

TABLE I
SIMULATION FIBER PARAMETERS

Parameter	Value
α_{1310}	0.5 dB/km
α_{1550}	0.4 dB/km
λ_{0min}	1300 nm
λ_{0max}	1324 nm
S_{0max}	$0.092 \text{ ps/nm}^2 \times \text{km}$

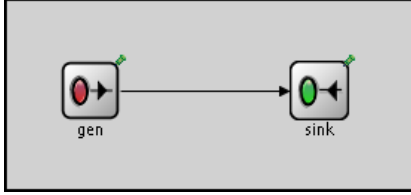


Fig. 2. Essential OMNeT++ simulation network consisting of traffic generator, sink and fiber model.

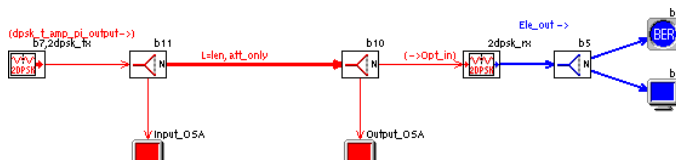


Fig. 3. Testing setup, consisting of traffic generator, fiber under test and resolution part.

Artis Optsim simulations are carried out using optical spectral analyzers (OSA). These OSAs are additionally used for signal supervision.

OSAs are very important for simulation supervision because they offer a first look at signal properties for different fiber length, ie. simulation steps. Artis OptSim BER estimation accuracy was directly monitored step-by-step using eye diagram and Q factor (8).

$$Q = \frac{I_1 - I_0}{\sigma_1 + \sigma_0} \quad (8)$$

where I_1 means level of logical 1, I_0 means level of logical 0, σ_1 means deviation of level 1 and σ_0 means deviation of level 1.

$$Q \cong \sqrt{OSNR} \quad (9)$$

The graph depicted in Fig. 4. is constructed from measured data given by Artis OptSim and a new OMNeT++ model. It is clear from the graph for OOK the modulation accuracy for the new OMNeT++ model and Artis OptSim model. On the other hand BPSK modulation results does not reach high relevance to Artis OptSim like OOK but the difference is in degree of 1^{-20} and 1^{-40} which both means 0 in real systems. This assumption is given by sensitivity and by technical resources of marketed systems. Important part in degree less than 1^{-9} is approximated correctly.

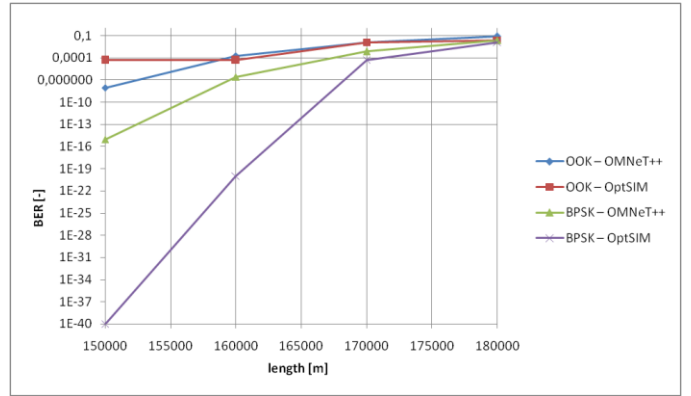


Fig. 4. BER estimation carried out from Artis OptSim and OMNeT++ fiber model for two different optical modulations.

V. FUTURE WORK

The previous chapter proves validity of the model and its usefulness for further research of IA-RWA. The validity is crucial because the model is going to be used for verification of mathematical algorithms taking into account BER, OSNR + Margin, PMD and Q-factor according [3]. Authors of this paper plan to further evaluate end-to-end delay as one of important parameters especially affecting transmission of voice centric services. Very important approach which authors are going to work on is a problem of network reachability on three different layers: transparent, opaque and wavelength tunable with coarse distribution of wavelength tuners (WR) and 3R regenerators. It must be mentioned that 3R regenerators introduce delay which is crucial for signaling and can lead to network misconfiguration but it extends the system reach and breaks the wavelength constraint. WR are lowering blocking probability in an AON but very expensive currently. Regarding these facts it is very interesting to evaluate accurate positions of these nodes in AON from viewpoint of their efficiency.

VI. CONCLUSION

Results of the model allow development and re-usage in extensive network simulations. Benefit of this model is that it can be used similarly to the model handling in Matlab. Another benefit of presented model is that it can be used in simulations of IA-RWA problem and along that it can be used for data transmission in data communication systems implemented by *inet* framework for OMNeT++ which provides for example Ethernet or any other Link layer protocols. Employment of IA-RWA can significantly improve transmission parameters such as bitrate or end-to-end delay. This topic is very interesting for future optical systems.

Uniqueness of fiber model presented here is that it introduces a transmission delay that depends on the length of the fiber or even lightpath which is not general feature in commercial optical simulators. Also the propagation time of a burst is calculated based on its length and modulation speed and format generated by the traffic generator.

ACKNOWLEDGMENT

This work was supported by grant The Research in the Area of the Prospective Information and Communication Technologies under project MSM6840770014, by grant Development and Optimization of the Simulation Modules for Communication Networks under project SGS11/124/OHK3/2T/13 and was partially supported by grant from Ministry of The Interior of Czech republic under project name „Guardsence" and number VG20102015053

REFERENCES

- [1] J. Aracil, F. Callegati, "Enabling Optical Internet with Advanced Network Technologies". [s.l.] : [s.n.], 2009. 224 s. ISBN 978-1-84882-277-1.
- [2] Y. Ed. Lee, G. Ed. Bernstein, W. Imajuku, "Framework for GMPLS and Path Computation Element (PCE) Control of Wavelength Switched Optical Networks (WSOs)," IETF, RFC Apr. 2011. [Online]. Available: <http://www.rfc-editor.org/rfc/rfc6163.txt>
- [3] Y. Ed. Lee, G. Ed. Bernstein, "PCEP Extensions for WSON Impairments," IETF, RFC 7 July. 2011. [Online]. Available: <http://tools.ietf.org/id/draft-lee-pce-wson-impairments-02.txt>
- [4] J. Leibrich. "Modeling and Simulation of Limiting Impairments on Next Generation's Transparent Optical WDM Transmission Systems with Advanced Modulation Formats". Kiel, 2006. 207 s. Dissertation thesis. Technischen Fakultät der Christian-Albrechts-Universität zu Kiel.
- [5] M. Ming; K. Liu. "Principles and applications of optical communications". USA : Hill companies, 1996. 1004 s.
- [6] Ch. Cieutat, L. N. Binh, "Routing and Wavelength Assignment in GMPLS based Optical Networks : An OMNeT++ modelling platform" [online]. Monash University, 2003. 90 s. Technical document. Monash University. Dostupné z WWW: <<http://www.ecse.monash.edu.au/techrep/reports/2003/MECSE-20-2003.pdf>>.
- [7] O. Libenský. "GMPLS network simulator". Prague, 2011. 54 s. Final thesis. CTU in Prague.
- [8] G.P.Agrawal, "Nonlinear Fiber Optics, Academic Press Inc"., Boston, 1995.
- [9] ITU-T G.652 – "Characteristics of a single-mode optical fibre and cable". United States : ITU-T, 2005. 22 s.

Dispersion Compensating Photonic Crystal Fiber with Defected Core

S. Kraus, K. O. Botah, M. Lucki

Department of Telecommunications Engineering, Faculty of Electrical Engineering, Czech Technical University in Prague, 166 27 Prague, Czech Republic

Abstract— The goal of this paper is to present a dispersion compensating fiber design, based on the index-guiding photonic crystal fiber, which can be considered for potential fabrication. Dispersion characteristics of the proposed fiber are investigated with a focus on the potential chromatic dispersion compensation of conventional single-mode fibers.

Index Terms—Photonic Crystal Fiber, chromatic dispersion, dispersion compensation fiber.

I. INTRODUCTION

SINCE the emergence of Photonic Crystal Fibers (PCFs), they have promised a next evolutionary step in the compensation of positive Group Velocity Dispersion (GVD), cumulated along the optical line in a single-mode fiber (SMF). This premise is based on their unique dispersion properties, incomparable with conventional step-index SMFs. A variety of fiber structural parameters allow one to design a Dispersion Compensating Fiber (DCF) with suitable dispersion characteristics. This flexibility of dispersion characteristics can be further extended by an appropriate choice of the fiber's background material and even of the material compounding microstructures, since these two parameters influence material dispersion. Considering a potential DCF usable for compensation of GVD in a wide range of wavelengths, caution should be taken in selecting the values of the fiber parameters, which provides the fiber with steady characteristics over the assumed wavelength range. This requirement is even strengthened if the proposed DCF is designed for potential fabrication, as the current state of fabrication technology has to be taken into account.

II. RELATED WORKS

A high negative dispersion is desired, if a PCF is designed for the compensation of GVD. Negative dispersion can be obtained by different design approaches. In particular, dual concentric cores with utilization of the mode coupling effect, highly doped core, or small microstructures are commonly used fiber layouts. Nevertheless, some negative aspects of the potential fabrication of such designs may arise. Selected examples are provided in this section.

As noted in paper [1], submicrometer holes are hard to fabricate, and therefore, they should be avoided in the design.

In another paper [2], a dual-concentric design with a dispersion value of $-1120 \text{ ps}\cdot\text{km}^{-1}\cdot\text{nm}^{-1}$ at 1550 nm is proposed. The low dispersion value shown in the paper is only achieved in a very narrow wavelength range (approx. 20 nm), which makes it unsuitable for GVD compensation purposes in modern optical transmission systems. A remarkable note regarding the utilization of a doping technique is stated in paper [2] — high values of refractive index (1.5-2.8) of doped cores should not be considered due to their unsuitability for application in real optical systems. Further problems related to other proposed DCF designs, are values of geometrical parameters (e.g. pitch), as a precision of a hundredth of a μm is expected [3]. In that paper, a DCF design incorporating different sizes of holes and pitches among different rings, effectively increasing the number of parameters of the design, was also presented.

A promising simple design layout of a DCF is shown in the paper published by S. Mohammadnejad and N. Ehteshami [4]. Such a fiber design consists of a hexagonal lattice, which is modified by introducing a hole, smaller in comparison with the other holes, into the core of the Index Guiding Photonic Crystal Fiber (IGPCF). Nevertheless, the proposed parameters are difficult to meet from the fabrication point of view. Hence, a further study of the dependencies of the fiber's dispersion characteristics has been conducted and an optimization of parameters performed. Both are presented in the Results section of this paper.

III. METHOD

The results presented in this paper were obtained using the full vectorial Finite Difference Frequency Domain method [5]. This method enables solving of mode profiles and provides information about the effective modal index n_{eff} . Knowledge of the effective modal index can be used to compute GVD expressed as the dispersion coefficient D

$$D = -\frac{\lambda}{c} \frac{\partial^2 \text{Re}\{n_{\text{eff}}\}}{\partial \lambda^2} \frac{1}{L}, \quad (1)$$

where λ is wavelength, c speed of light in vacuum, and L stands for length of fiber. Furthermore, Dispersion Slope (DS) S can be computed as a derivative of D with respect to

wavelength as in (2).

$$S = \partial D / \partial \lambda \quad (2)$$

The effectiveness of compensation of GVD, cumulated in a SMF along the optical line, and compensation of DS can be expressed by (3)-(4). Lower indices of DCF denote compensating fiber, whereas symbols without indices are pertinent to the compensated SMF.

$$LD + L_{DCF}D_{DCF} = 0 \quad (3)$$

$$LS + L_{DCF}S_{DCF} = 0 \quad (4)$$

Based on (3)-(4), a definition of the Relative Dispersion Slope (RDS) can be obtained (5). Ideally, values of SMF and DCF are equal, which means ideal compensation.

$$RDS = S_{DCF} / D_{DCF} = S / D \quad (5)$$

The simulations were conducted in a wavelength range covering not only currently used optical bands (S, C, L) for Wavelength Division Multiplexing (WDM), but also over bands (e.g. U), which might be used in the future. A solid material of the proposed PCF has a refractive index n of 1.444 at 1550 nm. Microstructures in the PCF are formed by air of refractive index $n=1$.

IV. RESULTS

Introduction of a small air hole into the solid core of an IGPCF, significantly alters the mode field profile, as in Fig.1. Due to the presence of the small hole, which resembles a barrier to the propagating light, the mode field is extended to the first ring of microstructures.

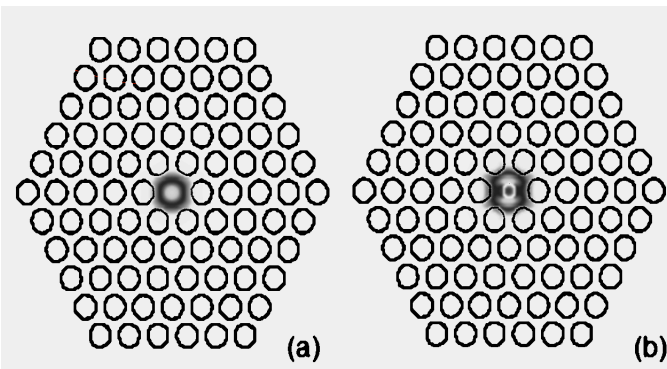


Fig. 1. Modal field profile of IGPCF (a) and PCF with air hole in the core (b).

This change in mode field profile is reflected in the waveguide dispersion, thus dispersion characteristics of the compared fibers are different, as illustrated in Fig. 2. Both fibers have the same geometrical parameters, specified in Table I. In the case of the PCF with a hole in the core, dispersion characteristic has a negative DS of approx. $-25 \text{ ps.km}^{-1}.\text{nm}^{-2}$ in the range of 1200-1800 nm wavelengths. Such a characteristic is suitable for the dispersion

compensation of a SMF.

TABLE I
PARAMETERS OF INVESTIGATED PCF

Symbol	Quantity/Description	Value
N_r	number of rings (-)	5
A	pitch (μm)	1.4
d	hole diameter (μm)	1
d/A	normalized hole diameter (-)	0.714
d_c/A	normal. hole diameter of the core hole (-)	0.4
n	refractive index of solid material (-)	1.444
λ	operating wavelength (nm)	1.55

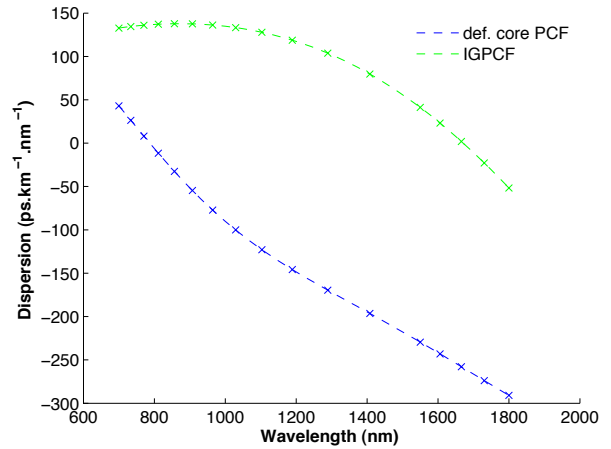


Fig. 2. Chromatic dispersion of IGPCF and investigated PCF fiber with a small hole in the core

Parametric sweeping is useful in determining the redundancy inherited in the fiber design. Fig. 3 depicts dispersion characteristics with the hole diameter as a parameter. The best resistance to change of dispersion characteristics with a change in parameter value is assured, if the hole is chosen to have a value of $1 \mu\text{m}$, because of the difference in values between the neighboring curves. This parameter choice should be taken, despite the fact, that GVD is lowest for the hole size of $0.8 \mu\text{m}$. Moreover, the dispersion curves for the different value of the hole diameter intersect at certain wavelengths as depicted in Fig. 3. This happens, if the different mode profiles exhibit the same waveguide dispersion properties.

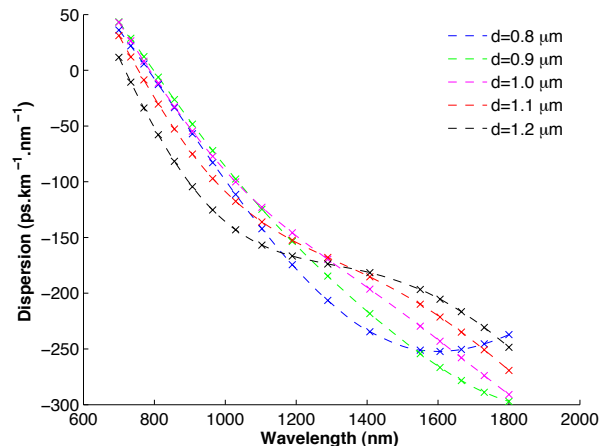


Fig. 3. Dependency of GVD on wavelength with hole diameter as a parameter

Based on the gathered results, an optimization process of the fiber's parameters is performed with respect to potential dispersion compensation. The goal of the optimization is to achieve the same value of RDS for both the compensating PCF and compensated SMF at the 1550 nm wavelength. Dispersion characteristic of SMF, necessary to determine RDS characteristic is computed according to the third equation in [6]. Equation constants specific for the given SMF are provided in [6] and taken from the data of Corning SMF-28, which is compliant with ITU-T G.652 recommendation. The optimized fiber parameters are summarized in Table II.

TABLE II
PARAMETERS OF OPTIMIZED PCF

Symbol	Quantity/Description	Value
N_r	number of rings (-)	7
A	pitch (μm)	1.6
d	hole diameter (μm)	1
d/A	normalized hole diameter (-)	0.625
d_c/A	normal. hole diameter of the core hole (-)	0.25
n	refractive index of solid material (-)	1.444
λ	operating wavelength (nm)	1.55

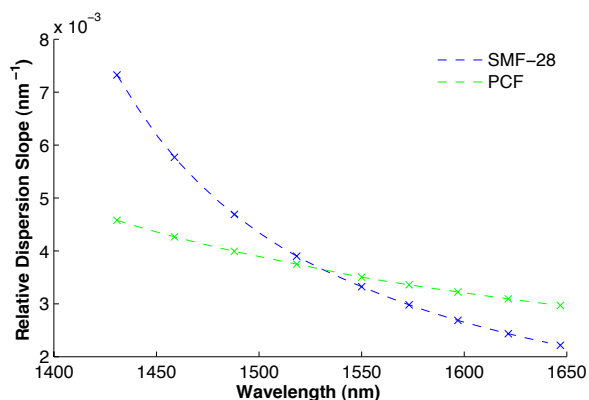


Fig. 4. Resulting RDS after optimization process (closer values mean better compensation capabilities)

The proposed fiber exhibits a RDS value, which is close to the SMF in the wavelength range of 1510-1565 nm, where the difference in RDS is below 10%. At the 1550 nm wavelength, the compensated SMF has a target RDS value of 0.0033 nm^{-1} , whereas the PCF has a value of 0.0035 nm^{-1} .

A positive aspect of the proposed fiber is its low value of confinement loss equal to 0.03 dB.km^{-1} at 1550 nm.

V. CONCLUSION

A PCF with a linear negative dispersion characteristic is presented. It is shown from numerical results that by optimization of the geometrical parameters an optimal RDS can be achieved. Although, a future work could focus on better implementation of the proposed fiber for better effective mode area properties that could be achieved by optimization of the lattice structure.

ACKNOWLEDGMENT

This work has been supported by the CTU grant under project SGS10/275/OHK3/3T/13.

REFERENCES

- [1] S. Yang et al., "Experimental demonstration of very high negative chromatic dispersion dual-core photonic crystal fiber (Presented Conference Paper style)," presented at Conference on Optical Fiber Communication and the National Fiber Optic Engineers Conference (OFC/NFOEC), Anaheim, CA, Mar. 25-29, 2007, Paper OThA6.
- [2] L. Yao et al., "High negative dispersion and low confinement loss photonic crystal fiber," in *2007 Proc. Optical Fiber Communication and Optoelectronics Conference*, pp.373-375.
- [3] F. Begum et al., "Design of broadband dispersion compensating photonic crystal fibers for high speed transmission systems (Presented Conference Paper style)," presented at Conference on Optical Fiber Communication (OFC), San Diego, CA, Mar. 22-26, 2009, Paper JTh6A.
- [4] S. Mohammadnejad, N. Ehteshami, "Novel design to compensate dispersion for index-guiding photonic crystal fiber with defected core," in *2010 Proc. International Conference on Mechanical and Electronics Engineering (ICMEE 2010)*, vol.2, pp. V2-417-V2-421.
- [5] Z. Zhu, T. G. Brown, "Full-vectorial finite-difference analysis of microstructured optical fibers," *Optics Express*, vol. 10, no 17, pp. 853-864, Aug. 2002.
- [6] B. Zsigri, J. Laegsgaard, A. Bjarklev, "A novel photonic crystal fibre design for dispersion compensation," *Journal of Optics A: Pure and Applied Optics*, vol. 6, no. 7, pp. 717-720, 2004.

Advanced testing of multimedia services in GEPON networks

Jan Latal, Petr Koudelka, Petr Siska, Jan Vitasek, Jan Skapa, Vladimir Vasinek

Department of Telecommunications, Faculty of Electrical Engineering and Computer Science, VSB - Technical University of Ostrava, 17.listopadu 15/2172, 708 33 Ostrava-Poruba, Czech Republic

Abstract— The article deals with the testing of multimedia services in GEPON networks by using special equipment IxChariot, which simulates traffic for individual services and measure the QoS parameters. Gradually, were from available xPON networks (GEPON networks), created various topologies and the quality of triple play multimedia services was tested. The advanced measurement devices were used for verification of simulation results made by IxChariot device during tests.

Index Terms — triple play, network, IxChariot, GEPON, VoIP, QoS.

I. INTRODUCTION

The requirements of end users on sufficient internet connection increased markedly in the last years. The providers have to find technologies, which are able to guarantee stability and high-quality high-speed connection. Nowadays technologies like xDLS, Wi-Fi – wireless and wire technologies do not satisfy to connection needs of end users, therefore the optical networks began to be used in greater extent. These optical networks, which were at first built only in backbone nets, were brought to end users thanks to access networks. According to the position of optical fiber termination the optical networks are classified into FTTx (Fiber To The x), where x means position of optical fiber end. The providers are mostly constructing passive optical networks (PON) due to financial demand on build-up. Optical access networks showed a great progress and now they are able to provide data rates in orders of Gbit/s. Above all the optical access networks based on Ethernet are used within EPON, GEPON. The optical access networks EPON and GEPON use time multiplex. For downstream is used TDM time multiplex (Time Division Multiplex) and for upstream is used TDMA (Time Division Multiple Access), which means time multiplex with multiple access of several users to shared optical fiber. The new generation of passive optical networks brought benefit of more effective utilization of optical fibers bandwidth. They use wavelength division multiplex (WDM), which allows parallel transmission of more wavelengths in one optical fiber. These optical networks are called WDM PON. When building-up of optical hierarchy for end user the provider has to choose efficient structure of network and possibilities of triple play services setting. This means setting of telephone centers, multimedia servers, which yields high

demand on quality and extent of network topology with a view to servicing and monitoring. All services have their own critical parameters. Therefore is necessary to set correct setting and guarantee of the quality of services (QoS) in network topology by proper choice of network active elements. With QoS we are able to define bandwidth for individual services thereby solve problems with jitter, latency and packet loss. The measurement was then realized in the “Laboratory of optical access network”, which is placed in building of Department of Telecommunications, Faculty of Electrical Engineering and Computer Science, VSB – Technical University of Ostrava. The VoIP, IPTV services, theoretical analysis of critical parameters for voice signals and video streams are described in the following parts. In the other parts there are described methods of simulation, setting of VoIP and IPTV services for measurement in optical access network GEPON topology. The measurement results and future measurement in other optical networks are summarized in the conclusion.

II. TRIPLE PLAY

Triple Play offers three basic services: voice transmission (Voice over IP), video transmission (IPTV) and broadband Internet access. Advance and distribution of broadband access networks for end-users is revolution in offering voice and data services as IPTV, Video on Demand, video calls and playing online games. In other words it means more services and more devices, but only one network, one provider and one account. The providers offering the triple play services can be much better choice for end users, then providers offering only one service. This can be seen in broadband Internet connection, where services and prices are more favorable for end-users using Triple Play provider.

III. INTERNET PROTOCOL TELEVISION

Analog transmission of TV is ending nowadays; digital transmission is already working and is widely spread to customers. Digital television transmission has few variants: satellite television (DVB-S, DVB-S2), cable television (DVB-C), terrestrial television (DVB-T) or mobile television transmission (DVB-H). Another way how to watch TV is technology called IPTV (Internet Protocol Television). The television broadband is compressed by some of few possible

codecs and compression types in IPTV, as listed in following table 1.

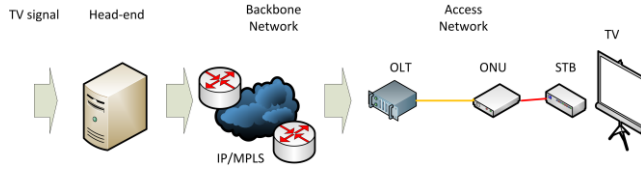


Fig. 1. IPTV infrastructure

Input video signal can be analog or digital. Analog signal is digitalized and compressed using right compression type. For IPTV transmission, UDP (User Datagram Protocol), RTP (Real-time Transport Protocol) or IGMP (Internet Group Management Protocol) protocols are usually used.

IV. IXCHARIOT ANALYZER

IxChariot is testing tool for realtime application simulation. It can predict and load system using realistic conditions. IxChariot allows considering performance characteristics of any application running under wired or wireless network. It supports TCP, UDP, RTP, IPX, SPX, IPv4, IPv6 protocols and many VoIP codecs (G.711, G.723, G.726, G.729), it can also simulate applications as Telnet, FTP, ICQ, etc. When using IxChariot, two computers with installed Endpoints are needed, as they are simulating end-devices, e.g. phones or TV.

TABLE I
CODECS AND COMPRESSION TYPES ARE USED IN IPTV

Transmission quality	Compression type	Bit rate [Mbps]
SDTV	MPEG-2	4 - 7
SDTV	MPEG-4/H.264	2 - 3
HDTV	MPEG-2	18 - 20
HDTV	MPEG-4/H.264	

SDTV - Standard-definition television; HDTV - Standard-definition television; MPEG - Motion Picture Experts Group; H.264 - AVC (Advanced Video Coding).

V. OBJECTIVE QUALITY MEASUREMENT

This method uses mathematical relations to express the image quality or the quality of video signal. Objective methods are simpler, faster and cheaper than the subjective methods. The test is performed by comparing original image frames against a compressed image version with degraded signal quality.

A. MSE a PSNR

MSE (Mean Square Error) is the mean square error of the received signal against the original [1]:

$$MSE = \frac{1}{MN} \sum_{i=0}^{M-1} \sum_{j=0}^{N-1} (x_{ij} - y_{ij})^2, \quad (1)$$

where x is the original image, y is the received image, i, j are elements of the image matrix, M is the quantity of pixels in the image height, N is the quantity of pixels in the image width. MSNR (Peak Signal-to-noise ratio) is the most widely used objective quality measurement. The signal in this case is the original sequence and the noise is an error. PSNR represents the ratio between the highest value of the signal against MSE and is given in decibels (typically in range of 30 to 40 dB):

$$PSNR = 10 \log \frac{m^2}{MSE}, \quad (2)$$

where m is the maximum value, which pixel can obtain.

B. SSIM

SSIM (Structural Similarity Index) is a new method for measurement of similarity between two images. SSIM was designed with the aim of improving methods such as PSNR and MSE, which showed to be inconsistent with the perception of the human eye. To express the structural similarity between two video signals x and y is used following relation:

$$SSIM(x, y) = [l(x, y)]^\alpha [c(x, y)]^\beta [s(x, y)]^\gamma, \quad (3)$$

where $l(x, y)$ compares the signal brightness, $c(x, y)$ compares the signal contrast and $s(x, y)$ measures the structural signal correlation.

C. Using of objective quality measurement method

Figure 2 represents the video sequence, which is computer processed in digital form. Sequence duration was approximately 20 s, which is the optimum time to load the video sequences during streaming. Parameters selected for the video sequences were as follows

- format: VOB
- resolution: 720x576 px
- sides ratio: 4:3
- time: 19s
- frames rate: 25fps
- video type: PAL
- audio format: AC3
- bit rate: 4,3 Mbps

In testing was used the same topology as during the measurement with IxChariot analyzer. QoS values of 5 Mbps, 2.5 Mbps and 1 Mbps had been used. Output video sequence was converted to lossy MPEG-2 compression, which was transmitted through the aforementioned topology via RTP protocol. Objective quality analysis was performed using the MSU Video Quality Measurement Tool. The results are described in the following figures 3, 4 and 5.

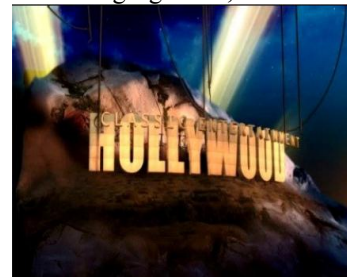


Fig. 2: Original video sequence.



Fig. 3: QoS = 5 Mbps, PSNR = 21,47 dB, SSIM = 0,55.



Fig. 4: QoS = 2,5 Mbps, PSNR = 8,94 dB, SSIM = 0,32.



Fig. 5: QoS = 1 Mbps, PSNR = 8,31 dB, SSIM = 0,22.

From the measured values is evident that reducing of the bit rate leads to decreasing of values of objective methods parameters. When bit rate is limited by the QoS below the codecs standard bit rate, then parameters of objective methods showed a lower image and video signal quality.

VI. MEASUREMENT OF IPTV QUALITY USING IxCHARIOT

Measurement was specified on QoS impact on IPTV quality in Triple Play service. Topology used for measurement is on the following figure 6.

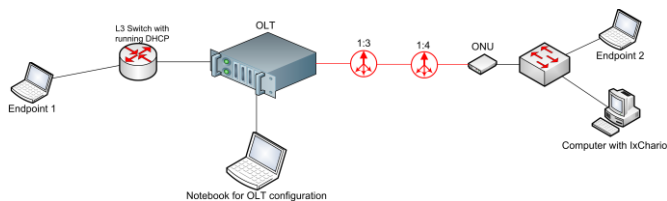


Fig. 6. Topology used for measurements

Topology was created to simulate real application of optical access network. Seven measures were made on this topology and for every measure QoS parameters was changed on OLT. Short brief on results are shown on next table 2.

From this table is evident that connection bit rate lower than 5 Mbps can make a lot of troubles and would affect IPTV quality a lot.

VII. DESCRIPTION OF VOICE SERVICE VOIP

Voice over IP is a service, which enables a voice transmission in internet networks by IP (internet protocol)

TABLE II
SET QoS AND MEASURED PARAMETERS

Bit rate [Mbps]	Average throughput	Average Delay Factor	Avg MLR [media frame per second]	Average Jitter	Packet Loss
50	3,749	2	0	0	0
25	3,749	2	0	0	0
10	3,749	2	0	0	0
5	3,749	3	0	0	0
2,5	2,363	13	920,752	0,719	36,92
1	0,944	32	1 861,241	0,308	74,76
0,512	0,471	170	2 166,683	1	87,33

network protocol. VoIP service enables cheaper calling in Ethernet networks than classic analog telephones. By the help of VoIP it is possible to transmit other services like fax or sending short text and voice messages. The telephone center can be created by software application Asterisk. Except IP protocol it uses VoIP and other protocols e.g. RTP, UDP, TCP/IP, SIP, H. 323, MGCP, RTCP or SDP. There are used two types of packets for VoIP i.e. signal and user. User packet carry useful data in form voice samples. For signalization there are used SIP and H.323 protocols.

Protocol H.323 is used for transmission of signalization of transport layer of OSI model called TCP, which in case packet loss guarantees message delivery by retransmission. SIP protocol allows using one of these protocols UDP or TCP at the transport layer. UDP, unlike TCP does not guarantee delivery of data; therefore the SIP defines resending of messages in the absence of a message delivery confirmation. Losses are therefore reflected in higher transmission delay for both protocols, but with the exception of link failure the message delivery is guaranteed. SIP also allows using of TLS (Transport Layer Protocol), which ensures the security of signaling messages. Voice samples are encoded/decoded using the codecs, such as G. 711, G. 726, G. 729, G. 723.1, GSM, iLBC, Speex.

Individual codecs varies in bit rate of data and compression type of voice samples. The main problems occur with packets that transmit voice samples. These packets are transmitted using UDP, which ensure only possibility to address specific applications within the target IP address and the integrity of transmitted data using the CRC. Each voice packet can be lost or delivered multiple times. Their order can be mixed up. RTP protocol provides specific services for voice and video samples transmission, defines information about the sample type, time, and the order of individual samples. In order to guarantee sufficient quality of the call, the packets must be delivered lossless (packet loss), with an overall low delay (latency) and with low variation of delay (jitter).

According to fact that VoIP communicates in real-time, it was necessary to set up measurement of VoIP service quality. Most used methods for evaluation quality of VoIP service are MOS (Mean Opinion Score) and E-model. There are two ways how to make quality measurement – active, or passive.

Active way of measuring sends known voice sample to network from one end-point to another end-point. End-point in role of receiver compares sample with original one and sends

result of this comparing. This method is not suitable for real-time testing according to its computational complexity.

Passive methods don't use voice sample, because they are usually used for measuring in real-time and built networks.

VIII. MEASURING VOIP QUALITY USING IXCHARIOT ANALYZER

During measurement, two parameters of IP networks were changing and their influence on VoIP quality were monitored. The first parameter was QoS (Quality of Service), the second one was packet loss simulated by Simena Network Emulator. To find QoS influence on VoIP quality, the following scheme was used (fig. 7):

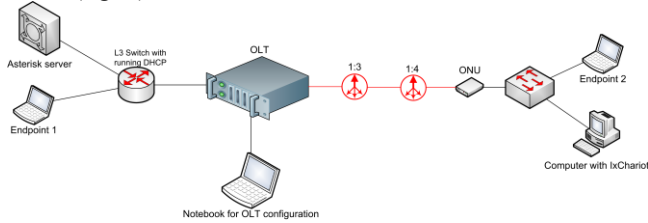


Fig. 7. Measurement of QoS influence on VoIP call

As a result, QoS does not change quality of VoIP transmission, as bit rate needed for VoIP transmission is quite low. Results can be seen in following graph (fig. 8):

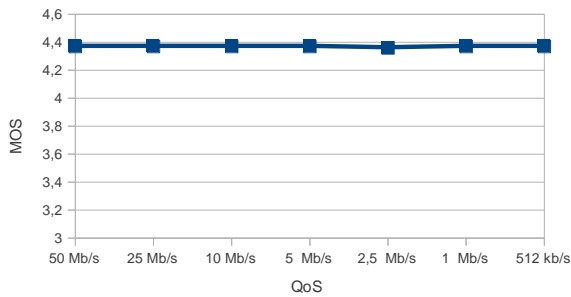


Fig. 8. Measurement of QoS influence on VoIP call

In this measurement was used codec G.711 with 64 kbps bit rate. Unfortunately, OLT provided for this measurement doesn't allow setting of QoS bit rate lower than 512 kbps, however lower rates would not change quality of VoIP transmission.

In the next step was monitored, what will happen to VoIP quality, if packet loss in IP network will change. Packet loss is really important parameter that can rapidly reduce VoIP quality. Measurements were made with two codecs, G.711 and G.729. Following topology was used (fig. 9):

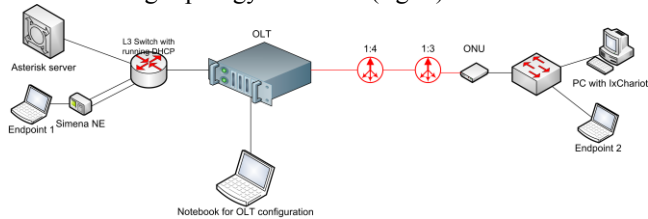


Fig. 9. Influence of packet loss on the VOIP

Results of the measured average values for the packet loss influence on the quality of VoIP services for G.711 and G.729 codecs are shown on fig. 10, 11.

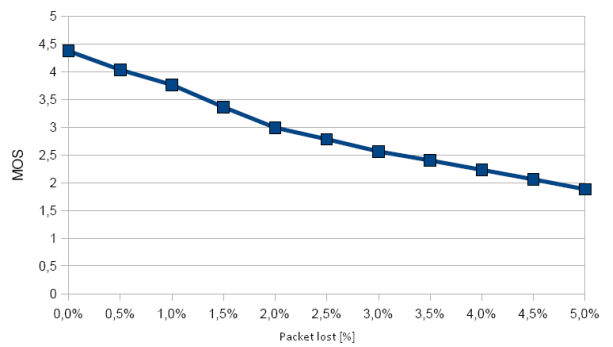


Fig. 10. The dependence of VoIP quality (MOS) on packet loss in case of G.711 codec.

As it is possible to see from graph, the limit of packet loss, when the VoIP call using codec G.711 was still clearly understandable, is 2%. Different result was obtained, when the codec G.729 was used, because this codec has bit rate 8 kbps only. (fig. 11):

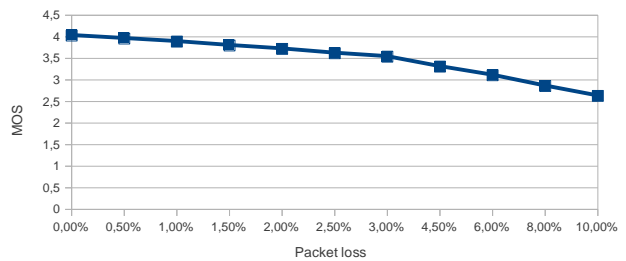


Fig. 11. Dependence of VoIP quality (MOS) on packet loss in case of G.729 codec.

IX. CONCLUSION

From all these measurements it is possible to state, that IPTV is more influenced by QoS and needs bigger bandwidth than VoIP. VoIP can be provided on almost every IP network. With higher requirements the higher bit rates are transmitted and IPTV is also sensitive for packet loss. The VoIP codecs demandingness varies in terms of bandwidth and therefore it is important to be aware of that if the better codecs are deployed in to the network is necessarily must to make sure that sufficient reserves for the increase of network data stream were ensured. In case of video stream is necessary to take into account the same thing, but with the difference that with video streams quality are not only growing a problems with sufficient transmission network capacity, but also the video server, which distributes data streams must be powerful enough for the video signals processing.

ACKNOWLEDGMENT

This work was supported in part by a FRVS G1 1270/2011, CESNET 429/2011 and SP2011/47.

REFERENCES

- [1] Gupta, P., Londhe, P., Bhosale, A., "S IPTV end-to-end performance monitoring," in *Communications in Computer and Information Science 193 CCIS (PART 4)*, pp. 512-523.
- [2] Shibeshi, Z.S., Ndakunda, S., Terzoli, A., Bradshaw, K., *Delivering a personalised video service using IPTV*. International Conference on Advanced Communication Technology, ICACT , pp. 1489-1494.
- [3] Lazar, G., Blaga, T.M., Dobrota, V., *Framework for IPTV QoS*. Proceedings Elmar - International Symposium Electronics in Marine 1, art. no. 4747461, pp. 161-164
- [4] Ma, X., He, L., Lan, J., Mao, J., Zhang, B. "Study on the optimal QoS utility scheduling in multiple-plane and multiple-stage switching network", Proceedings - 7th International Conference on Grid and Cooperative Computing, GCC 2008 , art. no. 4662890, pp. 380-385.

Sharing of Fibers by Transmission Systems and Open Photonic Transmission Systems

Josef Vojtěch, Stanislav Šíma, Lada Altmannová, Miloslav Hůla, Jan Radil and Pavel Škoda

CESNET z.s.p.o.

Abstract—The paper addresses motivation for and possible options of fiber-sharing by more transmission systems. Furthermore, the suitability of open photonic transmission systems for this task is described.

Index Terms — DWDM transmission systems, fiber-sharing, open photonic transmission systems, optical communications

I. INTRODUCTION

THE usage of fibers for data transmission has multiplied transmission capacities several times and transmission systems have developed from simple and static point-to-point into systems allowing complicated topologies with dynamic addition/removal of channels or whole wave bands. However, deployment of transmission systems is also limited by high prices of new installations or rental of fibers. Fiber-sharing would allow simultaneous operation of more (typically two) transmission systems over single fiber pair. Suitable candidates for fiber sharing are open transmission systems that offer unlimited and full access to the lowest layer of a network (in the sense of the ISO/OSI model [1], [9]).

II. FIBER-SHARING BY TRANSMISSION SYSTEMS

A rental of long distance fibers is rather expensive [2]. Another situations can be found where it looks reasonable to run more (typically two) transmission system simultaneously over the same fiber pair. For example, there could be no additional unused fiber pair available. Typically, annualized cost coefficient of a transmission system c_t is lower than the cost coefficient of annual fiber rental c_f . In [2] average c_f of 0.5 EUR/meter/year can be found.

From the same source it can be determined annualized cost coefficient of transmission system (4 year amortization is assumed) c_t about 0.12 EUR/meter/year for commercial transmission systems and from 0.035 to 0.047 EUR/meter/year for open transmission systems. These numbers apply for 10 Gbps transmission system with traditional all optical chromatic dispersion compensation.

Thus it can be stated:

$$(1) \quad 0 < c_t < c_f$$

Obviously, it is more reasonable to operate two systems over a single fiber pair than two systems over two fiber pairs.

$$(2) \quad 2 \cdot c_t + c_f < 2 \cdot c_t + 2 \cdot c_f$$

Mentioned composition (operation of two systems over a single fiber pair) brings only very slightly complicated hardware in comparison with the hardware required for a single fiber bidirectional transmission. The annualized increase in price can be determined as less than 0.0015 EUR/meter/year from [2].

Furthermore, due to gradual exhaustion of the available fiber plant, significant increase in prices of fiber rental between “old” (from years after .com bubble bursts) and “new” rentals can be observed. Where it is necessary to operate multiple (2 or more) transmission systems over a single fiber line, some kind of multiplex must be used. The multiplex obviously causes that the total transmission capacity is divided among the systems and therefore the capacity available for separate systems is decreased. Nevertheless, the present „ordinary“ transmission systems offer transmission of 88 channels in C band, each carrying up to 100Gbps of traffic, see for example [3]. Also, transmission in L band (transmission systems for L band are commercially available) offers up to 80 additional channels. Furthermore, efficient amplification for transmission in S band is also under development, see e.g. [4] and commercially available devices can achieve small signal gains up to 30 dB and output powers up to 20 dBm.

Band	Description	Wavelength Range
O band	original	1260 to 1360 nm
E band	extended	1360 to 1460 nm
S band	short wavelengths	1460 to 1530 nm
C band	conventional ("erbium window")	1530 to 1565 nm
L band	long wavelengths	1565 to 1625 nm
U band	ultra-long wavelengths	1625 to 1675 nm

Tab. 1. Transmission bands overview

With a given fiber pair, the first possibility is to multiplex in space. Obvious solution is each fiber from the fiber pair hosts one single bidirectional system, see Fig 1. CESNET has long experience with fiber sharing between directions in single fiber bidirectional transmission systems that are being deployed since 2002. In 2006 the 10 Gbps DWDM bidirectional transmission with no inline equipment has been

reported over 210km, see [10]. Today these systems are in operation over more than 900 km of fiber lines.

The isolation of the systems is perfect but the solution is limited to 2 systems only (blue and red on Fig 1.) and the availability of single fiber bidirectional systems is limited due to very small number of vendors able to deliver such systems. The operation principle of a bidirectional system is typically based on sharing transmission spectrum between the two directions and the total transmission capacity of a bidirectional system is only one half of the traditional fiber pair system capacity.

Spatial multiplex can be also achieved in few-mode or multi-core fibers. In these fibers each mode or core carries one data channel. Usage of these fibers is still under research, and many potential challenges must be solved, e.g. cross-talk, splicing, connectors, amplification. For more details see e.g. [12], [13].

The second possibility is to multiplex over the optical frequency spectrum. It allows operation of more systems than two, but brings possible mutual influence between the systems. An intuitive division of the transmission spectrum appears to be a division according transmission bands where the first transmission system uses one band and the second system uses the other band. The mutual influence of the transmission systems is relatively limited as each system uses its own amplifiers, multiplexers and a supervisory channel. Nevertheless, the nonlinear Raman interaction can play its role in transfer of energy from higher frequency to lower frequency channels.

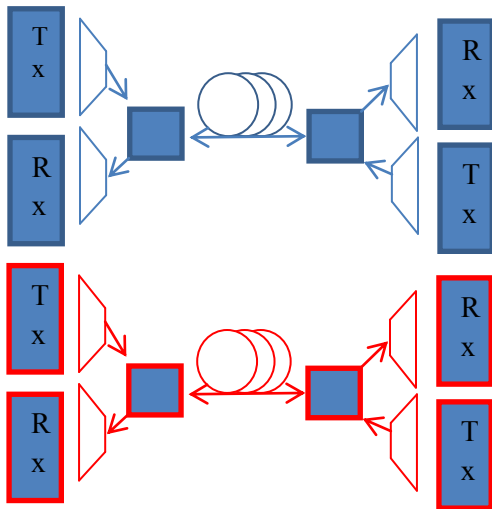


Fig. 1. Two bidirectional transmission systems in operation over fiber pair

A good example can be coexistence of C and L band systems over a single fiber pair. The systems are independent, they just share the same fiber pair. With decreasing available bandwidth in C and L bands, expansion of transmission systems into S band can be expected and, based on this fact, more possibilities of fiber-sharing on the band basis can be expected. See Fig. 2. Supervisory channels of transmission systems are shown with lower powers compared to data channels.

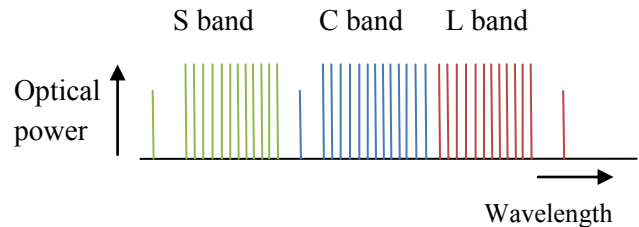


Fig. 2. Possible arrangement of transmission bands including their supervisory channels

Another possible scenario is a division of one transmission band into sub-bands. The mutual influence is of the systems is higher than in the previous case. It can be limited via guard-bands, but they cause waste of bandwidth.

Still another option is spectral interleaving of channels of transmission systems. There is no waste of bandwidth, but the mutual influence, via for example cross phase modulation and four-wave mixing, can be an issue. The last two scenarios represent a subset of a general scenario deploying variable division of the transmission spectra that is emerging with the availability of wavelength selective switching devices working with dynamic spectrum allocation. For this set of scenarios applies that it will be necessary to harmonize supervisory channels of these systems so that they do not collide with each other. The economy of the above described intra-band solution (sub-bands, interleaving and variable apportioning of spectrum inside a band) expressed in CAPEX (capital expenditure) per channel can be worse than in case of apportioning whole transmission bands due to wasted bandwidth.

III. OPEN TRANSMISSION SYSTEMS - RESEARCH AND TECHNOLOGY TRANSFER

As ‘open’ here are considered the systems which are free to additional development by users. An equivalent approach applies for open software. The opposite case represents the ‘closed’ systems typically offered by traditional vendors, where specifications are not publicly available. In case of open systems, important improvements and adding of features can be done by end users (i.e. researchers) or by third parties without any limitations and obstacles. Some parallel can be found in open software systems and it is (or it should be) up to users whether open or closed system is preferred or, in other words, what is more suitable for their ultimate goals. For more details see [11].

The CESNET Association has quite long experience with using dark fibers. The very first intercity link was acquired in 1999 [5]. Since then, CESNET has been aware of importance of full access to dark fibers and its network has been planned with this goal in mind – network should be based on dark fiber wherever possible. This concept was first presented on the Customer Empowered Fiber (CEF) networks workshop [6]. Later, CESNET started development of advanced optical equipment to be deployed on some of CESNET’s dark fiber links. The two main reasons were better economy and to secure technological advancement of its network.

The open photonic systems have been in operation since 2004 in the Czech Republic, utilizing over 2660km of dark fibers from the total of over 4000km. They also have been used during international workshops and demonstrations, e.g. [7], where all optical multicast of uncompressed HD streams has been demonstrated. Gradually, many components of transmission and photonic switching systems have been developed [8] and their development still continues.

ACKNOWLEDGMENT

This work was supported by the Ministry of Education, Youth and Sport of the Czech Republic under The *CESNET Large Infrastructure* project.

REFERENCES

- [1] ISO/IEC standard 7498-1 (1994), [http://standards.iso.org/ittf/PubliclyAvailableStandards/s020269_ISO_IEC_7498-1_1994\(E\).zip](http://standards.iso.org/ittf/PubliclyAvailableStandards/s020269_ISO_IEC_7498-1_1994(E).zip)
- [2] S. Sima et al.: Deliverable D3.2v3 of Porta Optica project: Economic analysis, dark fibre usage cost model and model of operations http://www.porta-optica.org/publications/POS-D3.2_Economical_analysis.pdf
- [3] Ciena 6500 family technical information: <http://www.ciena.com/products/6500/technical/>
- [4] P. Peterka et al.: Thulium-doped silica-based optical fibers for cladding-pumped fiber amplifiers, *Optical Materials*, vol 30, no.1, pp. 174-176
- [5] J. Radil, J. Vojtěch., M. Karásek , S. Šíma: Dark Fibre Networks and How to Light them, 4th Quilt Optical Networking Workshop, Fort Lauderdale: <http://czechlight.cesnet.cz/documents/publications/fiber-optics/2006/radil-quilt.pdf>
- [6] The Customer Empowered Fibre (CEF) network workshops, Prague (2004-2010), <http://czechlight.cesnet.cz/en/homepage/cef-networking/>
- [7] P. Holub, J. Vojtěch, J. Radil et al.: Pure Optical (Photonic) Multicast, GLIF 2007 Demo, Prague (2007).
- [8] J. Vojtěch, J. Radil: Transparent All Optical Switching Devices in CESNET, The APAN 25th Meeting,, Honolulu (2008).
- [9] L. Altmanova L. et al.: Deliverable DS1.1.1.2 of GN3 project: Final GEANT Architecture, http://www.geant.net/Media_Centre/Media_Library/Media%20Library/GN3-10-279_DS1.1.1.2%20Final%20GEANT%20Architecture_v1.pdf.
- [10] M. Karásek, J. Vojtěch, J. Radil: Bidirectional Repeaterless Transmission of 8x10 GE over 210 km of Standard Single Mode Fibre Proceedings of ICTON 2006, vol. 4, ICTON, 2006
- [11] J. Vojtěch et al.: Světélé zítřky s WDM, 1st WDM Summit 2010: [http://www.wdmsummit.cz/files/13_CESNET_Vojtech-SvetleZitckyWDM6.4%20\(2\).ppt](http://www.wdmsummit.cz/files/13_CESNET_Vojtech-SvetleZitckyWDM6.4%20(2).ppt)
- [12] R. Ryf et al.: Coherent 1200-Km 6x6 MIMO Mode Multiplexed transmission over 3-core Microstructured Fiber, paper Th.13.C.1, ECOC 2011, Geneve.
- [13] E. Ip et al.: 88x3x112-Gb/s WDM Transmission over 50km of Three-mode Fiber with Inline Multimode Fiber Amplifier, paper BTh.13.C.2, , ECOC 2011, Geneve.

A Nearly-Zero Ultra-Flattened Dispersion Photonic Crystal Fiber with Low Confinement Loss for Broadband Transmission Systems

R. Zeleny, K. Botah, M. Lucki

Faculty of Electrical Engineering, Czech Technical University in Prague

Abstract—The presented paper describes a novel index guiding photonic crystal fiber, in which its core is surrounded by air holes with three different values of diameter. A nearly-zero ultra-flattened dispersion photonic crystal fiber with low confinement loss is presented. The simulation of the proposed design was carried out using the finite difference frequency domain method. From the numerical simulations, it can be observed that ultra-flattened dispersion can be obtained in the wavelength range of 1400–1700 nm with confinement loss lower than $0.1 \text{ dB} \cdot \text{km}^{-1}$ in the considered wavelength range. Finally, an ultra-flattened curve with zero chromatic dispersion at 1550 nm was achieved by optimizing the hole to hole spacing.

Index Terms—confinement loss, nearly-zero ultra-flattened dispersion, photonic crystal fiber, zero chromatic dispersion

I. INTRODUCTION

AN index guiding photonic crystal fiber (IG-PCF) [1] consists of a solid glass region within a lattice of air holes. It is designed with a low-index cladding region around an un-doped silica core. IG-PCFs have been intensively studied in recent years due to their novel optical properties, not only for applications related to fundamental fiber optics. IG-PCFs have been extensively investigated due to their applicable properties, such as endlessly single mode regime of operation [2], large mode area [1], engineered zero dispersion [3], and ultra-flattened dispersion property, which make those fibers attractive for advanced applications.

The value of dispersion plays a significant role in modern optical high-speed transmission systems. It is responsible for the spreading of light pulse causing inter-symbol interference, and consequently, limiting the bit rate of optical systems. There are two fundamental ways to transmit broadband optical signals without dispersion. Either a dispersion compensating fiber (DCF) is used at the receiver side [4] to compensate dispersion, or dispersion is avoided by the use of a fiber with zero chromatic dispersion in a wide wavelength range along the entire length of the optical path. However, a zero value of dispersion can be problematic for a receiver, since undesirable nonlinear effects, such as four-wave mixing can occur in the optical fiber [5]. Therefore, **nearly-zero ultra-flattened dispersion fibers** are more suitable for telecommunication applications. Nevertheless,

zero dispersion can be of significant use in nonlinear optics, especially in supercontinuum generation (SC). This was investigated by K. P. Hansen in [6].

A parameter critical for telecommunication applications of photonic crystal fibers (PCFs) is leakage or confinement loss [6]. The presence of confinement loss is due to the finite number of air holes that can be made in the fiber geometry. As a result, all the PCF guided modes are leaky. For this reason, the ratio between air hole diameter and the pitch should be made large enough to confine light into the core, and the number of rings around the core should be optimized.

II. RELATED WORK

In recent studies, dispersion flattened PCFs have been obtained, for example, by the following fundamental arrangements of PCF cross-sections:

A. High-index doped core

The basic approach to achieve a flattened dispersion characteristic is to dope the fiber's core with a high-index material. Y. L. Hoo et al. [8] report a study, where the SiO_2 core was doped with GeO_2 , which increases the final core-index in the fiber design. A doped PCF with ultra-low and ultra-flat dispersion variation of less than $6 \cdot 10^{-2} \text{ ps} \cdot \text{km}^{-1} \cdot \text{nm}^{-1}$ over the C band was theoretically designed. However, fibers with a doped core imply significant propagation losses that can be undesirable. Consequently, there should be a trade-off between propagation loss and the required dispersion characteristics in the actual fiber design.

B. Reduced air holes diameter of the first ring

In the next approach, PCFs with reduced diameters of the air holes belonging to the first and second rings were investigated to obtain the desired dispersion characteristics.

N. M. Hai et al. [9] demonstrated the structure, which successfully achieves flat-dispersion characteristics as well as extremely low confinement loss. The ultra-low and ultra-flattened dispersion property with a total dispersion value between $\pm 0.28 \text{ ps} \cdot \text{km}^{-1} \cdot \text{nm}^{-1}$ from 1500 to 1800 nm was investigated by introducing three rings of elliptical air holes, positioned alternately perpendicular.

The study of S. M. A. Razzak et al. [10] involved a simple structure of octagonal PCF with one defected ring, which had a relatively small air hole diameter for ultra-flattened dispersion equal to $\pm 0.5 \text{ ps} \cdot \text{km}^{-1} \cdot \text{nm}^{-1}$, which was obtained within the 1310 to 1700 nm wavelength range. Confinement loss was less than $0.001 \text{ dB} \cdot \text{km}^{-1}$.

C. Threefold symmetry core

A highly nonlinear PCF consisting of a triangular hybrid core region, obtained by replacing four air holes with a central germanium doped area and three fluorine doped regions was recently proposed by K. P. Hansen [11]. The study shows that ultra-flattened dispersion equal to $\langle -1.4; -1.2 \rangle \text{ ps} \cdot \text{nm}^{-1} \cdot \text{km}^{-1}$ can be achieved in the (1460; 1655) nm wavelength range, with confinement loss of the proposed fiber being equal to $7.9 \text{ dB} \cdot \text{km}^{-1}$. The presence of different dopants in the fiber offers new possibilities to control dispersion and nonlinear coefficient. Nevertheless, this advantage increases the technological effort required in the fabrication process.

An improved structure has been reported by M. Chen et al. [12], where the regions doped with a low index material are substituted by air holes. Dispersion of the investigated PCF is less than $0.8 \text{ ps} \cdot \text{km}^{-1} \cdot \text{nm}^{-1}$ and is larger than $-0.7 \text{ ps} \cdot \text{km}^{-1} \cdot \text{nm}^{-1}$, from 1515 to 1622 nm. Moreover, confinement loss does not exceed $0.35 \text{ dB} \cdot \text{km}^{-1}$.

III. RESULTS

To create the model of a novel IG-PCF structure, the full-vectorial Finite Difference Frequency Domain method (FDFD), which was described by Zhu et al. [13], was adopted. Consider the schematic cross-section structure of the optimized IG-PCF, as shown in Fig. 1. It is composed of air holes in the cladding region arranged in a hexagonal array with a constant lattice pitch Λ . The diameter of holes in the first ring, denoted as d_1 is the key design parameter and the diameters of the second and remaining rings of air holes are denoted as d_2 and d respectively.

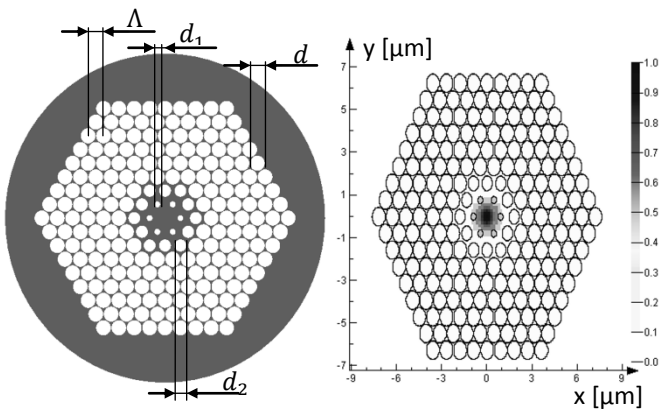


Fig. 1. Schematic cross-section and the fundamental mode field distribution (right) of the investigated IG-PCF.

The optimized fiber exhibits a very low confinement loss equal to $0.1 \text{ dB} \cdot \text{km}^{-1}$ due to the six outermost air hole rings. Removing one of those rings results in a rapid increase in confinement loss of the order of hundred, and dispersion characteristics are changed. Nevertheless, by modifying the innermost first and second ring air hole diameters, the characteristics can be reverted to the initial one. High accuracy in the fabrication process is critical in this design because a change of about 1% highly affects the final flattened dispersion characteristics. This is achieved by the accurate tuning of all the above mentioned parameters, which are summarized in Tab. 1.

TABLE I
SPECIFICATION OF PARAMETERS FOR THE PROPOSED IG-PCF

Parameter	Value	Unit
Dispersion $D^{(1)}$	-0.08	$\text{ps} \cdot \text{km}^{-1} \cdot \text{nm}^{-1}$
Core-index n	SiO ₂	-
Loss $L^{(1)}$	0.034	$\text{dB} \cdot \text{km}^{-1}$
Pitch Λ	0.9	μm
Hole diameter in 1 st ring d_1	0.3378	μm
Hole diameter in 2 nd ring d_2	0.684	μm
Hole diameter d	0.86	μm
Number of rings N	8	-

⁽¹⁾For the considered wavelength of 1550 nm.

Fig. 2 illustrates the wavelength dependence of chromatic dispersion for the proposed PCF presented in Fig. 1. It is shown that ultra-flattened dispersion is maintained with $\pm 1\%$ and $\pm 2\%$ variations of the d_1 optimized parameter, but there are changes in the position of the initial characteristics. The presented PCF is less sensitive to all the other geometrical parameters reported in Tab. 1. It is therefore needless to show these changes, since the same conditions should be applied to them, as in the case of the d_1 parameter during the fabrication process. The wavelength range within which the PCF's ultra-flattened dispersion remains between $\langle -0.173; -0.042 \rangle \text{ ps} \cdot \text{nm}^{-1} \cdot \text{km}^{-1}$ is from 1400 to 1700 nm.

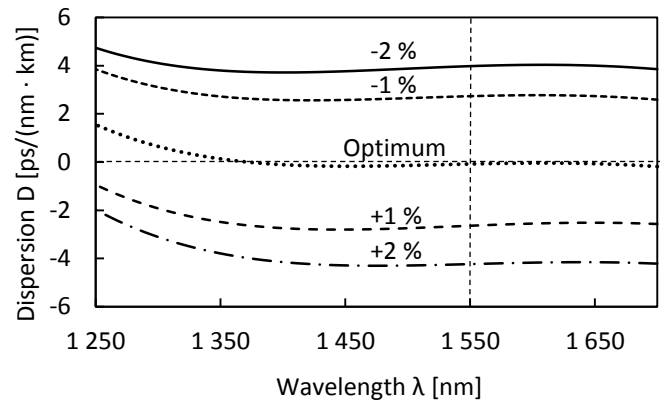


Fig. 2. Nearly-zero ultra-flattened chromatic dispersion with fabrication tolerances of $\pm 1\%$ and $\pm 2\%$.

Zero dispersion is achieved at 1370 nm in Fig. 2, but the wavelength of 1550 nm is more suitable for modern telecommunication optics. However, by adjusting the parameters: $\Lambda = 1$, $d_1 = 0.3334$, $d_2 = 0.669$, $d = 0.91$ (all in μm), it is possible to obtain zero value of dispersion at 1550 nm , as depicted in Fig. 3.

As illustrated in Fig. 3, two zero dispersion wavelengths (ZDWs) are found in the modified fiber at the wavelengths of 1450 and 1550 nm . Dispersion of the proposed IG-PCF is less than $0\text{ ps} \cdot \text{km}^{-1} \cdot \text{nm}^{-1}$ and larger than $-0.065\text{ ps} \cdot \text{km}^{-1} \cdot \text{nm}^{-1}$ between these ZDWs and exhibits a very flattened curve over the S and C bands. Therefore, the modified fiber should be suitable for nonlinear optics like SC generation, rather than for telecommunication applications. Moreover, by varying the mentioned geometrical parameters, the position of ZDW could be tuned.

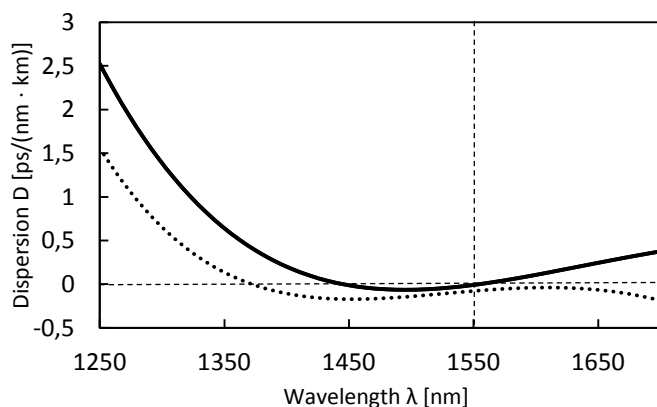


Fig. 3. Achieved chromatic dispersion of both presented IG-PCFs. The dotted line represents the original fiber from Tab. 1. The solid line shows the results after fiber modification with two achieved ZDWs.

IV. CONCLUSION

An IG-PCF with nearly-zero ultra-flattened dispersion, and low confinement loss has been investigated and reported. It has been shown that by modifying the geometrical parameters in the cross-section of the presented structure, the position of the zero dispersion wavelengths could be tuned. The presented fiber is very sensitive to deviations in geometry, and therefore high accuracy is required during the fabrication process. As a result, deviations should be less than 1%. Future work will focus on the proposal of a fiber, immune to structural changes.

ACKNOWLEDGMENT

This work has been supported by the Czech Science Foundation under project 102/09/P143.

REFERENCES

- [1] F. Poli, A. Cucinotta, S. Selleri, "PCF properties and applications," *Springer*, 2007, ch. 1, ISBN: 4020-6325-1
- [2] B. T. Kuhlmey, R. C. McPhedran, C. M. Sterke, P. A. Robinson G. Renversez, D. Maystre, "Microstructured optical fibers: where's the edge?," *Optics Express* 1285, Vol. 10, No. 22, 2002.
- [3] M. H. Frosz, P. Falk, O. Bang, "The role of the second zero-dispersion wavelength in generation of supercontinua and bright-bright

- soliton-pairs across the zero-dispersion wavelength," *Optical Society of America*, 2005, Vol. 13, No. 16/Optics Express 6181.
- [4] M. Nishimura, "Optical fibers and fiber dispersion compensators for high-speed optical communication," *Springer Science, J. Opt. Fiber Commun.*, Rep. 2, 2005, pp. 115–139.
- [5] C. W. Thiel, "Four-Wave Mixing and its Applications," Available from: <<http://www.physics.montana.edu/students/thiel/docs/FWMixing.pdf>>
- [6] K. P. Hansen, "Introduction to nonlinear photonic crystal fibers," *Springer Science, J. Opt. Fiber Commun.*, Rep. 2, 2005, pp. 226–254.
- [7] S. M. A. Razzak, Y. Namihira, F. Begum, K. Miyagi, Sh. Kaijage, N. H. Hai, T. Kinjo, and N. Zou, "Dispersion and Confinement Loss Control in Modified Hexagonal Photonic Crystal Fibers," *Optical Review*, Vol. 14, No. 4, 2007, pp. 165–168.
- [8] Y. L. Hoo, W. Jin, J. Ju, H. L. Ho, D. N. Wang, "Design of photonic crystal fibers with ultra-low, ultra-flattened chromatic dispersion," *Optics Communications* 242, 2004, pp. 327–332.
- [9] N. H. Hai, Y. Namihira, F. Begum, S. Kaijage, T. Kinjo, S. M. A. Razzak, K. Miyagi, N. Zou, "A Novel Ultra-flattened Chromatic Dispersion Using Defected Elliptical Pores Photonic Crystal Fiber with Low Confinement Losses," *IEEE*, 2007, pp. 2233–2236, ISBN: 1-4244-0878-4
- [10] S. M. A. Razzak, N. Yoshinori, F. Begum, "Tailoring Dispersion and Confinement Losses of Photonic Crystal Fibers Using Hybrid Cladding," *Journal of lightwave technology*, Vol. 26, No. 13, 2008, pp. 1909–1914.
- [11] K. P. Hansen, "Dispersion flattened hybrid-core nonlinear photonic crystal fiber," *Optics Express* 1503, Vol. 11, No. 13, 2003.
- [12] M. Chen, Sh. Xie, "New nonlinear and dispersion flattened photonic crystal fiber with low confinement loss," *Optics Communications* 281, 2008, pp. 2073–2076.
- [13] Z. Zhu, T. G. Brown. "Full-vectorial finite-difference analysis of microstructured optical fibers," *Optics Express* 853, Vol. 10, No. 17, 2002.

Low Cost Free-Space Optical System and Its Application

Pavel Lafata, Břetislav Bakala

Czech Technical University in Prague, Faculty of Electrical Engineering, Department of Telecommunication Engineering, Czech Republic

Abstract—This paper deals with the design and realization of free space optical link (FSO) implemented on the basis of the modified project RONJA. The main goal was to design free space optical system with the lowest cost possible and to implement several improvements and upgrades. The first part of this article describes the basic blocks and their function, while the second one presents a process of subsequent installation and practical operation of a sample constructed at the Department of Telecommunication Engineering, FEE, CTU in Prague. The improvements concern mainly constructional parameters, mechanical fixing system for aiming and focusing the optical beam, internal lenses heating, external powering and data connection etc. We also implemented a diagnostic and monitoring module, which enables remote monitoring and measuring of several parameters, such as the level of optical received signal and temperature of critical components. The firmware for controlling the whole system can be uploaded remotely, therefore it is possible to upgrade the system further. This paper also contains practical information and experience obtained during the operation of a whole free space optical system.

Index Terms—Diagnostic Module, Free-Space Optics, Low Cost Solution.

I. INTRODUCTION

THE free space optic represents a specific solution for modern local access data networks, especially in cities and towns with tower blocks and skyscrapers. It usually offers high speed data transmission similar to the standard optical fibers technologies, however only for much shorter distances and together with several limits. The transmission medium is a free space environment, thanks to that no optical fibers and problems and expenses with their installation are necessary, on the other hand, there are several atmospheric phenomena and parameters, which can negatively influence the transmission parameters of the whole optical link. Modern professional free space optics (FSO) systems can offer transmission speed up to 10 Gbps for distances of several kilometers together with cutting edge technologies for optical beam aiming, auto tracking, optical transmitting power controlling, monitoring and remote diagnostic etc. However, these professional systems are usually very expensive and are not very useful for small local operators and internet providers. That's why several community projects for designing and realization of

low cost FSO systems are available. One of the most famous projects is RONJA (Reasonable Optical Near Joint Access), which represents a typical open-source project for low cost and affordable FSO system with limited transmission parameters and functions. The complete documentation of the project is available at [1].

This paper presents our investigation, which was focused on the designing and realization of free space optical link (FSO) implemented on the basis of the modified project RONJA. The main goal was to design free space optical system with the lowest cost possible and to implement several improvements and upgrades [2]. The improvements concern mainly constructional parameters, mechanical fixing system for aiming and focusing the optical beam, internal lenses heating, external powering and data connection etc. We also implemented a diagnostic and monitoring module, which enables remote monitoring and measuring of several parameters, such as the level of optical received signal and temperature of critical components. The firmware for controlling the whole system can be uploaded remotely, therefore it is possible to upgrade the system further.

The paper also describes practical remarks and experience concerning installation and operation of the whole system. Several photos and measured results are also attached to demonstrate the characteristics of the optical link.

II. DESCRIPTION OF REALIZED FSO SYSTEM

The realized optical link consists of two prototypes based on RONJA project with several modifications and changes. These modifications are useful especially for easier optical link installation, optical beam focusing and aiming and also for remote diagnostic and measurements. The entire system consists of several separate modules that provide specific functions. The principle diagram of the optical link is presented in Figure 1. Module INT ensures compatibility with Ethernet 10Base-T and connects the transmission part of the optical link into local data network hub or switch.

Module TX provides an electro-optical signal conversion; it contains necessary LED excitation circuits and acts as a transmitter of the final optical beam. Module RX re-converts received optical signal back to electrical and works as a

receiver. Diagnostic module D performs mainly diagnostic functions and it also evaluates measured data from connected sensors and from the output of an AD converter. The module provides online information about the level of received optical signal (RSSI) and about temperatures simultaneously via the RX module's connection into the local network.

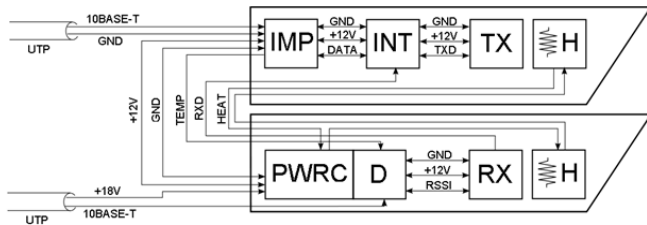


Fig. 1. Detail block diagram of one side of the FSO system. TX – transmitter module, RX – receiver module, INT – interface module, D – diagnostic module, PWRC – power and control module, IMP – module for impedance matching, H – heating of optics, TEMP – 1-wire interface for temperature monitoring, RXD – receiver interconnection, TXD – transceiver interconnection, RSSI – RSSI signal connection, GND – grounding and shielding, DATA – data signal interconnection, 10Base-T – 10 Mbps Ethernet output/input

The whole FSO system is powered remotely via unused pairs of the UTP data cables. Supply voltage 18 V was used mainly for the purpose of potential long cables (attenuation), the minimum operating voltage meets the minimum required supply voltage of 12 V for the input stabilizer. The stabilizer for 3.3 V creates a great loss of at least 10 V, that's why this redundant voltage is used for an internal heating system. This heating system heats both lens of receiver and transmitter to prevent the water condensation or their freezing.



Fig. 2. The realization of TX module. The main processor of the diagnostic module is a microcontroller Microchip PIC18F67j60, which has an integrated physical layer for Ethernet, and does not need many peripherals for their functionality. The microcontroller is connected to 3 temperature sensors DS18B20 placed in the transmitting and receiving tube and also outside to monitor the air temperature. The sensors communicate using 1-Wire protocol. The output of one channel of AD converter is

connected to the RSSI receiver module and thanks to that it is possible to measure the current level of received signal. The microcontroller is connected via SPI to EEPROM memory for storing the last measured data, the frequency of measurements and the required format of data stored in memory can be adapted for several specific situations. These data can be remotely retrieved from memory and they can be processed and evaluated into graphical representation over a longer time period. They can be further analyzed and it is possible to study the impact of weather and other events and various atmospheric conditions (the influence of atmospheric phenomena) on the transmission parameters of the whole optical link.

The interpretation of measured data is provided by a TCP/IP stack from Microchip. Information about the actual state and stored values for elapsed time are available via http protocol by any browser remotely; rendering the graphs and curves is solved by a Java script. Another part of the diagnostic module consists from eight-level LED indicator that displays the actual signal level. This indicator was very useful in the process of aiming and focusing the optical link. The firmware and software of a diagnostic module can be additionally updated and its new version can be remotely uploaded via TFTP protocol.

The optical link was installed on the roof of the Faculty of Electrical Engineering and the Faculty of Mechanical Engineering. The total distance of a link is 120 m. Several photos were taken during the link's installation and they are presented in Fig. 3.



Fig. 3. The photos of realized FSO link.

III. MEASUREMENTS AND RESULTS

Before the measurements themselves, the process of accurate aiming and focusing of the optical beam had to be performed first followed by the process of calibration and fine tuning. It was also necessary to upgrade the firmware several times during the testing period of the whole optical link.

The graphical interface of the diagnostic and control window was designed to be clear and simple and to contain only the most important functions. The actual firmware version does not cover all planned functions and features, that's why it will be necessary to further implement and finish some of them. However, most of the features are already implemented. The main functions are:

- current local time and date,
- actual value of RSSI and its conversion to the attenuation,
- 3 values of temperature – internal temp. of RX module, internal temp. of TX module and external air temperature,
- 5 graphs for the interpretation of measured values during a certain time period (RSSI, attenuation, 3 temperatures),
- remote firmware uploading (password protected),
- detail configuration and diagnostic (password protected),
- calibration – for calculation of the attenuation from RSSI value (password protected).

The functions that are planned to implement further:

- availability of link – thanks to a simple ping test and flooded ping test, the availability of the whole link (packet loss) can be estimated,
- continuous re-calibration and advanced calibration system, which could enable more detailed and accurate measurements and calculations of the attenuation.

The testing and demonstrational interface is available via any web browser using standard http protocol at: <http://ronja.styxx.cz:8080/>. The illustration of actual graphical interface is presented in the next Fig. 4.



Fig. 4. The interface of remote link's diagnostic and control window.

The diagnostic and remote functions are still under the development; however, several measured results and practical experience were already obtained. The next graphs in Fig. 5 present the situation of RSSI (Received Signal Strength Indication) and its dependence on the external air temperature (weather conditions) during the 3 days testing and measurements.

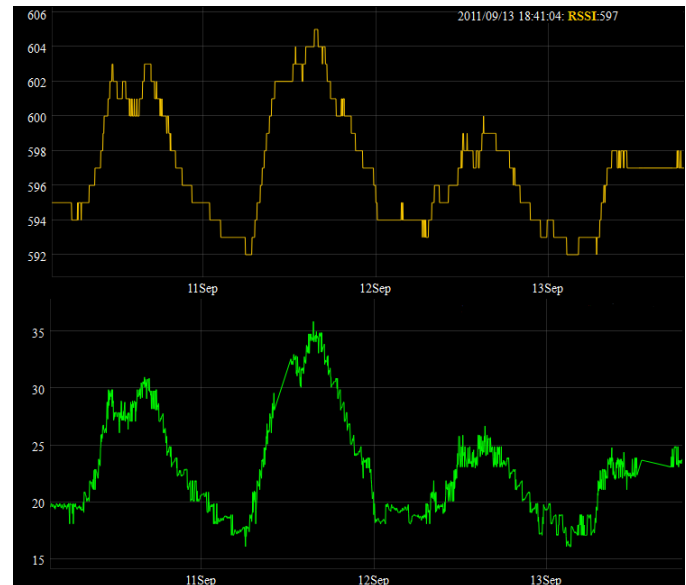


Fig. 5. The development of RSSI (yellow line) and air temperature (green line) in the period of 3 days.

The time development of RSSI (yellow line) shows an evident dependence on the external weather conditions (air temperature – green line). During the night period, probably thanks to the water condensation and mist, the RSSI is always lower than in the mid-day period, when the sun is shining and the air temperature is much higher. However, the difference is not very significant yet (these measurements were performed during completely sunny days of 10.-13. September), but can be more significant in autumn or winter days. Certainly, it will be interesting to observe the dependence of RSSI during heavy raining, fog or snowing period. We were also able to detect the interruption of optical beam caused probably by a bird, as it is illustrated in the next Fig. 6.



Fig. 6. Significant drop of RSSI caused probably by beam interruption by a bird.

The value of RSSI in Fig. 6 during the beam interruption is not completely 0, while the value is measured in sec intervals, however, several values are averaged (because the capacity of memory for storing the results is limited).

There are many mathematical models describing the

propagation of optical beam through the atmosphere in various different weather conditions and situations, and the dependence of the atmosphere attenuation on the weather conditions can be accurately estimated, that's why our future effort is to compare our measured results with the predictions given by these models and simulations.

IV. CONCLUSION

This paper presented the possibilities of designing and realization of low cost FSO system with limited transmission speed and characteristics. We used an open-source project RONJA and we implemented several various modifications and improvements. The remote diagnostic and controlling mechanisms are still under the development, however, several measurements and practical outputs were already obtained. This optical link will probably serve as a testing and demonstrational for the purpose of teaching in subjects concerning access networks and transmission systems at the Department and for the purpose of bachelor and diploma thesis from the field of simulations of FSO links and atmospheric phenomena.

Our next goal is to design and realize similar low cost FSO system for short and mid distances with transmission speed of 100 Mbps. We expect to use the experience and results obtained by operating the 10 Mbps optical link presented in this paper.

ACKNOWLEDGMENT

This work and paper was supported by the Grant Agency of the Czech Technical University in Prague, grant No. SGS 10/275/OHK3/3T/13 and grant the Ministry of Industry and Trade of Czech Republic No. FR-TI2/621.

REFERENCES

- [1] K. Kulhavy, "Twibright Labs, Ronja," [online], 2007, [cit. 10-12-2011]. <<http://ronja.twibright.com/>>.
- [2] B. Bakala, "Realization of optical link," Bachelor project, Department of Telecommunication Engineering, Czech Technical University in Prague, Faculty of Electrical Engineering, 2011.

Adaptive Techniques in Free-Space Optical Networks

J. Libich and S. Zvanovec

Czech Technical University in Prague, Faculty of Electrical Engineering, Czech Republic

Abstract—Free-space optical link is an alternative instrument to transmission of information in data rates up to tens gigabits per second. Although evolution of this technology proceeds several years, many factors still affect propagation of optical beam. Therefore several mitigation techniques are used or in a state of research. Between the most significant appertain beam tracking, adaptive optics, diversity techniques or new modulation schemes. In this paper, diversity techniques are discussed. First result from a measurement campaign are introduced.

Index Terms—Free-space optics, weather influence, turbulence, diversity gain.

I. INTRODUCTION

Free-space optics (FSO) is a continuously evolving technology providing transmission of information using an optical beam and atmosphere or free-space as a transmission medium. In contrast to radio band systems, FSO offer larger bandwidth, which results in higher data rates, more safety, no licensing and interferences, fast deploying and fewer prices contrary to fiber optics [1]. Unfortunately, FSO is strongly affected by weather conditions. Suitable wavelength is chosen with regard to molecular and aerosol extinction, but many effects cannot be eliminated. Constantly present turbulence causes inhomogeneity of the refractive index. Optical beam passing through this random medium spreads out and wanders and the wave-front of the optical beam is distorted [2]. Therefore, researches tries to mitigate these effects by various techniques, for instance beam tracking, adaptive optics, diversity techniques or new modulation schemes. The result is enhanced availability of FSO link, which is required by end users. Quality of data transmission is expressed by bit-error-rate (BER).

Propagating optical beam interacts with atmosphere owing to its composition consisting of variety molecules and particles. The interaction causes extinction of the optical beam. Extinction is defined as a decrease of the optical beam intensity. Extinction is caused by absorption and scattering and it can be subdivided into two size domains: molecular and aerosol extinction.

The paper is arranged subsequently. In Chapter I, FSO technology is introduced and fundamental terms are defined. In the next part, weather influence on FSO links is recapitulated. Diversity techniques as are spatial, route and

wavelength diversity techniques are described. Chapter IV examines the diversity gain of two FSO links incorporated within a star topology network. Chapter V summarizes results based on data measured so far. The last chapter concludes using of a route diversity technique in FSO networks.

II. WEATHER INFLUENCE

A. Atmosphere influence

Atmosphere is composed of molecules of air (N₂, O₂, H₂, CO₂, H₂O) and aerosols (fog, smoke, haze, maritime spindrift particles and sea salt, soil and rock debris). Extinction owing to these particles is permanent as well as turbulence within air. Attenuation by atmosphere is strongly dependent on the wavelength of used light [3]. Therefore, the wavelength has to be chosen carefully. Nowadays FSO systems usually work at wavelength of 850 nm.

B. Turbulence influence

Non-homogeneous distribution of the refractive index results in widening and wandering of the optical beam. On the site of the receiver, the optical power fluctuates in frequency range from 0.01 up to 200 Hz [2]. The frequency and amplitude of scintillation depend on cells diameter to beam diameter ratio. Random speed of fluctuation of a fluid results in turbulences. In the atmosphere, there are two different type of motion, laminar and turbulent. Contrary to laminar flow, turbulent flow is the cause of constant dynamic mixing of media and creates smaller flow areas called eddies which occupy areas from tens of centimeters to units of kilometers..

The variance σ_x^2 of the received optical power is represented by Rytov variance expressed by the next equation [4]:

$$\sigma_x^2 = 1.23 C_n^2 \left(\sqrt{\left(\frac{2\pi}{\lambda} \right)^7 L^{11}} \right) \quad (1)$$

where C_n^2 introduces the refractive index structure parameter, λ stands for the wavelength and L denotes length of the link.

C. Rain and fog influence

Rain consists of water droplets whose are various in the size, number and the space distribution. The shape of the

raindrop is dependent on the size and it graduates from sphere to flatted ellipsoid. Rain attenuation is mainly caused by scattering effect. In infrared region, wavelength is much smaller than the diameter of the droplet. Total attenuation by rain is dependent on the quantity of raindrops in propagation path.

The worst condition for transmission of the FSO signal is under fog and mist. Size of small droplets comprising fog is comparable to wavelength of light. Therefore, Mie scattering is main reason of attenuation of the optical beam passing through fog. The scattering coefficient is related to the meteorological visibility V by the following equation [5]:

$$\beta_n(\lambda) = \frac{3.91}{V} \left(\frac{\lambda}{550 \text{ nm}} \right)^{-q} \quad (2)$$

Model defined by Kim [6] defines q as:

$$q = \begin{cases} 1.6 & V > 50 \text{ km} \\ 1.3 & 6 \text{ km} < V < 50 \text{ km} \\ 0.16V + 0.34 & 1 \text{ km} < V < 6 \text{ km} \\ V - 0.5 & 0.5 \text{ km} < V < 1 \text{ km} \\ 0 & V < 0.5 \text{ km} \end{cases} \quad (3)$$

III. DIVERSITY TECHNIQUES

Since FSO signal propagates through atmospheric channel, the optical beam is affected by various phenomena. The most important effects were discussed in previous chapters. These result in fading and fluctuation of the received optical power and subsequently decreasing of the FSO link availability. In order to mitigate atmospheric effects, following diversity techniques can be used.

A. Spatial diversity

One of the feasible solutions is the use of the spatial diversity. Multiple apertures on the site of the transmitter or/and the receiver (MIMO) provide additional redundancy and lead to enhance of the performance [6]. Moreover, reducing of possibility to blind of the laser beam is suppressed. Nowadays FSO links uses more than one transmitting and receiving apertures. For instance LightPointe Strata G terminal, used in the measuring network described below uses four optical beams transmission.

B. Route diversity

FSO systems can be used in FSO networks for interconnecting buildings of campuses, different buildings of corporations or a hospital complex in various network topologies. Availability of the whole network depends on either each component and on arrangement of links. If the

connection is lost owing to failure of one of the links within a ring topology network, another direction is used to establish a connection. A star topology is based on connection of all links to central multipoint unit (MPU) which is composed of several FSO transceivers. Since each of the links is connected directly to MPU, protection against failure is not secure. Furthermore, malfunction of the MPU causes breakdown of the whole network. High availability due to several possible connections offers a mesh network topology [1]. FSO networks also can be supplemented by classical radio band communication systems.

C. Wavelength diversity

Molecular absorption is one of the effects causing fading of the received optical power. By reason of existence of opaque and transparent windows, the used wavelength must be chosen carefully. Comparison between influences on 850 nm and 1550 nm was discussed in several publications, for instance [7]. Nowadays, combinations of optical links and radio frequency systems are very often used. Dense fog represents almost opaque barrier for the FSO signal. Therefore, joint radio frequency links are installed as a backup in case of FSO link outage [8].

IV. MEASURING NETWORK

Experimental measuring network was set up in the university campus of the Czech Technical University in Prague (CTU). The network consists of tree FSO link and comprises a star topology network. Parameters of particular optical links are characterized in terms of lengths, wavelengths and positions of transceivers characterized in table 1.

TABLE I
Parameters of used FSO links

	Link A	Link B	Link C
Type	WaveBridge 500	LightPointe Strata G	MRV Telescope 700
Length (m)	120	450	390
Wavelength (nm)	800 - 900	850	830 - 860
Optical Source	LED	LD	LD
Divergence (mrad)	17.5	2.0	3.5
Max Data Rate (Mbps)	155	1250	155
1. point of the link	CTU Campus	CTU Campus	CTU Campus
2. point of the link	CTU Campus	ORLIK Dormitory	BUBENEC Dormitory

Arrangement of the network and sensors is then depicted in Fig. 1. Weather conditions are observed by two meteorological stations collecting air temperature and humidity, atmospheric pressure, wind velocity and amount of precipitations. In order to investigating of influence of buildings on FSO link, set of thermal sensors was installed between at first quarter of the link A. In the next step, the measuring network will be extended to a mesh topology. New FSO link will be added and it will enclose links B and C.

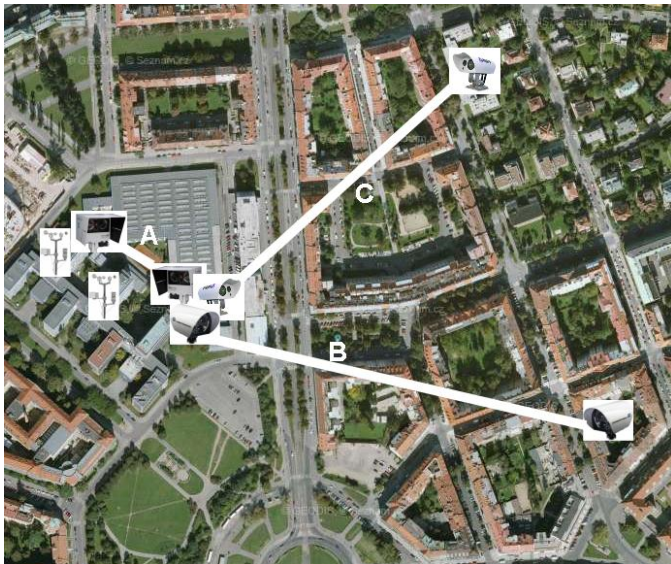


Fig. 1. Measuring network and sensors arrangement

V. RESULTS

Data from two FSO links A and B as a part of a star topology network were analyzed in order to investigate diversity statistics. In order to obtain these results, cumulative distribution functions (CDF) were analyzed and compared. All above mentioned propagation impairments were dealt and recalculated especially with their spatial properties. Because of different length of the links, the diversity gain was recalculated to 1 km long propagation path.

Table II gives the diversity gain of two FSO links derived from measured statistics during April to May 2011. Availability of single links A and B was enumerated at first. In next step it was distinguished improvement of such statistics when the second link was added. As can be seen diversity gains up to 8 dB can be yielded. This contribution can introduce very perspective possibility especially within dense FSO networks during drops of particular network segments (links) due to the harsh atmospheric conditions.

TABLE II
Diversity Gain Derived from Statistics of Two Adjacent Links

Availability (%)	Diversity Gain (dB) Link A	Diversity Gain (dB) Link B	Availability (%)	Diversity Gain (dB) Link A	Diversity Gain (dB) Link B
99.00	0.75	5.27	99.975	1.05	7.02
99.25	0.81	5.42	99.990	1.07	7.49
99.50	0.85	5.74	99.9925	1.10	7.60
99.75	0.89	6.03	99.9950	1.17	7.74
99.90	0.94	6.39	99.9975	1.23	8.02
99.925	1.01	6.67	99.9990	1.27	8.36
99.950	1.04	6.79			

VI. CONCLUSION

The route diversity gain of two FSO links incorporated in a star topology measuring network in university campus of the CTU was evaluated. The availability of whole network is possible to increase using the route diversity technique. The diversity gain evaluated from measured data reaches up to tens of decibels per 1 km long link. Next research steps will be focused on extending measuring network to a mesh topology by adding new FSO link connecting both of dormitories directly and evaluation of the route diversity gain of a more complex mesh topology network.

ACKNOWLEDGMENT

This work was supported by the Grant Agency of the Czech Technical University in Prague, grant No. SGS11/065/OHK3/1T/13.

REFERENCES

- [1] A. K. Mujamdar and J. C. Ricklin, *Free-Space Laser Communications: Principles and Advances*. New York: Springer, 2008.
- [2] L. C. Andrews, *Field guide to atmospheric optics*. Bellingham, Wash.: SPIE Press, 2004.
- [3] "Propagation data required for the design of terrestrial free-space optical links," ed: Rec. ITU-R P.1817, 2007.
- [4] L. C. Andrews and R. L. Phillips, *Laser beam propagation through random media*, 2nd ed. Bellingham, Wash.: SPIE Press, 2005.
- [5] L. Dordova and O. Wilfert, "Free space optical link range determination on the basis of meteorological visibility," in *Radioelektronika, 2009. RADIOELEKTRONIKA '09. 19th International Conference, 2009*, pp. 333-336.
- [6] L.-q. Han, *et al.*, "Performance of free space optical communication through gamma-gamma turbulence channels with spatial diversity," in *Computer and Communication Technologies in Agriculture Engineering (CCTAE), 2010 International Conference On, 2010*, pp. 109-112.
- [7] M. Grabner and V. Kvicera, "Fog attenuation dependence on atmospheric visibility at two wavelengths for FSO link planning," in *Antennas and Propagation Conference (LAPC), 2010 Loughborough, 2010*, pp. 193-196.
- [8] F. Nadeem, *et al.*, "Weather Effects on Hybrid FSO/RF Communication Link," *Ieee Journal on Selected Areas in Communications*, vol. 27, pp. 1687-1697, Dec 2009.

Wave Effects in FSO Links and Their Influence on Transmitted Laser Beam

Juraj Poliak^a, Jiri Komrska^b and Otakar Wilfert^a

^a*Institute of Radio Electronics, Brno University of Technology, Purkyňova 118, 612 00 Brno (Czech Republic)*

^b*Institute of Physical Engineering, Brno University of Technology, Technická 2, 616 69 Brno (Czech Republic)*

Abstract — The paper introduces a propagation model of light wave which takes into consideration diffraction effects on transmitter aperture. Scalar diffraction theory was applied and its results were used in the model developed in the MATLAB environment. The model was compared with experiment and its validity proved.

Index Terms — Fresnel Diffraction, Free-space Optical Communications, Fourier Transform, Gaussian Beam.

I. INTRODUCTION

IN recent years, new techniques and technologies have been developed in FSO. This is due to many reasons, mainly the possibility of achieving high data rates, directivity of the link and use in non-licensed bands. During the shaping of the transmitted laser beam, various physical phenomena occur on the path, changing the laser beam profile, reducing the signal-to-noise ratio, and causing the automatic tracking system to fail. Many approaches based either on numerical or on analytical analysis of the system have been developed to simulate these effects.

The most critical effect distorting the transmitted laser beam profile is diffraction [2]. For the use in practice, the scalar theory of diffraction is used to describe the effect of optical elements on this laser beam profile. The transmitter lens and transmitter aperture were identified as the main source of diffraction.

The paper deals with data provided by the scalar diffraction theory. As the computation of the intensity distribution is demanding, many approaches have been developed [7]. The most widely used approach is based on the Fourier transform. Furthermore, the paper introduces an important solution of the wave equation – the elliptically symmetrical Gaussian beam. The main part is focused on the approach based on the FFT algorithm and its use in the simulation of diffraction is discussed. Also, a simple user-friendly program for the simulation of diffraction of elliptically symmetrical Gaussian wave on a circular aperture is discussed. In the final part, simulated results are compared with experiment.

II. KEY TO UNDERSTANDING

Diffraction effects are usually described by means of scalar diffraction theory. Its results are based on the Huygens-Fresnel principle and lead to the general formula

$$\psi(x, y) = -\frac{jk}{2\pi} \iint_{S_0} \psi_0(x_M, y_M) \frac{\exp(jks)}{s} dx_M dy_M, \quad (1)$$

cf. fig. 1. This equation expresses the wave function $\psi(x, y)$ in the plane of observation (i.e. the receiver plane) in terms of the incident wave $\psi_0(x_M, y_M)$ in the plane of the transmitter aperture S_0 . The computation of the integral on the right-hand side of equation (1) requires to compute the double integral for every point $P(x, y)$ of the plane of observation. To avoid such computationally extensive challenge, one may approximate the equation by means of different approaches.

One of the most straightforward approaches is based on the Fresnel approximation [1, 7] of the spherical wave

$$\frac{\exp(jks)}{s} \approx \frac{\exp(jkz)}{z} \exp\left[\frac{jk}{2z}(x-x_M)^2 + (y-y_M)^2\right], \quad (2)$$

where according to fig.1, the exponential term on the left side of equation (2) is the divergent spherical wave coming from the point M . Further development of the quadratic term in equation (2) leads to the final form of equation (1)

$$\psi(x, y, z) = -\frac{jk}{2\pi} \frac{e^{jkz}}{z} e^{\frac{jk}{2z}(x^2+y^2)} \cdot \iint_{S_0} \psi_0(x_M, y_M) e^{\frac{jk}{2z}(x_M^2+y_M^2)} e^{-\frac{jk}{z}(xx_M+yy_M)} dx_M dy_M. \quad (3)$$

The wave function of the diffracted wave is then expressed by means of the Fourier transform of products of wave function ψ_0 in the plane of diffraction aperture S_0 and the phasor $e^{\frac{jk}{2z}(x_M^2+y_M^2)}$.

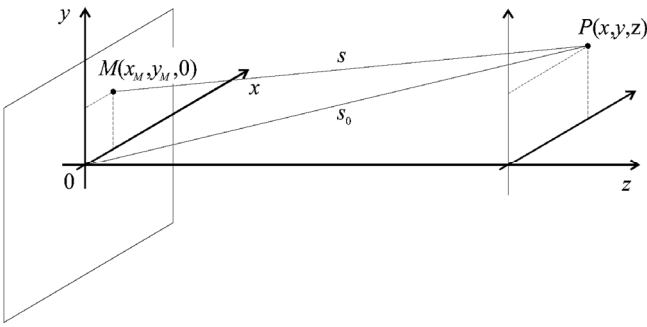


Fig.1. Representation of the Fresnel approximation. [7]

III. SIMULATIONS

In practical applications one benefits from the built-in FFT algorithm included in many modern programming languages. Simulations were based on equation (3) and were developed in the MATLAB[®] environment. However, in practice the intensity distribution instead of the wave function is needed. Using the relation between optical intensity and wave function, equation (3) provides the resulting formula

$$\psi\psi^* (x, y, z(n)) = I(x, y, z(n)) \propto \left| \mathbb{F}\mathbb{T} \left\{ \text{circ} \left(\frac{x_M^2 + y_M^2}{\rho_0^2} \right) e^{\frac{jk}{2z}(x_M^2 + y_M^2)} \right\} \right|^2, \quad (4)$$

where the circ function refers to the circular shape of the transmitter aperture. Simulation based on this approach enables us the following parameters to change:

- ✓ wavelength λ ,
- ✓ distance z between the receiver and the transmitter,
- ✓ beam widths w_x and w_y of the Gaussian beam in both axes,
- ✓ radius of the transmitter lens ρ_0 ,
- ✓ linear resolution of the simulation,

After entering the parameters and pressing the *Evaluate* button, the results are displayed as shown in figure 2. At the top of the figure, an elliptical Gaussian beam in the transmitter plane and the transmitter aperture S_0 are displayed. At the center, the intensity distribution of the laser beam in the receiver plane and at the bottom, 2 perpendicular cross-sections are shown. As can be seen, the ratio of beam width to aperture radius has a strong impact on the shape of the distribution.

Sometimes, usually for teaching purposes, one needs to use a number of Fresnel zones [5] as the parameter. The distance where the desired number of Fresnel zones is visible can be easily calculated using the $FZ \Rightarrow z$ button after entering the input parameters.

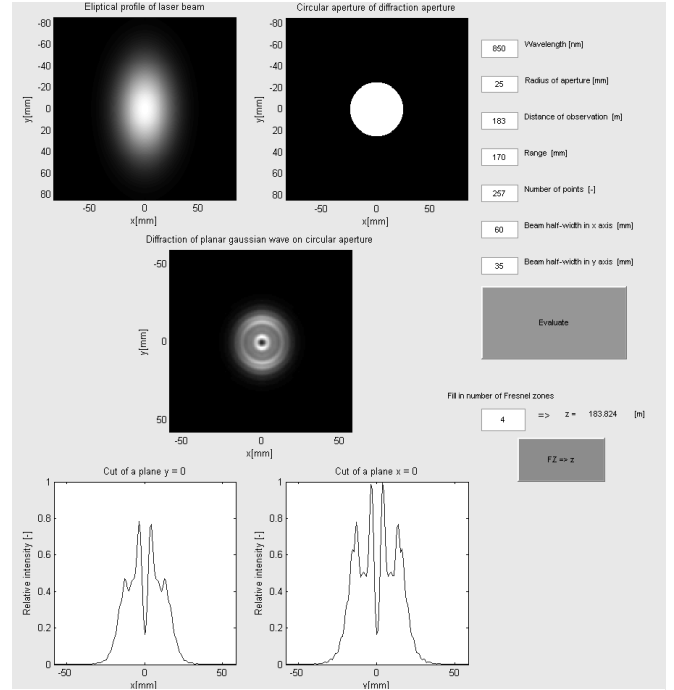


Fig.2. Results of simulation using MATLAB GUI script based on FFT with following parameters: $\lambda = 850$ nm, $\rho_0 = 25$ mm, $z = 183$ m, $w_x = 60$ mm and $w_y = 35$ mm.

IV. EXPERIMENT

To prove experimentally the simulated results, one has to consider the limits and conditions introduced by the theory. These limits concern source coherence (both spatial and time) as well as the shape of the wave front. To satisfy these conditions, an experimental setup according to figure 3 was proposed.

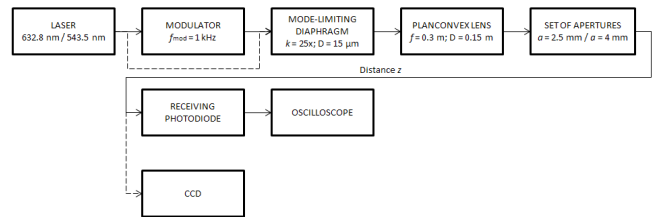


Fig.3. Experimental setup.

A He-Ne laser was used for its pure spectrum and laser beam shape, although only a circularly symmetrical beam could be achieved. This beam was input for the simulation of the experiment (see fig.4). To reduce the number of modes in the beam, a mode-limiting diaphragm was used [4]. Crucial for the experiment was to collimate the laser beam very precisely. To achieve this, a plan-parallel plate was used [8].

The results of the experiment carried out according to the proposed setup are given in figure 5 and figure 6. In figure 5, intensity distribution of the diffracted wave is captured on CCD chip in the given distance. This figure can be visually compared with the central plot in the simulation in figure 4.

To compare the results of simulation and measurement more precisely, both were plotted in figure 6. Measured results are obtained using a photodiode and an oscilloscope. As can be seen, the measured results mostly fall into 7% error. This interval represents various effects that may have affected the experiment [6].

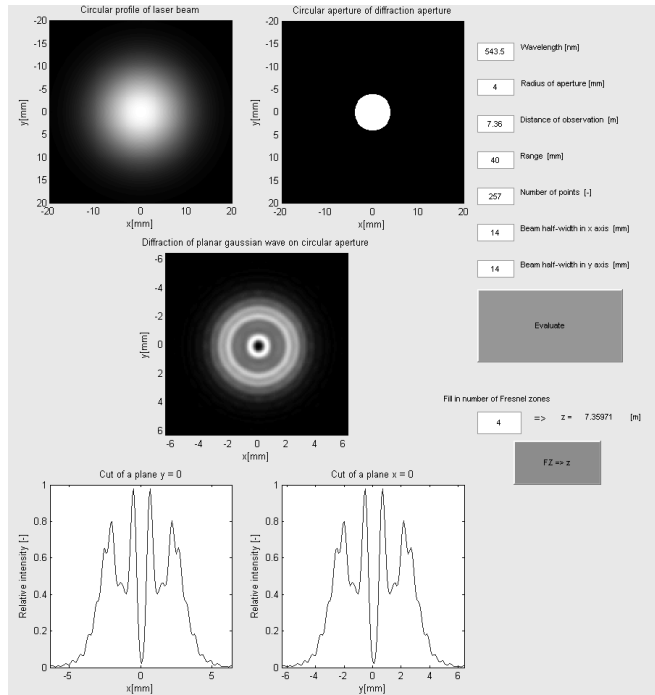


Fig.4. Simulation of the diffraction pattern intensity distribution with following parameters:
 $\lambda = 543,5 \text{ nm}$, $\rho_0 = 4 \text{ mm}$, $z = 7,36 \text{ m}$, $w_x = w_y = 14 \text{ mm}$.

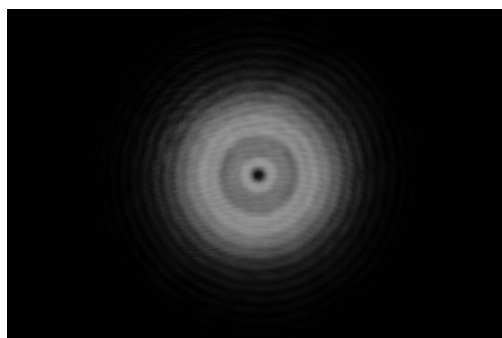


Fig.5. The diffraction pattern intensity distribution captured on the CCD chip during experiment with following parameters:
 $\lambda = 543,5 \text{ nm}$, $\rho_0 = 4 \text{ mm}$, $z = 7,36 \text{ m}$, $w_x = w_y = 14 \text{ mm}$.

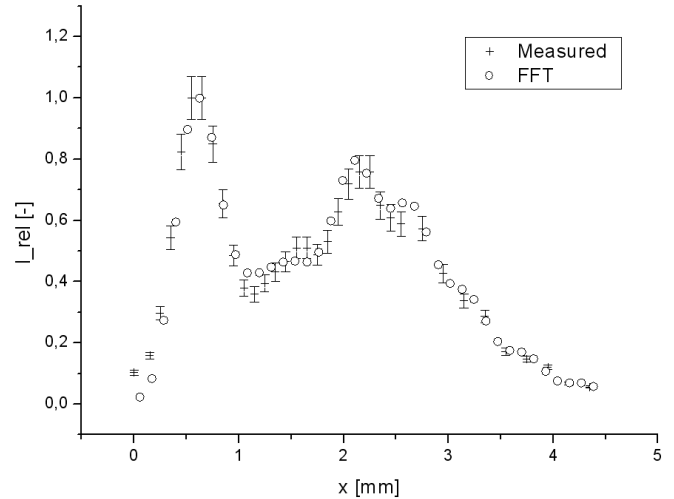


Fig.6. Comparison of the simulated and measured results of the diffraction pattern intensity distribution. Parameters of the experiment: $\lambda = 543,5 \text{ nm}$, $\rho_0 = 4 \text{ mm}$, $z = 7,36 \text{ m}$, $w_x = w_y = 14 \text{ mm}$.

V. CONCLUSION

In the paper, scalar diffraction theory and its contribution to modeling the wave effects of the laser beam were discussed. A qualitative as well as a quantitative analysis of the simulated results in the near-field were performed and compared with the measured results.

It was shown, that the transmitter aperture can have significant influence on the shape of the beam in the receiver plane. An example of the intensity distribution was shown, with emphasis on several maxima in the distribution that may cause a lower SNR and subsequently also higher BER.

ACKNOWLEDGMENT

The research described in the paper has been supported by the Czech Science Foundation under grants No. 102/09/0550, No. P102/11/1376, No 102/08/H027 and by the research program MSM0021630513. The research has been also supported by the projects CZ.1.07/2.3.00/09.0092 and CZ.1.07/2.3.00/20.0007 WICOMT in the frame of the operational program Education for competitiveness and by the Czech Ministry of Industry and Trade under grant agreement No. FR-TI2/705.

REFERENCES

- [1] J. D. Schmidt, *Numerical simulation of optical wave propagation with examples in MATLAB*. Bellingham, Washington: SPIE Press, 2010.
- [2] J. Schuster, H. Willebrand, S. Bloom, E. Korevaar "Understanding the performance of Free Space Optics", *Journal of Optical Networking*, Vol. 2, No. 6, 2003, p. 178-200.
- [3] G.R. Osche *Optical detection theory for laser applications*. New Jersey: John Wiley, 2002.
- [4] M. Born, E. Wolf *Principles of optics*. London: Cambridge university press, 2003.
- [5] B.E.A. Saleh, M.C. Teich *Fundamentals of photonics*. New York: John Wiley, 1991.
- [6] J. Poliak "Effect of optical elements on transmitted laser beam". Master thesis, Dept. of Radio electronics, Fac. Of Elec. Eng., Brno Univ. of Tech., Brno, Czech Republic, 2011.

OK 2011

- [7] J. Komrska “Vlnová optika”. Brno: Akademické Nakladatelství CERM, 2004.
- [8] J. Světlík “Simple methods for the measurement of laser beam parameters” in *Applied Physics*, vol. 13, no. 6, pp. 1276 – 1278, June 1974.

Experiment with Simple Prototype for Visible Light Communication

J. Vodrážka, J. Hrad

Czech Technical University in Prague, Faculty of Electrical Engineering, Department of Telecommunication Engineering, Czech Republic

Abstract—This paper deals with implementation and testing of data transfer technology using visible light, especially VLC (Visible Light Communication), which uses white LED for data transfer and it is integrated to lighting devices. The paper provides overview of VLC technology development and it describes real demonstration thereof. The electronic circuits of a prototype for visible light communication are inspired by free space optical link (FSO) that originated in RONJA project. The first part of this paper describes the basic blocks and their functions. The second part illustrates practical operation and discusses the results of a sample constructed at our Department.

Index Terms—Wireless Optic Communication; Visible Light Communication; Free-Space Optics.

I. INTRODUCTION

THIS paper deals with designing and implementation of a free space optical link (FSO) built on the basis of modified Ronja. [1], [3] The main goal was to design free space optical systems for the lowest possible cost and to implement several improvements and upgrades.

Below we describe the implementation and testing of data transmission technology using visible light, especially VLC (Visible Light Communication). VLC uses white LEDs as data signal sources, which also act as an ordinary light sources. In this paper we introduce an overview of VLC technology development and describe practical demonstration of its utilization. The electronic circuits of the prototype for visible light communication are derived from free space optical link in Ronja and other similar projects. [2], [4]

The first part describes the basic blocks and their function; the second part is dedicated to practical operation and results of a sample constructed at the Department of Telecommunication Engineering.

II. VISIBLE LIGHT COMMUNICATION

Visible Light Communication (VLC) technology uses optical spectrum between 400 nm and 700 nm for transmission of data. One of the motivating facts fostering the development of such technology is that the traditional bulbs are being successively replaced by energy-saving and more efficient light sources based on electroluminescent diodes (LED) – these promising devices are rapidly developing, thus becoming

more powerful and affordable. One of their most important features is that their output light can be modulated by signals in frequency range from units to hundreds of MHz. Together with the advancement of LED lighting, this opens the way to the development of wireless data transmission system that could use lighting devices.

VLC is being developed as an alternative to wireless networks based on radio transmission (such as WiFi). The goal is to design a complementary wireless technology that could be deployed at places where radio transmission is limited or forbidden (hospitals, airports, airplanes, etc.) or impossible because of interference.

White LEDs composed of blue LED and luminophore are most usual in lighting applications. Modulation bandwidth of blue diodes used for production of white LEDs is 20 MHz and 12 MHz for those with small chip and with large chip area, respectively. When the luminophore used for white LEDs is applied, the available bandwidth is reduced, typically to 2-3 MHz (in case of complete spectrum detection).

One of the main problems related to VLC systems is compensation of background light influence caused e.g. by natural daylight or fluorescent tubes. It is important to achieve independence of data transmission from the intensity of background light. Therefore the applied modulation method must be robust enough. Since VLC systems are integrated into lighting devices, the modulation methods must also ensure satisfactory lighting intensity.

Typical use of VLC technology is in downlink communication. Implementation of uplink is more demanding, and there are several options – infrared transmission, reflected beam or RF (radio frequency) communication. [6], [7], [8]

III. VISIBLE LIGHT COMMUNICATION EXPERIMENT

A. System Description

The prototype of visible light optical link was produced [5] on the basis of open-source available Ronja project as well. The red LED using the wavelength of 650 nm was replaced by a white light power LED (product of FORYARD OPTOELECTRONICS, type FYL-P20AWC-1W). Block diagram of the system is shown in Figure 1.

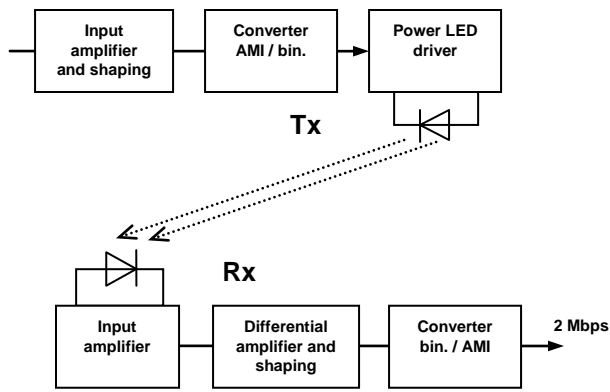


Fig. 1. Block diagram of visible light communication prototype.

The transmitter is powered from DC source; the voltage is 12 V. However, the logical gates require a lower voltage; the stabilizer of 5 V is implemented inside the receiver. The input signal is brought to the VLC module over a coaxial cable and the first part of the transmitter performs signal amplification to the required level. The input signal should have amplitude of 700 mV. After amplification, the signal passes through an inverter for pulse shaping. The inverters connected in parallel control the output transistor that is connected also in parallel to power LED. This parallel combination is connected through a resistor to power supply; the power LED output is thereby modulated.

The receiver is powered from DC source of 12 V, too. Unlike the transmitter, there is no need to supply voltage of 5 V in the receiver; it contains light detector based on a silicon PIN photodiode connected in a resistive mode. The signal from the photodiode is conducted to a low-noise input amplifier transistor BF998. In the next step, the signal is processed in differential amplifier NE592, designed primarily for video amplifiers, which provides enough amplification of the signal. From there the signal is lead to the output amplifier. Details of the design (both receiver and transmitter) are shown in Figures 2 and 3.



Fig. 2. Design of transmitter part of visible light communication prototype.



Fig. 3. Design of receiver part of visible light communication prototype.

B. Results of Testing

Firstly, the prototype of visible light optical link was tested by common impulse signal. The sensitivity and frequency band are shown in Figures 4 and 5. The optical axis of receiver was identical to the optical axis of the transmitter in this test.

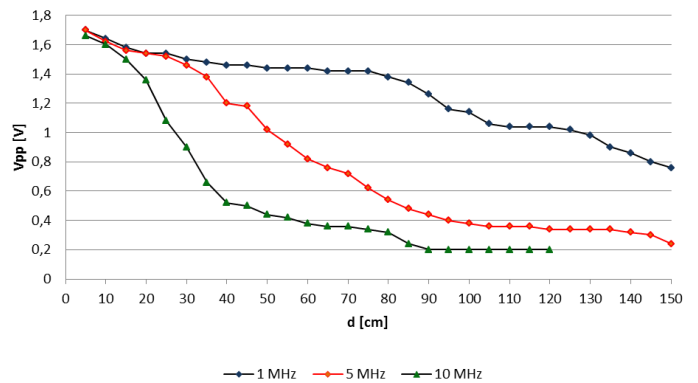


Fig. 4. Dependence of transmitting level distance for 3 frequencies.

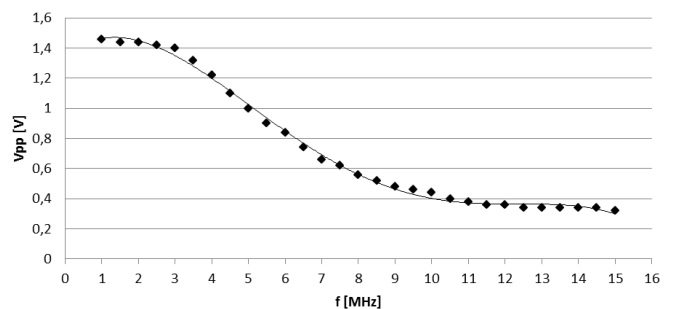


Fig. 5. Dependence of transmitting level frequency for distance 0.5 m.

With respect to relatively low power of the lighting LED, the resulting values are acceptable. If a LED with higher power (or LED array) should be used, the range would be adequately longer, i.e. acceptable for medium-sized interiors.

C. Real Communication Experiment

Secondly, the prototype was tested using E1 digital signal with line code AMI and transmission rate 2.048 Mbps. For this purpose, the binary/AMI and AMI/binary convertors are designed and connected to the receiver and transmitter.

The maximum distance of the transmitter and receiver, for which the 2.048 Mbps data analyzer indicated working synchronization, was 12 cm. The optical axis of receiver was identical to the optical axis of the transmitter in this test. The radiation characteristic of LED allows the rotation of axis by an angle of ± 30 degrees. Until this point, all measurements were conducted without any additional optical elements that could extend the range of the optical link. Since the distance of 12 cm is insufficient, an optical lens with refractive power of 5 D was inserted between the transmitter and receiver; the resulting range was extended to 160 cm, which is satisfactory. If a LED with higher power (or LED array) should be used, the range would be adequately longer, i.e. acceptable for medium-sized interiors.

IV. CONCLUSION

The established optical links will be used for demonstration purposes in education; students will get in touch with optical transmission free space FSO system and VLC technology. The measured results and practical experience will also serve for research purposes (examining the phenomena influencing free space attenuation). The follow-up Student Grant at the Czech Technical University in Prague is expected to explore the possibilities concerning production of affordable free space optics for short and medium distances featuring transmission rate of 100 Mbps.

ACKNOWLEDGMENT

This work was supported by the project No. MSM6840770014 (Czech Ministry of Education, Youth and Sports) and grant No. SGS 10/275/OHK3/3T/13 (Grant Agency of the Czech Technical University in Prague).

REFERENCES

- [1] K. Kulhavy: Twibright Labs, Ronja. [online], 2007, [cit. 12-30-2010]. <<http://ronja.twibright.com/>>.
- [2] Visible Light Communications Consorcium. <http://www.vlcc.net/?ml_lang=en>.
- [3] B. Bakala: Realization of optical link. Bachelor project, Department of Telecommunication Engineering, Czech Technical University in Prague, Faculty of Electrical Engineering, 2011.
- [4] T. Matsumara: 10Mbps Visible Light Transmission System. 2008 [cit. 2010-05-05]. <<https://mentor.ieee.org/802.15/file/Public/08/15-08-0171-01-0v1c-10mbps-visible-light-transmission-system.pdf>>.
- [5] J. Ondra: Communication with lighting electroluminescent diodes. Diploma project, Department of Telecommunication Engineering, Czech Technical University in Prague, Faculty of Electrical Engineering, 2011.
- [6] K. Navin, L. N. Rafael: LED-Based Visible Light System: A Brief Survey and Investigation. Journal of Engineering and Applied Sciences. 2010.
- [7] H. Elgala, et al.: OFDM Visible Light Wireless Communication. Vehicular Technology Conference, VTC2007-Spring. 2007.
- [8] M. Amand, P. Mishra: A Novel Modulation Scheme for Visible Light Communication. India Conference (INDICON). 2010.

The Fiber-optic Sensor for Perimeter Guarding

Jiří Hladík^a, Ladislav Šašek^a, Leoš Boháč^b

^a*Safibra, s.r.o*

^b*Faculty of Electrical Engineering, Czech Technical University in Prague*

Abstract— This paper deals with the practical application of the optical fiber sensors for the specific purpose of intrusion detection systems and the integrity protection of critical infrastructures. Currently, the use of security equipment is primarily based on metallic lines that generally integrate also surveillance cameras, free space detection lasers and other complicated security equipment. This paper shows one of the principles of using glass optical fibers as sensors for dynamic perimeter intrusion detection systems based on perturbation of the optical transmission properties of sensor zone fiber. The bending-pressure perturbations are used to induce optical speckle patterns at the end of sensing multimode fiber. These patterns are further spatially filtered by connected single mode fiber. The use of optical sensor systems has its advantages compared with conventional metallic systems that include stable parameters in time, potential greater guarding coverage due to low attenuation of the zone sensor driving fibers, passive mode of operation without using of active components in a guarded area, and great resistance to electromagnetic interference.

Index Terms— perimeter, optical fiber, sensor, multimode fiber, speckle.

I. INTRODUCTION

It is obvious that the everyday life of our civilized cultural society is increasingly dependent on the infrastructure and especially on certain critical parts of it such as electricity distribution network, data transmission networks, telecommunication mobile operators and ISPs. Similarly, it could be very dangerous for civilization, if there were significant disruptions of functionality for other infrastructure networks, such as air traffic control or public passenger transport in cities.

In this respect our modern civilization is very vulnerable, that is what the extremists are a very much aware of. And just this vulnerability can be relatively easily used to create pressure on governments and citizens. Most of the risks could be prevented by obtaining timely information about the attack of an unauthorized person, with strict security guarding of critical infrastructures and their surrounding areas through a system of vibration sensing and continuous signal evaluation using Fast Fourier Transform (FFT) [2] analysis, possibly using vibration sensors along the whole monitored zone. The problem lies in the fact that in practice it is usually required to assure security guarding in a large space or distance, but the classic electric vibrometers are not suitable for prolonged use

in the field in terms of aging and the need for periodic calibration.

Electrical cables and sensors can also be easily detected and localized by metal detection devices and thus function of the security system can be easily disengaged or influenced. Compared with the disadvantages of electrical sensors for guarding applications the optical and especially fiber-optic sensors appears be very suitable for this purpose, especially for their long life (min. 20 years), good stability of properties, usually without any necessary calibration for the whole life span, and especially for their full dielectric structure, which can be quite insensitive to external electromagnetic field.

This is an advantage especially when it comes to use in an outdoor environment near metal structures (eg, systems for monitoring of fences around important objects), while these sensors as composed of a pure dielectric materials are very difficult to be found by an unauthorized person. In addition, fiber sensors offer substantial possibility of different arrangements, where it is possible to gain high vibration sensitivity along a considerable length of a sensor or on other hand it possible to assure a transfer of optical sensing information for a long distances without influencing the transmission in fiber by disturbing vibrations from its surroundings. This allows zonal arrangement of sensors with sufficient sensitivity to vibrations in the localized detection zones.

II. SPECKLE MODAL DETECTION PRINCIPLE

It is well known, that multimode fiber with its large core diameter supports a large number of simultaneously propagating electromagnetic modes. The exact number of propagating modes depends on the index profile of the fiber, core diameter and wavelength of travelling light. Each mode has its own group velocity and propagation constant, but all interfere with others as they share the same medium. There are hundreds of modes in a typical multimode fiber.

A multimode optical fiber can be used as a vibration sensor using principles based on the phenomena of modal noise [1-11]. When the fiber starts to vibrate the intensity and phase of each individual mode is slightly modified, each to a varying degree [7]. As the modulation of the modes in the distribution is different the light intensity in the pattern will change, though the intensity of the overall pattern will not vary. If the output pattern is spatially filtered then the signal current at the

photodetector will be modulated too.

If the light output of the end of multimode fiber is projected on screen it forms so called speckle pattern (see Fig. 1). This speckle pattern forms a number of speckles each having its own specific intensity profile. This is clear evidence that if normalized frequency exceeds its critical value for multimode excitations (2,405 for step index fiber), light truly travels in many modes through fiber. Any change in optical path property affects propagation of various modes that couples inside the core among themselves and as such interfere at the fiber end differently forming also other speckle pattern with total summed intensity in all modes remaining the same [11].

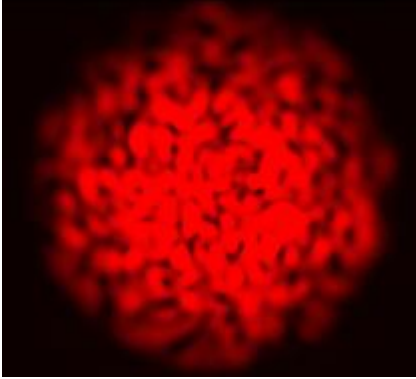


Fig. 1. The well known speckle pattern emanating out of the multimode fiber end projected on the screen.

In [1] is shown that intensity of a one speckle is proportional to the force $F(t)$ perturbing the fiber by following expression

$$I_i = A_i \{1 + B_i [\cos(\delta_i) - F(t)\phi_i \sin(\delta_i)]\} \quad (1)$$

where A_i represents a degree of mode self-interaction, and the next two terms cross-mode interactions, the first one (B_i) takes into considerations the modes steady state condition, and the second one ϕ_i corresponds to a degree of cross-mode interactions if a fiber is being perturbed in some way or other. The signal output that sums absolute value of changes in intensity pattern is given by equation [1]:

$$\Delta I_T = \left[\sum_{i=1}^M |C_i \sin(\delta_i)| \right] \left| \frac{dF(t)}{dt} \right| \quad (2)$$

A various forces applied upon a fiber can change modes propagation characteristics and thus their interference conditions resulting in different speckle distributions out of the fiber end on the screen. An exact analysis of changes in propagation parameters for each mode arising from application of the force is an extremely difficult, but in most cases studying only variations in speckle pattern itself at the fiber end is sufficient enough. From these variations it is also possible easily not only detect vibrations but also obtain information about the vibration pattern itself that is characterized by amplitude and the frequency. What is more,

such a sensor system can be built with cheap and widely available components that are at the same time lightweight, which makes it an interesting product in the sensor market for integration in, already mentioned, smart structures.

III. OPTICAL FIBER BASED GUARDING SYSTEM

One of the real results of this paper will be eventually a design of fiber-optic system that is able to warn against attacks on critical infrastructure or unauthorized entry to the site of the guarded object. In addition to the advantages of a purely passive outdoor installation using dielectric fiber-optic cables the complete system will be able to identify possible intruders, and potential false signals will be minimized

Not all sites are around its perimeter protected by a fence. For this reason, the system sensors were tailored so that they could be placed not only on the fence, but also on (in) the ground as a tread sensor.

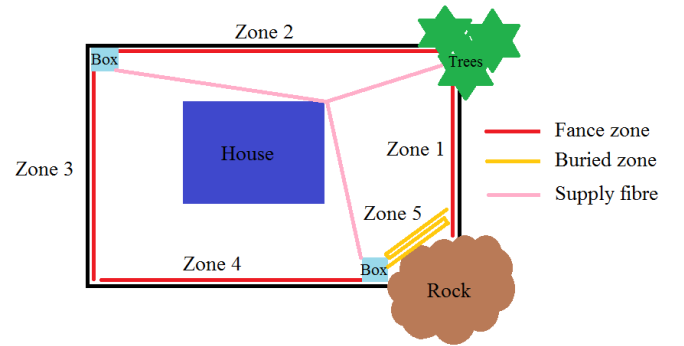


Fig. 2. The principle of the zoned perimeter guarding

For intruder position resolution a system can be divided into several zones (see Fig. 2), which do not affect each other. The power feeding fibers of all zones in turn lead to the central security unit, which is located for example in the home or centralized emergency alert system. Some sites are very large (eg airport) and so power feeding fibers can be very long, In this case telecommunications singlemode optical fibers with low losses are used.

Both fibers in the fence and in the ground can capture vibrations from their surroundings, and subsequently evaluate them. Vibrations may not only be created by an intruder, but also by a nature. For this reason, there must be set a threshold or resolution pattern, which varies for different applications.

IV. FIBER SENSOR MEASUREMENTS

The basic configuration of the sensor for measuring the effect of vibration is shown in Fig. 4. As can be seen, configuration is quite simple. At the left a semiconductor laser was used to couple light of appropriate wavelength into a feeder singlemode fiber section of approximate length of 500 m. The feeder fiber is on its end directly spliced to following 100 m section of a detection multimode fiber. Its end is again spliced firmly to the last feeder section of

singlemode fiber that is connected to optical intensity detector. A first section of singlemode fiber couples and excites optical modes in multimode fiber. The role of last singlemode feeder section is not just only to carry light to the detector for longer distances but also to spatially filter only a part of speckle pattern that is most sensitive to vibration. As the singlemode feeder fiber does not contribute to the signal attenuation we have further concentrated more on the measurement setup in Fig. 5. To preserve the influence of spatial filtering at the points of splices we have left the singlemode feeders on both sides of detection multimode fiber intact but used only a short length of them.

We have measured at two wavelengths (1550 nm and 1300 nm), in the spectral regions commonly used for telecommunications transmissions. There were two kinds of tests for the same sensor. The first test should simulate a position on the fence and thus the detection optical fiber was inserted into the of-the-shelf plastic protective strip. The second test was adapted tread arrangement and multimode fiber including all buffers was placed between the rubber sheets (see Fig. 3). **In all cases, the weight of 100 g was used to simulate the impact by its free fall from height of 20 cm.** First measurement was conducted to simulate situation on the fence in the protective strip. The fiber length of detection zone was 100 m. The fiber was stretched in a protective strip in length of 2 m. The first effect was measured at the very beginning of detection zone fiber and then at the end. The graph in Fig. 6 shows the measured signal intensity curves versus time.

At the beginning of the detection zone, in the moment of weight impact, the measured signal was about 60 % of the original signal (non impact) for both light sources. But at the

end of the fiber it was just about 12 % compared to the original signal at wavelength of 1300 nm and about 30 % compared to the original signal at wavelength of 1550 nm.



Fig. 3. Illustration of fiber sandwiched between two rubber sheets

The second arrangement, where we used rubber sandwich, the fiber sensor was placed on the ground between pair of rubber sheets that both protected and transferred vibrations to the detection fiber from its vicinity as far as 0.5 m. The detection fiber was stretched through these sheets. The result of impact signal measurement is given in Fig. 7.

In addition to the signal peak it is evident that character of the signal is quite different than in previous case where the fiber was placed in protective strip alone. In rubber tread sheets case the vibrations are filtered. This characteristic is important for further correlation analysis of the signal. Using FFT and other digital processing methods the authors hope to be able to use a signal from optical sensor a precisely identify a type of intrusion and also differentiate the right from false alarms.

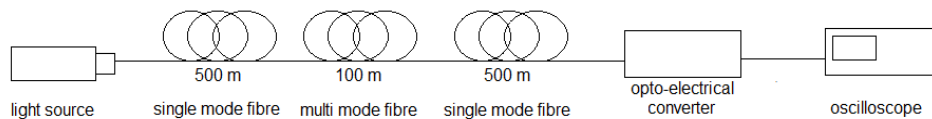


Fig. 4. The basic arrangement of measurement

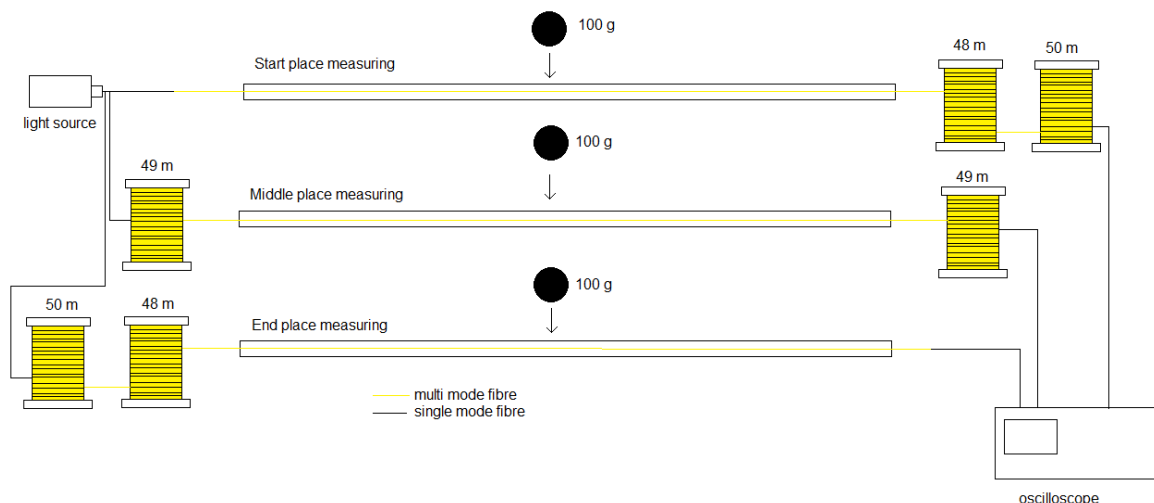


Fig. 5. The impact measurement in detection fiber

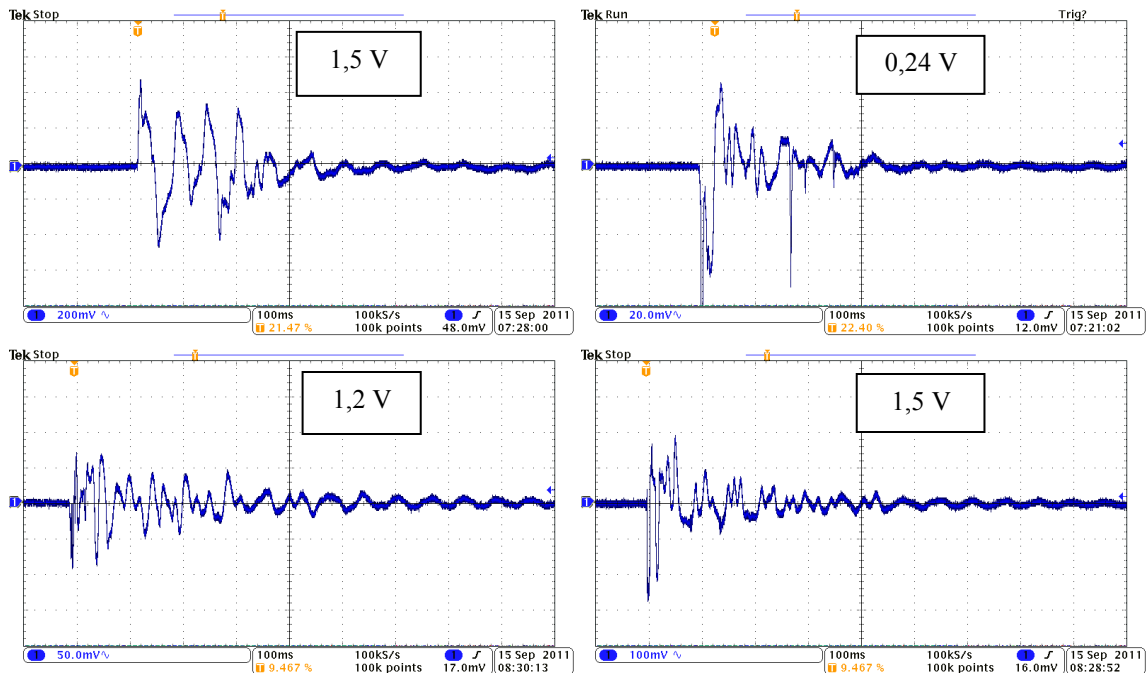


Fig. 6. The fiber in a protective bar measured at the beginning (top) and end (bottom) detection zone for a wavelength of 1300 nm (left) and 1550 nm (right)

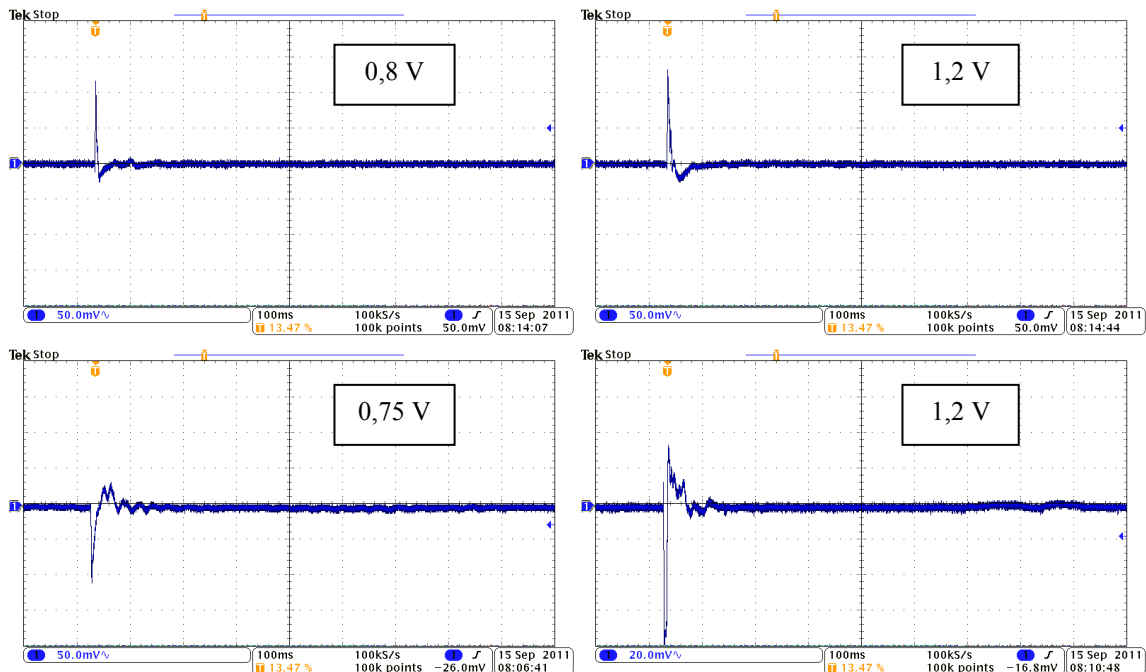


Fig. 7 The fiber sandwiched between the rubber sheets measured at the beginning (top) and end (bottom) detection zone for a wavelength of 1300 nm (left) and 1550 nm (right)

IV. CONCLUSIONS

We have practically demonstrated by measurement a sufficient sensitivity and practical applicability of optical fiber as a viable sensor for guarding critical infrastructure security and other objects.

The measured AC signal from the photodetector in

application to the perimeter fence simulating intrusion along as far as 100 m length of detection fiber is at least 12 % of the DC value of perimeter signal in idle (no intrusion) state. Results of tread sensor arrangement are above 12 % of the original signal in the case of one fiber.

The results of many measured experiments indicate that higher sensitivity to the measured vibrations at the beginning of the fiber was achieved in the spectral range of 1300 nm.

The measurements at the end of detection fiber (100 m) showed that sensitivity of the source of 1300 nm is still higher than it was at a wavelength of 1550 nm, but compared to the beginning of fiber it has decreased. Consequently, it is better to use a wavelength of 1550 nm at a distance greater than 200 m.

The measured results of testing two possible arrangement of fiber-optic perimeter showed that the sensor can potentially reliably detect intruders.

ACKNOWLEDGEMENT

This paper and work was supported by grant from Ministry of The Interior of Czech republic under project name „Guardsence” and number VG20102015053.

REFERENCES

- [1] Spillman W B Jr, dKline B R, Maurice L B and Fuhr P L. Statistical-mode sensor for fiber optic vibration sensing uses, *Appl. Opt.* 28 316676, 1989
- [2] Culshaw B. *Optical Fibre Sensing and Signal Processing*, 1984, London
- [3] H. J. Arditty and H.C. Lefevre, Sagnac effect in fiber gyroscopes, *Opt. Lett.* 6, 401-3
- [4] B. Zagar and S. C. Schneider, “A laser-speckle-shift strain gauge and its application in material testing,” in *Proc. IEEE IMTC*, Anchorage, AK, 2002, pp. 733–736.
- [5] I. Yamaguchi, “Speckle displacement and decorrelation in the diffraction and image fields for small object deformation,” *Opt. Acta*, vol. 28, no. 10, pp. 1359–1376, 1981.
- [6] V. T. Chitnis, S. Kumar and D. Sen, Optical fiber sensor for vibration amplitude measurement, *J. Lightwave Technol.* 7, 678-91
- [7] M. Kielu and P. R. Hercfeld, Novel fiber optic sensor based on modal power distribution, *Proc. SPIE Int. Soc. Opt. Eng.* 798, 1987, 331-6
- [8] Y. Kitagawa and A. Hayashi, Fiber optic sensor for distance and velocity measurements using speckle dynamics, *Appl. Opt.* 24, 1985, 955-9
- [9] M. Tsubokawa, T. Higashi and S. Seikai, Fiber optic sensor for measuring external forces distributed along a fiber, *Japan J. Appl. Phys.* pt 2 26, 1987
- [10] J. D. Weiss, Fiber optic strain gauge, *J. Lightwave Technol.* 7, 1989, p 1301-18
- [11] P. J. Kajenski, P. L. Fuhr and D. R. Huston, Mode coupling and phase modulation in vibrating multimode waveguides, *J. Lightwave Technol.*, Vol. 10, Iss. 9, 1992

SMART OPTICAL FIBER SENSORS

B. Korenko, J. Jasenek, J. Červeňová

Faculty of Electrical Engineering, Slovak University of Technology in Bratislava

Abstract— The paper concerns the intrinsic optical fiber (OF) sensors with distributed parameters. In the paper we focus on numerical simulations of interaction of the sensing fiber with the external factors using 3D modeling of different applied forces. Further we discuss the implementation of the advanced Optical Time-Domain Reflectometry (OTDR) based on the combination of Photon-Counting OTDR equipped with advanced zooming tool and Polarization OTDR. The correction of the detected backscattered signal due to higher optical power in photon counting method is discussed. The measured data are briefly explained.

Index Terms— optical fiber sensors, optical time domain reflectometry, numerical model of OF sensor, strain distribution measurement.

I. INTRODUCTION

Nowadays the optical fiber sensors with distributed parameters based on optical fibers are beginning widely used in practice. Nevertheless rather strong effort is being permanently focused on further development of more sophisticated sensoric systems using these principles. One can mention their application in civil engineering structures, airplanes, turbines and other structures for measurement of physical quantities like pressure, vibration etc. Designing a multidimensional structure with OF sensors provides the possibility to measure mechanical or other physical fields in more dimensional manner. Also real time measurement is possible. The advantage of usage of OF pressure sensors with distributed parameters instead of those using conventional methods is that only the access to one end of the sensing fiber is needed and it is also possible to measure on more dimensional structure with appropriate space resolution.

The crucial point in the designing of optical fiber sensors with distributed parameters for the picking up the space distribution of some physical quantity is the detail analysis and modeling of the processes that transform the changes of the physical quantity into those of index of refraction in the fiber core. The understanding of these transformations gives the possibility for the optimization of the sensing systems. The main results of this paper concern particularly the modeling of the mechanical stress on the index of refraction changes in sensing optical fiber. These induced index of refraction changes are detected by the OTDR method and its several modifications or by the combination of these modifications. At present time OTDR [1] and its several modifications [2] are

frequently used in many fields of OF sensors. Very attractive is the combination of Photon-Counting OTDR (PO-OTDR) and Polarization OTDR (PO-OTDR) that is used also at our laboratory.

II. 3D MODELING OF INTRINSIC FIBER SENSOR

In general intrinsic OF sensor means, that any mechanical stresses applied to the optical fiber cause a reaction – the dimension deformation and the change of OF local properties. To obtain the precise 3D OF model a cylindrical symmetric structure of silica material was modeled in ANSYS Multiphysics program (Fig. 1). The structure consists of three cylindrical areas consisting from different materials – the inner core with the diameter of $10\mu\text{m}$, the cladding with the $120\mu\text{m}$ diameter and the primary protection with $250\mu\text{m}$ diameter.

To simulate the difference of “optical density” between core and cladding the Young modulus parameter was set to 55 GPa for the core, 50 GPa for the cladding and 30 GPa for protection [3]. Each part was meshed for finite element numerical analysis.

The places of applied stress can be clearly seen from the simulation results although the area of the force application is very small. The equipotential contours with higher amplitude of the pressure are clearly located along the OF axis. Due to the pressure field in the atomic structure of fiber continuum, the index of refraction inside the core was changed [3].

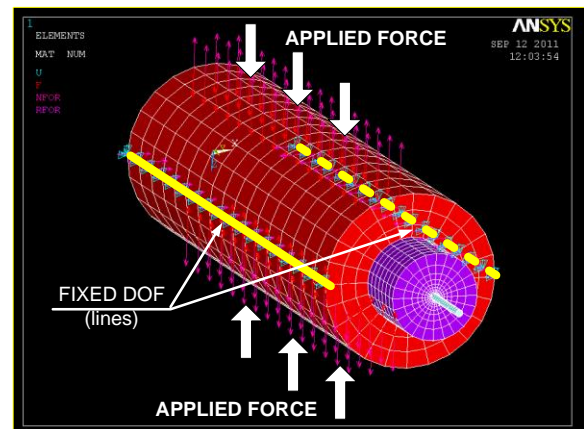


Fig. 1. Simulated model of OF sensor with lateral loading.

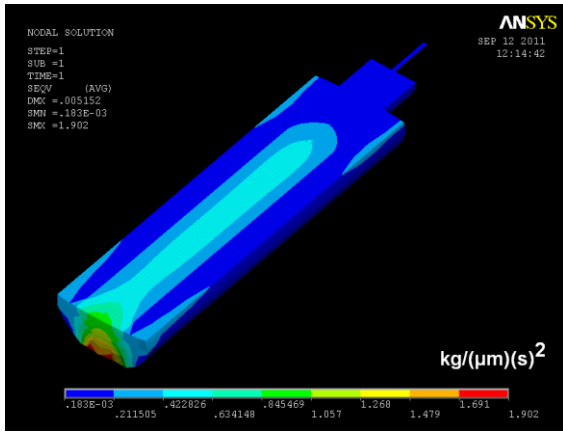


Fig. 2. Von Misses stress distribution in the cross-section caused by lateral force.

For better understanding of stress distribution caused by different force applications three specific model variants were realized.

The lateral loading is shown in Fig. 1. On 45 segments (nodes) of the 3D model the force of 1mN was applied from both sides (Fig. 1). The model geometry was fixed along the primary protection of the OF. There are no dimensions of freedom (DOF) for these lines. The simulation results concerning the longitudinal section are shown in Fig. 2. It is clear that applied force on the protection surface also affects the core structure.

Another case of the mechanical influence on the fiber core is that the OF is exposed to longitudinal strain Fig. 3. One end of the fiber was fixed as a plane area and the force was applied on the other end. At the end segments the force of 1mN was applied at each node on primary protection of the OF.

The results are shown on Fig. 4.

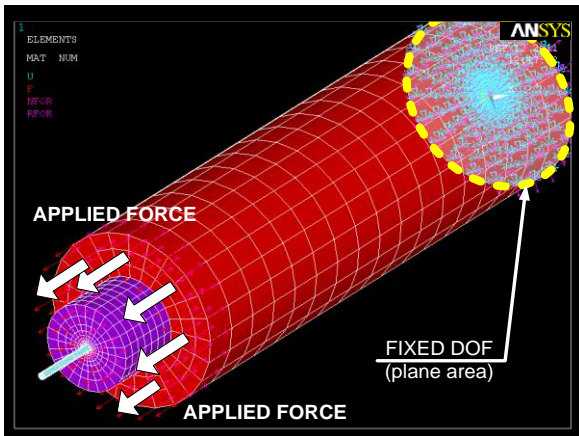


Fig. 3. Simulated model of OF sensor with longitudinal strain.

The third model implements torsion. On 10 nodes on each side of the OF, see Fig. 5, the force of 1mN was applied. From the simulation result, see Fig. 6, only the influence at the primary protection and cladding is present. This event is not so relevant for OF sensors.

If the polarization properties of the fiber are known before its exposure to the stress that is perpendicular to the fiber axis, polarimetric sensor with distributed parameters can be obtained.

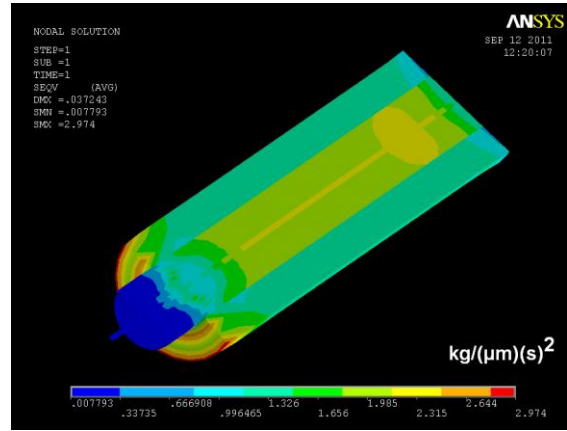


Fig. 4. Von Misses stress distribution in the cross-section caused by longitudinal strain.

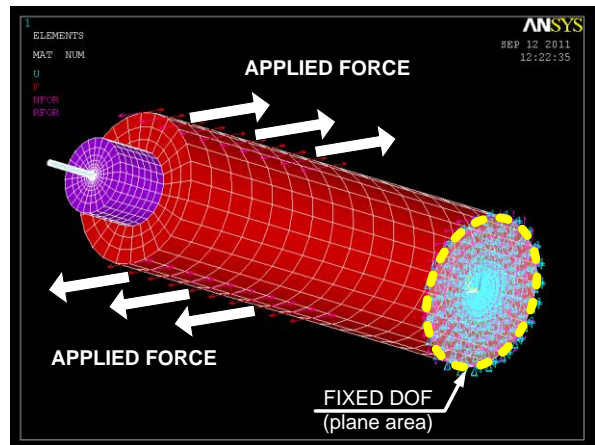


Fig. 5. Simulated model of OF sensor with torsion force.

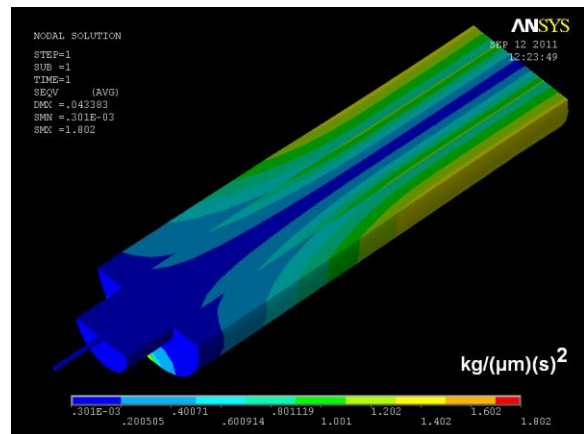


Fig. 6. Von Misses stress distribution in the cross-section caused by torsion.

The stress field distribution combined through the elasto-optic effect with the local change of refraction index gives the possibility to calculate local birefringence changes [3].

As it was shown in [4] the calculation of refraction index changes $\Delta n_{\text{eff}X}$, $\Delta n_{\text{eff}Y}$, $\Delta n_{\text{eff}Z}$ represents the tensor of optical density change due to the pressure fields.

For the purposes of the birefringence changes calculation only the axial values of pressure tensor vector σ_{XX} , σ_{YY} and σ_{ZZ} in the fiber core are needed [4]. The cross sections views demonstrate clear homogeneity of stress distribution inside the fiber core.

The results obtained from ANSYS clearly show that in comparison with 2D models [3] we achieved good approximation of the pressure distribution σ_{XX} , σ_{YY} and σ_{ZZ} . Due to these changes induced birefringence will affect the polarization and the periodicity of the beat length will be disturbed.

III. OTDR BASED ON PHOTON COUNTING

For using such kind of sensor as described above a sophisticated measuring method is needed. That's the reason why we use variant of one end measuring method based on OTDR [2]. For our measurement needs we use the combination of PO-OTDR [3] and PC-OTDR that is very advantageous due to high sensitivity, rather simple digital signal processing and the use of coupling between the external factors and measurable polarization changes caused in the fiber core.

PC-OTDR is based on the usage of Poisson statistics of backscattered ultra low level optical power. The simplified diagram of the signal processing in PC-OTDR is shown in Fig. 7.

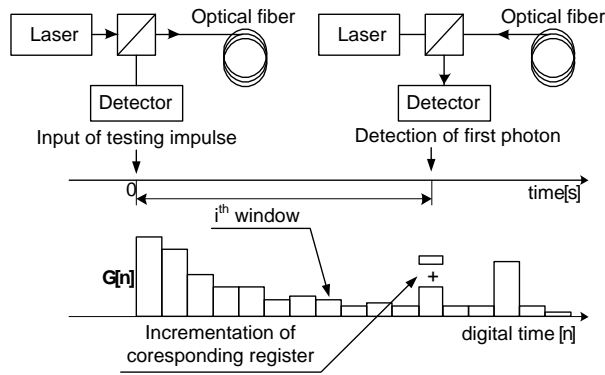


Fig. 7. The principle of PC-OTDR histogram forming.

In contrast with the classic OTDR it dominantly uses the digital signal processing. The optical source generates a test impulse which is launched through 3dB optical coupler into the optical fiber under test. Ultra low backscattered optical power from the tested fiber is given by a stream of discrete photons and is detected by a very sensitive detector based on the single photon avalanche diode (SPAD). The result of the measurement is a PC-OTDR histogram. As it can be shown in [6] under these ultra-low power conditions the probability of the first photon detection $R_1(t)$ at the time “t” in the time window of the duration “ τ ” is given by the relation:

$$R_1(t) = \eta\tau \cdot \left[\frac{P_{BS}(t)}{h\nu} \right], \quad (1)$$

where η is the quantum efficiency of the detector, $P_{BS}(t)$ is the time dependence of the back-scattered power, $h\nu$ is the photon energy. The expression (1) defines the mutual relation between the measurable first photon detection time and the time dependence of the back scattered power we are trying to measure. Under these ultra-low power conditions the measurement process may take a lot of time that is in practical measurement process not acceptable. Therefore it is necessary to realize the measurements at “a bit higher” optical powers but it results in the necessity of making some corrections of the originally derived formula (1). Due to rather long procedure of the precise correction derivation we bring the result published in [6]. At higher back-scattered optical powers the mutual relation between the measured numbers N_i of the first photon detection in the i -th time window determining the measured probabilities N_i/N (N is the total number of repeated measurements) and the true probabilities are given by the relation:

$$R_{li-true}(t) = \frac{N_i}{N - \sum_{j=0}^{i-1} N_j} + \frac{1}{2} \cdot \left(\frac{N_i}{N - \sum_{j=1}^{i-1} N_j} \right)^2. \quad (2)$$

The relation (2) makes possible to calculate from the measured data N_i and N true or corrected probabilities of the first photon detection defining the true time dependence of the measured back-scattered optical power.

OTDR based on photon counting demands usage of active quenching circuits for optical receiver. We use single photon avalanche diode PGA 408 from Princeton Lightwave. When the data processing is digital and it is possible to quench optical receiver at any time it gives us a possibility to measure fiber on specific regions “windows”. Such an approach in measuring gives us the possibility to do first preliminary measurement on the whole fiber network and then focus mainly on interesting part of the network like sensing region, for example. Below we show a simple experiment results from windowing - zooming method.

We measured optical link constructed from 2 optical fibers as shown in Fig. 8. The link was ended with non refractive coil. The measurement was done in 1550 nm region.

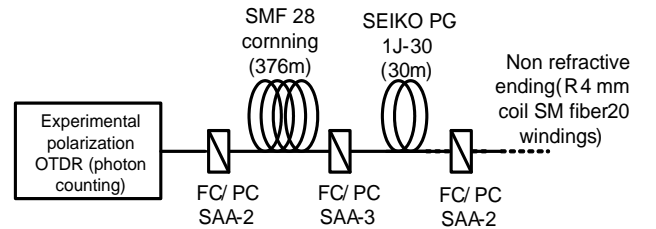


Fig. 8. Structure of measured optical net.

All measurements were done digitally according to [5], so it is not scaled in dB but in count rate. Number of realized measurements was 1 milion. For the first preliminary

measurement shown in Fig. 9 the active time for receiving avalanche diode was $4.38 \mu\text{s}$. The reversed bias voltage on SPAD was $62,6\text{V}$. The distance we measured was from 1^{th} to 13^{th} window. One window represents a distance of approximately 35m .

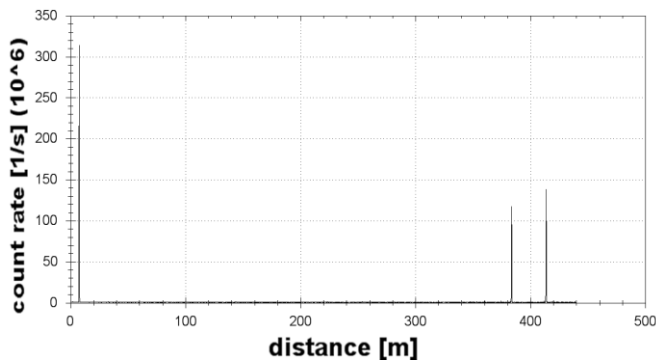


Fig. 9. Example of measured PC OTDR histogram.

From the Fig. 9 it is clear that the measured OTDR histogram corresponds to constructed optical net. More precise detail of the end section was measured only from 11^{th} to 13^{th} window.

The active time for receiving avalanche diode was $729.34\mu\text{s}$. The results of OTDR histogram zooming are shown in Fig. 10.

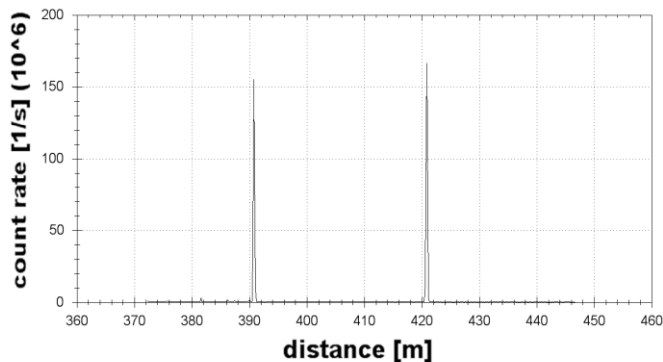


Fig. 10. Zooming on PC OTDR histogram.

The main advantage of zooming was not only the more detailed description of the optical net but also a serious impact on the time of the measurement that was approximately 10 times lower. With such a tool the realization of adaptable measurement algorithm could be realized. Also usage of active quenching circuits at the receiver SPAD diode lead to suppression of unwanted reflections “ghosts” and also the “memory effect” on the receiver is not present.

IV. CONCLUSION

In the first part of the paper the results of the numerical simulation of load, strain and torsion effect in the standard cylindrically symmetrical optical fiber are brought through the 3D modeling. The main result consists in the 3D evaluation of the space changes of the local refraction index in the optical fiber core under the defined mechanical strain, lateral loading and torsion. These changes imply the occurrence of induced local birefringence in optical fiber. The exact investigation of

the relation between the sensed physical quantity and induced birefringence is the crucial point for the construction of smart fiber optic sensors with distributed parameters.

Further advanced measuring method based on the photon counting OTDR is briefly explained according to its zooming possibilities. And correction for higher optical power is explained.

ACKNOWLEDGMENT

This work was done as a part of the solution of the VEGA projects No. VEGA 1/0617/09.

REFERENCES

- [1] M.K. Barnoski, S.M. Jensen, “ A novel technique for investigation of attenuation characteristics,” in *Applied Optics* , 1976, vol. 15, no. 9 , pp. 2112-2115.
- [2] A. J. Rogers, “ Polarisation-optical time domain reflectometry: a technique for the measurement of field distribution,” in *Applied Optics*, 1981, vol.20, no. 6, pp. 1060-1074.
- [3] K. M Hung, et al. “Theoretical analysis and digital photoelastic measurement of circular disk subjected to partially distributed compression,” in *Experimental mechanics*, 2003,vol. 43, pp. 216-224
- [4] S. A, Mastro, “Optomechanical behaviour of embedded fiber bragg grating strain sensors,” in *PhD thesis*, 2005, DREXEL UNIVERSITY, online: http://dspace.library.drexel.edu/bitstream/1860/515/10/Mastro_Stephen.pdf
- [5] B. Korenko I, J. Jasenek, J. Cerveňová, M. Hlaváč, “Optical fiber sensor with distributed parameters based on optical fiber reflectometry”, in *Advances in electrical and electronic engineering*. 2011, vol. 9, no. 1, p. 48-55.
- [6] J. Jasenek, “Optická vláknová reflektometria”, Slovak Technical University of Technology in Bratislava, 2004, ISBN 80-227-2002-X, pp.